Theoretical study of defect signatures in

III-V and II-VI semiconductors

Final Report

Period covered: Mar 2, 2005 – Mar 1, 2006

Prepared by

Assoc. Prof. Dr. Sukit Limpijumnong (P.I.)
Suranaree University of Technology,
Nakhon Ratchasima 30000

sukit@sut.ac.th

		Form Approved
Report Documentation Page		OMB No. 0704-0188

Public reporting burden for the collection of information is estimated to average 1 hour per response, including the time for reviewing instructions, searching existing data sources, gathering and maintaining the data needed, and completing and reviewing the collection of information. Send comments regarding this burden estimate or any other aspect of this collection of information, including suggestions for reducing this burden, to Washington Headquarters Services, Directorate for Information Operations and Reports, 1215 Jefferson Davis Highway, Suite 1204, Arlington VA 22202-4302. Respondents should be aware that notwithstanding any other provision of law, no person shall be subject to a penalty for failing to comply with a collection of information if it does not display a currently valid OMB control number.

1. REPORT DATE	2. REPORT TYPE	3. DATES COVERED
30 JAN 2008	**Final**	**23-03-2005 to 28-04-2006**

4. TITLE AND SUBTITLE	5a. CONTRACT NUMBER
Theoretical study of defect signatures in III-V and II-VI semiconductors	**FA520905P0309**
	5b. GRANT NUMBER
	5c. PROGRAM ELEMENT NUMBER

6. AUTHOR(S)	5d. PROJECT NUMBER
Sukit Limpijumnong	5e. TASK NUMBER
	5f. WORK UNIT NUMBER

7. PERFORMING ORGANIZATION NAME(S) AND ADDRESS(ES)	8. PERFORMING ORGANIZATION REPORT NUMBER
National Synchrotron Research Center, Suranaree University of Technology, P.O. Box 93, Nakhon Ratchasima 30000, Thailand, NA, NA	**N/A**

9. SPONSORING/MONITORING AGENCY NAME(S) AND ADDRESS(ES)	10. SPONSOR/MONITOR'S ACRONYM(S)
AOARD, UNIT 45002, APO, AP, 96337-5002	**AOARD-054013**
	11. SPONSOR/MONITOR'S REPORT NUMBER(S)

12. DISTRIBUTION/AVAILABILITY STATEMENT
Approved for public release; distribution unlimited

13. SUPPLEMENTARY NOTES

14. ABSTRACT
The study of defects in III-V and ZnO semiconductors was accomplished using ultrasoft pseudopotential (USPP) method. For that, a numerical approach was also implemented to calculate isotropic hyperfine-parameters for isolated defects based on a supercell method.

15. SUBJECT TERMS

16. SECURITY CLASSIFICATION OF:			17. LIMITATION OF ABSTRACT	18. NUMBER OF PAGES	19a. NAME OF RESPONSIBLE PERSON
a. REPORT **unclassified**	b. ABSTRACT **unclassified**	c. THIS PAGE **unclassified**	**Same as Report (SAR)**	**61**	

Standard Form 298 (Rev. 8-98)
Prescribed by ANSI Std Z39-18

Executive summary

During the first year contract, we have successfully initiated and continued our study of defects in III-V and ZnO semiconductors using ultrasoft pseudopotential (USPP) method as planned. We have also investigated and implemented a numerical approach to calculate isotropic hyperfine-parameters for isolated defects based on a supercell method. We have surpassed our original milestones in several aspects and already accomplished important calculations that aid ZnO and III-V research. a) Based on our calculations and experimental work by Dr. D.C. Look at AFRL/WPAFB, we together have identified a newly observed native defect donor in ZnO as a Zn_I-N_O defect complex. b) Through our collaboration with experimentalists at Linköpin University (Sweden), we identified the recently observed EPR signals in diluted GaPN to be Gallium interstitial (Ga_I) complexes. c) We have investigated and identified two important mechanisms that deactivate nitrogen doped ZnO and turns them into nitrogen-hydrogen complex (N_O-H) and substitutional diatomic molecules $(N_2)_O$. Our predicted infrared signatures of the complexes are in agreement with the infrared measurements by our collaborators at the National Renewable Energy Laboratory. d) We proposed a novel N-2H complex model in GaAsN that has the IR signature matching the observed result.

Publications:

1) **Appl. Phys. Lett. 86**, 211910 (2005).
   "Substitutional diatomic molecules NO, NC, CO, N_2, and O_2: Their vibrational frequencies and effects on p doping of ZnO"

2) **Appl. Phys. Lett. 86**, 151910 (2005).
   "Resolving hydrogen binding sites by pressure - A first-principles prediction for ZnO"

3) **Phys. Rev. B 71**, 125209 (2005).
   "Properties of Ga-interstitial defects in $Al_xGa_{1-x}N_yP_{1-y}$"

4) **Phys. Rev. Lett. 95**, 225 502 (2005).
   "Evidence for native-defect donors in n-type ZnO"

5) **Physica B 376-377**, 686 (2006).
   "Probing deactivations in Nitrogen doped ZnO by vibrational signatures: A first principles study"

6) **Physica B 376-377**, 583 (2006).
   "Ion relaxation and hydrogen LVM in H-irradiated GaAsN"

7) **J. Cryst. Growth 287**, 94 (2006).
   "Impurity effects in ZnO and nitrogen-doped ZnO thin films fabricated by MOCVD"

(Following work schedule and milestones are the same as previously submitted)

Work schedule:

Month 0:

- o Start state-of-the-art calculations for common native defects in GaP and GaAs using ultrasoft pseudopotential (USPP) and large supercell.

- o Investigate the first principles all electron codes in detail. Designing viable numerical approaches to calculate isotropic hyperfine-parameters for isolated defects using the supercell method. Develop the tools to streamline the results from USPP calculations to all electron calculations.

- o Study N_O-Zn_i complexes and other point defects in ZnO using USPP calculations *(in collaboration with experimentalists at AFRL/WPAFB)*.

Month 6:

- o Explore the formation of defect complexes in GaP and/or GaAs using USPP calculations. Identify potential complexes for further study.

- o Systematically calculate the isotropic hyperfine parameters for important native defects in GaP and/or GaAs.

- o Study the stability of Frenkel pairs in GaN and/or ZnO using USPP calculations *(in collaboration with experimentalists at AFRL/WPAFB)*.

Milestones:

6 month:

- o Complete USPP results on common native defects in GaP and GaAs.

- o Ability to calculate isotropic hyperfine parameters for point defects in semiconductors.

- o Results on stability of N_O-Zn_i complexes in ZnO and preliminary results on their electronic properties.

12 month:

- o USPP results on important defect complexes in GaP and GaAs.

- o Complete results on isotropic hyperfine parameters for common native defects in GaP and GaAs.

- o Results on stability of Frenkel pairs in GaN and/or ZnO and preliminary results on their electronic properties.

Method and Theory

Computational method

We performed our studies using a first-principles calculation approach, based on density-functional theory and *ab initio* ultrasoft pseudopotentials (USPP). We used the codes called Vienna Ab-initio Simulation Package (VASP) [R1]. For calculations of hyperfine parameters, the electron density near atomic cores is needed. In such cases, we use all electrons (AE) calculations based on Augmented Plane Wave method as implemented in the WIEN2k codes [R2]. Since AE calculations are quite demanding in terms of computational resources, we limited the use of WIEN2k calculations to only the final stage after the extensive atomic relaxation steps are performed using the less demanding yet accurate USPP codes (VASP). The detail of the parameters and approximations used in the calculations is slightly varied, depending on specific material. Further specific computational detail for each system under study can be found in each attached publications.

A brief description of the defect theory

Calculations for defects in semiconductor are calculated using a supercell containing 32 to 96 atoms and a set of non-Γ k-points sampling.

In supercell calculations, the formation energy of a defect X in charge state q is defined as

$$E_f[X^q] = E_{tot,SC}(X^q) - E_{tot,SC}(bulk) + n_\alpha \mu_\alpha + qE_F, \qquad [1]$$

where $E_{tot,SC}(X^q)$ is the total energy of a supercell containing the defect, $E_{tot,SC}(bulk)$ is the total energy of the same supercell but without any defect. n_α is the number of the atoms of specie α being removed from (positive value) or added to (negative value) a bulk supercell to form defect X. μ_α is the reservoir energy of specie α (the chemical potential). E_F is the Fermi level, referenced to the valence-band maximum of bulk (no defect), E_v.

The chemical potentials in Eq. [1] depend on the growth conditions. For example, (in the case of defects in ZnO) under Zn-rich case, μ_{Zn} = formation energy of solid metal Zn. In order for ZnO to be stable during the growth, we also require that $\mu_{Zn} + \mu_O = \mu_{ZnO}$

= constant Φ. This fixes $\mu_O = \Phi - \mu_{Zn}$.   The chemical potential of other elements are referenced to their natural phase. For example the chemical potential of N, μ_N is referenced to the N_2 gas precipitation limit, i.e. $\mu_N = E_{tot}(N_2)/2$.


Research Activities on ZnO

ZnO is a wide-band-gap semiconductor (3.4 eV). Most of its current applications, including varistors, phosphors, piezoelectric transducers, and transparent conduction films, do not directly benefit from its wide-band-gap properties. Large-area high quality bulk ZnO crystal could be produced by various growing methods. This combining with the recently reported *p*-type ZnO (as-grown ZnO is *n*-type), opens up the possibility of producing blue- and UV-range opto-electronics devices. Currently Nitrogen is one of the most promising p-type dopants in ZnO with limited success. To aid in understanding (*p*-type) doping difficulty, we have investigated several donor defects and defect complexes based on first principles calculations. We are particularly interested in the process that deactivated N acceptors, i.e. in the substitution N_O form.   To accomplish this investigation, we have calculated a wide range of possible defects and defect complexes involving N_O and native defects or predominant impurities that could be the end results of the deactivation process. Up to this point, we found three types of N_O complexes that are likely to form 1) Zn_I-N_O complex, 2) N_O-H complexes, and 3) Substitutional dimer molecules (SDM) such as $(N_2)_O$ and $(NC)_O$. Appropriate signature of each complex is calculated and compared with experimental measurements. Since H has been identified as an exclusive donor that could impede p-doping of ZnO, we studied isolated H in ZnO as well. Based on first principles calculations, we found that under applied pressure, local vibrational mode of H at different sites in ZnO, namely antibonding (AB) and bond-center (BC) sites, shifts differently. We, therefore, proposed that IR experiment under high pressure could be very beneficial in identifying the location of H in ZnO.

Zn_I-N_O complex

Zn interstitial (Zn_I) has been predicted to have high formation energy in *n*-type growth conditions [R3]. However, with its (2+)-charge state, the formation energy goes down twice as fast as the Fermi level moves down. While Zn_I might not be the

predominant cause of *n*-type in undoped cases, it could exist in a substantial amount in N-doped cases where the Fermi energy is shifted down from the CBM considerably. In addition, to place N on the oxygen site, an O-poor (or Zn-rich) growth condition is generally used. This also promotes Zn_I formation. During a cool down process, Zn_I can passivate N_O acceptor, forming Zn_I-N_O complex which is a single donor. To investigate the complex as well as finding a binding energy, we separately studied N_O, Zn_I and the Zn_I-N_O complexes.
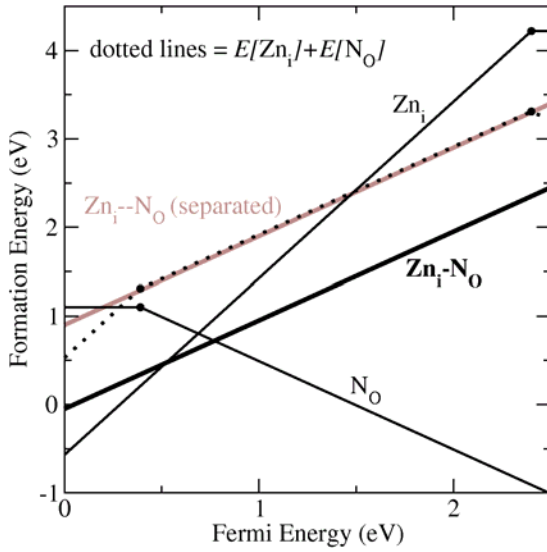
Fig 1. Calculated defect formation energy as a function of the Fermi level for N_O, Zn_I, and the Zn_I-N_O complex under the Zn-rich and N_2 precipitation limits. The Fermi level is references to the top of the VBM. The dotted lines show the sum of the formation energy of isolated Zn_I and isolated N_O. The calculations show that Zn_I binds with N_O to form the Zn_I-N_O with the binding energy of 0.9 eV (the energy difference between the thick black line and the thick brown line).

Isolated substitutional N_O has four Zn nearest neighbors. The N atom stays almost exactly on the T_d site with a small contraction of Zn-N bond comparing an an average Zn-O bond, i.e. contracted by 3.6 % and 2.6 % for the neutral and (1-)-charge state, respectively. The formation energy of N_O under Zn-rich condition and N_2 precipitation limit is shown in Fig.1.

Zn interstitial prefers a site near an ideal octahedral site (in the middle of a hexagonal channel). However, a strong repulsion between the interstitial atom and lattice cations (Zn) causes the Zn_I atom to shift vertically to be roughly in the middle between two [0001] Zn planes. The relaxation occurs such that neighboring anion lattice atoms (O) are attracted to the interstitial (due to Coulomb attraction) and are drawn inward whereas cation lattice atoms (Zn) are repelled by the interstitial and are pushed outward. Zn_I is stable in (2+)-charge state under *p*-type conditions. Our calculations indicate that the transition from 2+/0 could occur at E_F = 2.3 eV [$\varepsilon(2+/0)$ = 2.3 eV]. Since LDA

underestimates ZnO bulk band gap by a rather large amount, with band gap corrections the $\varepsilon(2+/0)$ level would lie very well above the CBM, implying that Zn_I is a shallow donor in agreement with previous calculations [R4] [R5].

Zn_I and N_O can form a donor-acceptor pair and become a single donor complex. The complex is most stable in a (1+)-charge state and has a *calculated* donor level $\varepsilon(+/0)$ = 2.7 eV above the VBM. Since this donor level is higher than the calculated $\varepsilon(2+/0)$ level of isolated Zn_I, which has been concluded to be shallow [R4][R5], the complex can therefore be argued to be a shallow donor as well. The binding energy of the complex is ~ 0.9 eV, which can be seen in Fig.1. Our calculated formation energies of N_O (solid line), Zn_I (solid line) and N_O-Zn_I complex (thick solid line) as a function of E_F are illustrated. The sum of the formation energies of N_O and Zn_I is plot with a dotted line. The binding energy is simply a total energy lowered when the complex is formed (the difference between the dotted line and the solid line).

A brief explanation of Zn_I-N_O complex study is published in conjunction with the photoluminescence results by Dr. Look in Phys. Rev. Lett. [P4]. The full detail of the theoretical part is under preparation for publication (tentatively for Phys. Rev. B).

N_O-H complex
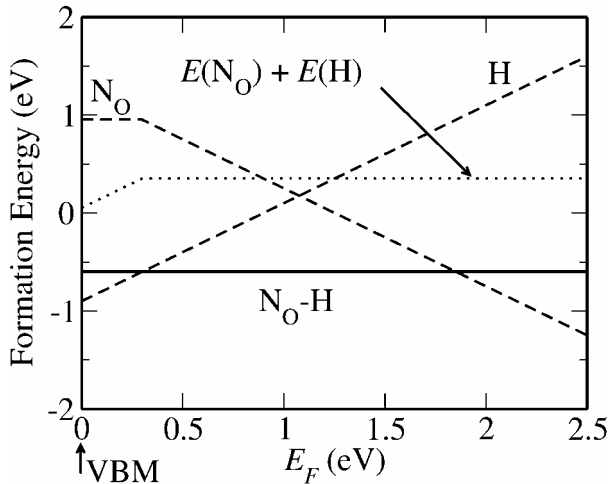
Fig 2. Formation energy of an interstitial H, N_O (dashed lines) and a N_O-H complex (solid line) in ZnO as a function of electron Fermi energy. The dotted line shows the sum of the formation energies of an isolated interstitial hydrogen and an isolated N_O. The Zn-rich condition, N_2 and H_2 phase precipitation limits were assumed. The energy difference between the dotted line and the solid line is the binding energy of the N_O-H complex.

Hydrogen, which is present in various growth techniques, could easily be incorporated in the ZnO film during growth. Hydrogen is known to be amphoteric in most semiconductors, but is identified as an exclusive donor in ZnO and can passivate

acceptors such as N_O [R7][R8]. Hydrogen and nitrogen can interact strongly to form a neutral defect complex, thereby reducing the maximum achievable hole concentration. Based on first principles calculations, we calculated the formation energies of an isolated interstitial H, a nitrogen acceptor N_O, and a N_O-H complex in ZnO. An isolated interstitial H is exclusively a donor in ZnO and always exists in the form of H^+. For an isolated H^+ location, there are four low-energy sites surrounding an O atom with the so-called $BC_\parallel$ site being the site with the lowest energy [R9][R10]. An isolated N_O is an acceptor. Currently the exact location of the ionization energy of N_O is still under debate [R11]. Over almost the entire Fermi energy range, the isolated N_O is stable in a (1-)-charge state whereas an isolated interstitial H atom is always stable in a (1+)-charge state. The two defects, therefore, have a Coulomb attraction and have a strong tendency to form a N_O-H defect complex. The formation energy of H^+ (at $BC_\parallel$ site) and N_O are plotted (dashed lines) as a function of Fermi level in Fig. 2 with the sum of the two formation energies shown as a dotted line. In the same figure, we plotted the formation energy of the N_O-H complex (thick solid line). The binding energy of the N_O-H complex is 0.95 eV, which is the difference in energy between the dotted and solid line. For the N_O-H defect complex, the $AB_{N\perp}$ configuration has the lowest formation energy. To compare with experiment, we calculated the infrared absorption signature of this complex and obtained the characteristic N-H stretch frequency of 3070 cm^{-1}. This is in a reasonable agreement with recently observed peak from an MOCVD sample at 3020 cm^{-1} [R11].

More detail of this work can be found in the attached manuscript (published in Physica B) [P5].

Substitutional dimer molecules (SDM) such as $(N_2)_O$ and $(NC)_O$

Based on total energy calculations, we found that carbon impurities and excess N strongly prefer to passivate N_O and form low-energy SDM on the Oxygen site, $(NC)_O$ or $(N_2)_O$, both of which are donors with several-eV binding energies. These SDMs have electronic and structural properties similar to free diatomic molecules (Lee *et al.* has previously illustrated for the case of $(N_2)_O$ [R12]).
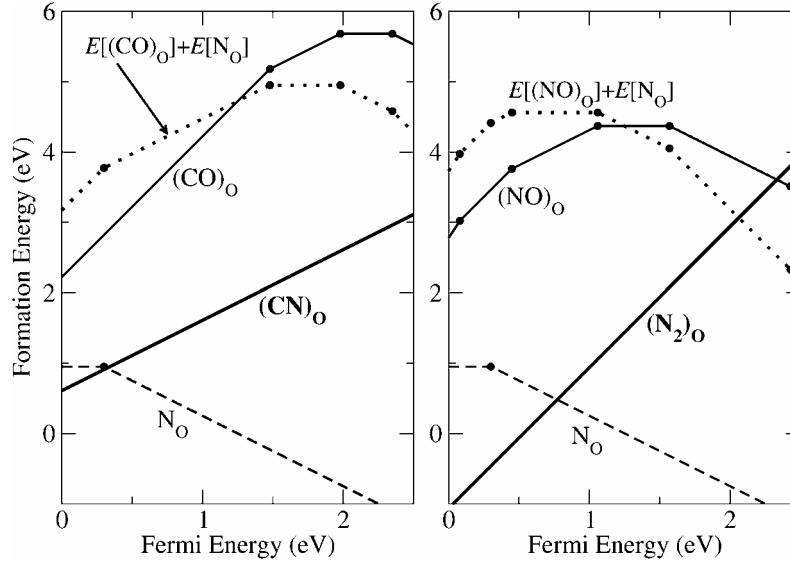
Isolated interstitials N_i and C_i have very high formation energies, they tend to immediately bind with the closest lattice O, forming $(NO)_O$ and $(CO)_O$. Figure 3 shows the formation energies as a function of Fermi energy for $(CO)_O$, $(NC)_O$, $(NO)_O$, and $(N_2)_O$. However, in the presence of N_O, $(NO)_O$ and $(CO)_O$ are unstable against the formation of $(N_2)_O$ and $(NC)_O$. Typical binding energies are several eV due in part to Coulomb attraction between oppositely charged impurities and in part to the combination of two impurities into one. In the right panel of Fig. 3, the formation energy of N_O and $(NO)_O$ are shown as a dashed line and a thin solid line with the sum of the two as a dotted line. The sum is to be compared with the thick solid line, which is the formation energy of $(N_2)_O$ defect. We can immediately see that the binding energy, which is the difference between the dotted line and the thick solid line, depends somewhat on the Fermi energy, but has a typical value of several eV. The binding energy is of similar magnitude for the case of $(NC)_O$, as shown in the left panel. The formation of SDMs are enhanced in the case of p-type ZnO, for which the binding energies are large enough to lower the energy of both $(N_2)_O$ and $(NC)_O$ below the isolated N_O. It is therefore expected that the formation of $(N_2)_O$ and $(NC)_O$ will compete with the formation of N_O acceptors. Since these SDMs are donors in p-type samples, their formation further hinders p-type doping by compensating the already lowered N_O acceptors.

Calculated frequencies for $(N_2)_O{}^{2+}$ and $(NC)_O{}^+$, which are the most stable charge states in p-type ZnO, are 2108 and 1995 cm^{-1}, respectively. These frequencies fall within 200 cm^{-1} of the experimentally observed values [R13]. In addition, recent XPS experiments have found strong signals of N-N and C-N bonds with similar characteristics to those of free diatomic molecules [R14].

These results suggest that one should be careful with a C impurity that can turn an existing N acceptor (N_O) into an $(NC)_O$ SDM, which is a donor. In addition, excessive N incorporation could lead to an unwanted $(N_2)_O$ SDM, which is a double donor, instead of the desired N_O acceptor.

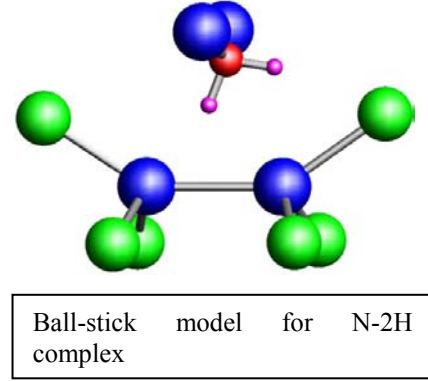More detail of this work can be found in an attached manuscripts [P1][P5].

Research Activities on III-V

III-V semiconductors are used extensively in electronic and optoelectronic devices, ranging from GaAs (1.42 eV) to wide band gap semiconductor GaN (3.4 eV). Recently, there are substantial interests on diluted-nitride alloys, for instant GaAs$_{1-x}$N$_x$, based on their interesting characteristics. Due to the large size mismatched between N and As (or P), a small percents of N can drastically change the electronic and optical properties of the host GaAs or GaP samples. For example, the small amount of N can dramatically reduce the band gap of GaAs. During the course of the program, we have three main themes of research related to III-V semiconductors. a) H is known to neutralize the effects of N in diluted-nitride alloys back to normal bulk properties. This includes the recoveries of band gap, electron effective mass, and lattice constant. We have investigated several possible N-H complex configurations that are likely to form in GaAs. Based on comparison with experiments, N-2H complex emerges as the top candidate that can explain how H neutralize the effects of N. b) Native defects in traditional semiconductors, GaP and GaAs, are not well theoretically studied. We have systematically calculated simple native defects in GaP that should provide an important foundation for further study of defects in these III-V materials. c) Recent optically detected magnetic resonance (ODMR) measurements found ODMR lines that correspond to Ga$_i$ but has much weaker Fermi contact values. We believed that the observed FC

came from a Ga_i which is a part of a defect complex. To aid in this identification, we have explored some of the complexes that could explain the observed smaller FC values.


N-2H complex in GaAsN

Large size-mismatched dilute alloys such as GaAsN and GaPN are promising alloy semiconductors with unique physical properties. For example, with only an atomic percent of N incorporated into GaAs, the band gap decreases by several hundred meV [R15]. On the other hand, H irradiation causes a nearly full recovery of the GaAs band gap and lattice parameter from those of

Ball-stick model for N-2H complex

GaAsN [R16]. The formed H complexes after H irradiation should be charge neutral due to their large concentration ($>10^{20}$ cm^{-3}). While there are existing complex models, such as $\alpha - H_2^*(N)$ complex that can explain the experimental observations, a recent infrared experiment [R17] on H-irradiated samples did not observe any Ga–H modes, hence, contradicting the $\alpha - H_2^*(N)$ model. Based on first-principles calculations, we show that the hydrogen configurations in GaAsN are actually depended on how hydrogen is introduced into the sample. Since proton and neutral H have different ground states, the proton injected into the sample by H-irradiation follows a unique energy pathway to form a charged dihydride, instead of the charge-neutral H_2^* monohydride. The subsequent charge neutralization causes the spontaneous canting of the dihydrides. The resulting canted N–2H structure explains the recent puzzling IR observation, the recoveries of the GaAs band gap and lattice parameter, and the dihydride symmetry determined by the XANES experiment.

More detail of this work can be found in the attached manuscript (published in Physica B) [P6].

Native Defects in GaP

We have investigated fundamental native defects in GaP, including Ga_i, P_i, V_{Ga}, V_P, Ga_P, and P_{Ga} using supercell approach with 32-atom supercell size. The formation energies of defects are referenced to an fcc-Ga (μ_{fcc-Ga} = -2.90 eV/atom) and a P_2-dimer ($\mu_{P2-dimer}$ = -4.52 eV/atom) phases. Our calculated GaP heat of formation is μ_{GaP} = -9.18 eV/pair.
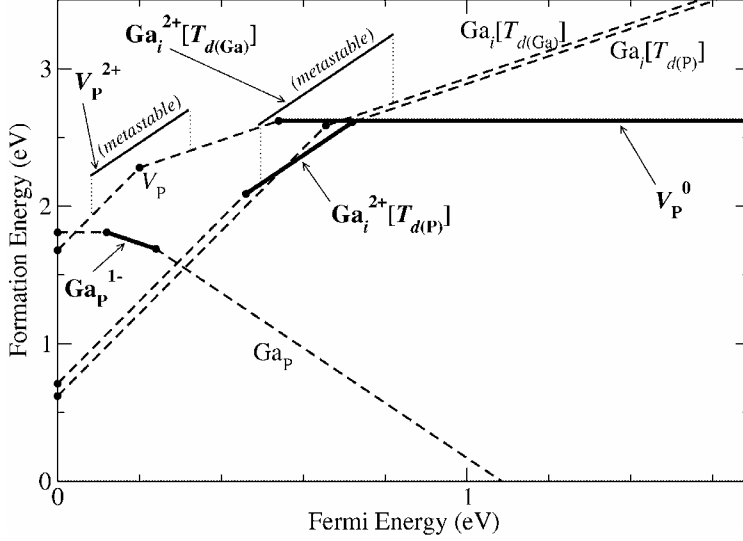
Fig 4. Formation energies of native defects in GaP under Ga-rich conditions. Solid lines indicate EPR active states (the defect state is half occupied). Under Ga-rich condition, Ga_i has the lowest energy in p-type samples whereas Ga_P has the lowest energy in n-type samples.
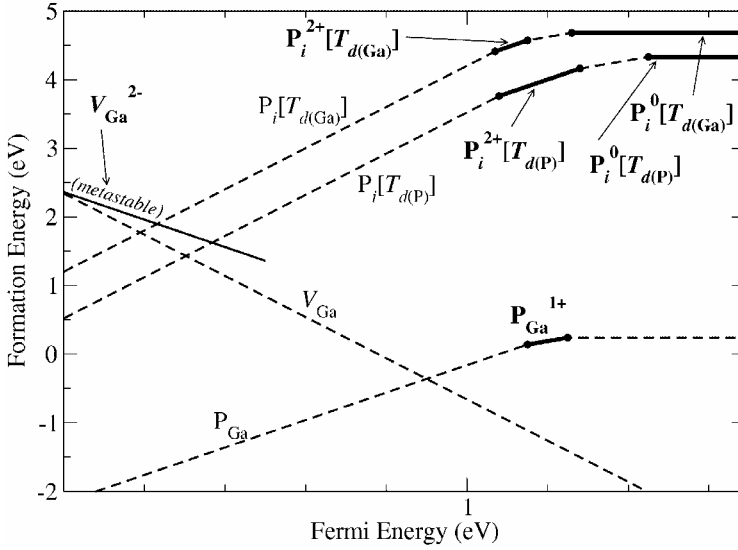
Fig 5. Formation energies of native defects in GaP under P-rich conditions. Solid lines indicate EPR active states (the defect state is half occupied). Under P-rich condition, P_{Ga} has the lowest energy in p-type samples whereas V_{Ga} has the lowest energy in n-type samples.

Under *Ga-rich condition*, the calculated formation energies of native defects are shown in Fig.4. As a result of high Ga partial pressure, Ga_i, Ga_P, and V_P become low-energy defects. Under p-type condition (where Fermi energy, E_F, is near the VBM), Ga_i in the (3+)-charge state (triple donor) has the lowest formation energy. This means it would serve as the leading native donor as one tries to dope GaP p-type. Ga interstitial

prefers to stay in a tetrahedral site T_d (also called a cage site) in GaP. In the zincblende structure, there are two types of T_d sites, one is surrounded by four Ga ($T_{d,\text{Ga}}$) and the other is surrounded by four P ($T_{d,\text{P}}$). Ga_i at both sites have similar formation energy. However, only the Ga_i at $T_{d,\text{P}}$ has a stable (2+)-charge state which is EPR active. As the Fermi energy goes up, the Ga antisite, Ga_P, which is an acceptor has the lowest formation energy among the the native defects. With its (2-)-charge state, it will counteract the attempt to dope GaP n-type. Note that, our reference for phosphorus chemical potential is somewhat too high (we used P_2 instead of black phosphorus), the actual position of Ga_P should be around 1 eV higher in relative to other defects in the plot.

Under *P-rich condition*, calculated formation energies of native defects are shown in Fig.5. As a result of low Ga partial pressure and high P partial pressure, P_{Ga}, V_{Ga}, and P_i become low-energy defects. Under *p*-type conditions, P_{Ga} in the (2+)-charge state (double donor) has the lowest formation energy. This means it would serve as the leading native donor as one tries to dope GaP *p*-type. At higher Fermi energy, the Ga vacancy (V_{Ga}), which is an acceptor, has the lowest formation energy. With its (3-)-charge state, it will counteract the attempt to dope GaP *n*-type. P_i has rather high formation energy and is unlikely to exist in a noticeable concentration under usual growth conditions.

To aid in identification of these native defects, we plan to perform calculations of hyperfine parameters for each important defect explained above. At this point, we have finished calculating isotropic hyperfine parameters (Fermi contact, FC) of three out of four important native defects in GaP, i.e. P_{Ga}, Ga_P, and Ga_i.

Table I. Isotropic hyperfine parameters of selected native defects in GaP.

Defect	Central			Nearest Neighbor		
	Atom (# atoms)	ρ spin/Å^3	$A \times 10^{-4}$ cm^{-1}	Atom (# atoms)	ρ spin/Å^3	$A \times 10^{-4}$ cm^{-1}
P_{Ga}^+	P(1)	9.71	984	P(4)	0.51	53
Ga_P^-	Ga(1)	0.09	5	Ga(4)	1.44	76
$Ga_i^{2+}[T_{d,Ga}]$	$Ga_i(1)$	35.40	1876	Ga(4)	1.55	82
$Ga_i^{2+}[T_{d,P}]$	$Ga_i(1)$	30.18	1599	P(4)	0.39	35

Phosphorus antisite (P_{Ga}) can exist in three charge states, 2+, 1+, and neutral depending on the Fermi level as shown in Fig.5. Out of the three charge states, only the (1+)-charge state has an unpaired electron. Our calculated FC for P_{Ga}^+ at the central P atom and at the four neighboring P atoms are 984 x 10^{-4} and 53 x 10^{-4} cm^{-1}, respectively. These are in good agreement with earlier measurement by Kaufmann *et al.* who reported the corresponding values of (966 $\pm$ 13)x10^{-4} and (81.5 $\pm$ 4) x10^{-4} cm^{-1}, respectively [R18].

Gallium antisite (Ga$_P$) can be stable in three charge states: neutral, 1-, and 2- as shown in Fig.4. Only (1-)-charge state has an unpaired electron. We found that the unpaired electron is not localized on the central Ga atom but is distributed out to four nearest neighbors (Ga) atoms. The spin density at the nucleus of the central Ga atom is only 0.09 spin/Å^3. This is very small in comparison to the spin density of 1.44 spin/Å^3 at the nuclei of the nearest neighbor Ga atoms. These spin densities lead to FC values of 5x10^{-4} and 76 x 10^{-4} cm^{-1} for the interaction at the central Ga atom and at the four nearest neighbor Ga atoms, respective.

Gallium interstitial (Ga$_i$) prefers to stay at a tetrahedral site. While the formation energies are similar for Ga$_i$ at both $T_{d,Ga}$ and $T_{d,P}$ sites, only the later has a stable (2+)-charge state (which has an unpaired electron). The (2+)-charge state for Ga$_i$ at $T_{d,Ga}$ is metastable. We calculated the FC of Ga$_i$ at both sites and found that an unpaired electron

is strongly localized[*] at the central interstitial Ga atom with charge densities of 35.40 and 30.18 spin/Å^3 for an interstitial at $T_{d,\text{Ga}}$ and $T_{d,\text{P}}$, respectively. These correspond to large FC values of $1876\text{x}10^{-4}$ and $1599\text{x}10^{-4}$ cm^{-1}. Recent optically detected magnetic resonance (ODMR) measurements on AlGaPN by our collaborators (the group of Prof. Weimin Chen *et al.*, Linköping University, Sweden), found two sets of pattern of ODMR lines that are proved to come from Ga interstitial and labeled them Ga_i-A and Ga_i-B. However, the measured FC values of both Ga_i defects are much smaller than the calculated values of isolated Ga_i, i.e. $770\text{x}10^{-4}$ cm^{-1} for Ga_i-A and $1150 \text{ x } 10^{-4}$ cm^{-1} for Ga_i-B. We believed that the observed FC came from a Ga_i which is a part of a defect complex, not an isolated Ga_i. This model is supported by recent observations (both theory and experiment) that Ga_i in GaN has a low diffusion barrier and should diffuse at around room temperature. Since GaP is less dense than GaN, all existing Ga_i should able to diffuse easily and form defect complex with other defects. We, therefore, should not detect any isolated Ga_i. To aid in this identification, we have explored some of the complexes that could explain the observed smaller FC values.

Some Defect Complexes in GaP

Our first assumption was that an Al-atom replacing lattice Ga (Al_{Ga}) near a Ga_i might strongly reduce the FC value of an isolated Ga_i. For this, we have investigated a Ga_i at the $T_{d,\text{Ga}}$ site (labeled as $\text{Ga}_i^{2+}[T_{d,\text{Ga}}]$). And replace one nearest neighbor Ga atom with an Al atom, leading to a *Ga_i-Al_{Ga} complex*. Since Al and Ga are isovalent, the charge state of this complex that results in an unpaired electron is the same as the charge state of an isolated Ga_i, i.e., the 2+ charge state. For a quick test, we use the fully relaxed atomic structure of an isolated $\text{Ga}_i^{2+}[T_{d,\text{Ga}}]$ defect and just replace one nearest neighbor Ga atom with an Al atom. To justify this assumption, the structural relaxation test were performed using a pseudopotential codes. We indeed found only a small atomic relaxation. The FC results show that replacing a Ga nearest neighbor by an Al atom leads to a very small reduction in the central FC (see Table II). The FC value of this complex

---

[*] The unpaired electron's density is 42-49% of our calculated atomic-Ga 4s electron. ($\left|\psi_{4s}(0)\right|^2 = 72.7 \text{ e}^-/\text{Å}^3$)

is still way too large in comparison to any of the observed ones. Therefore, we concluded that Ga_i-Al_{Ga} defect complex could not explain the measured FC.

Next, we aimed our attentions toward *Ga_i-Ga_P complex* since Ga_i and Ga_P are both have low formation energies under Ga-rich condition. Ga_i should serve as the leading donor and Ga_P as the leading acceptor if there are no other lower-energy impurities (see Fig. 4). As the sample is cool down, both complex are attracted to each other and can combine to form Ga_i-Ga_P complex which is a donor-acceptor pair.
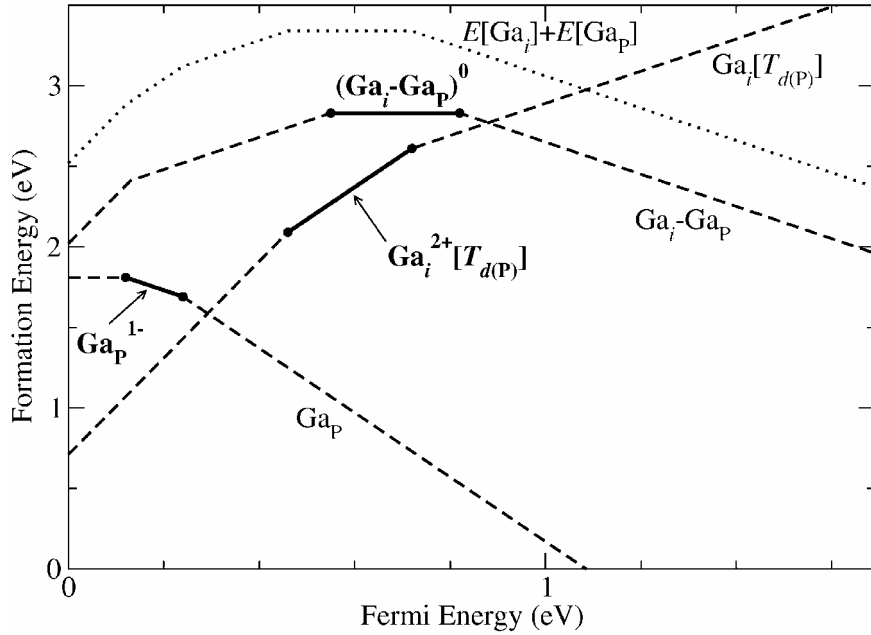
Fig 6. The formation of Ga_i-Ga_P complex. The charge states with an unpaired electron are plotted with thick solid lines with boldface labeling including the charge state numbers. The dotted lines show the summation of the formation energy of the isolated defects forming the complex.

To minimize the donor-acceptor pair distance, the Ga_i binds to the Ga_P on the T_d site with (originally before the Ga atom substitute on the P site) 4 P atoms. Since a P atom is substituted by a Ga atom, the Ga_i is left with three P and a Ga nearest neighbor atoms. Substituting a neighboring group V atom with a group III atom results in a loss of two electrons. Therefore, the charge state of the defect, that has an unpaired electron, changes from 2+ in an isolated Ga_i case to neutral in this $Ga_i - Ga_P$ complex. From an energetic viewpoint, we find that the complex is "bound" with a binding energy of about

0.5 eV (the energy different between the dotted line and the energy of $Ga_i - Ga_P$ complex in Fig. 6). The formation energy of each constituent defect and the complex is plotted as a function of the electron Fermi level in Fig. 6. Calculated FC values of $(Ga_i - Ga_P)^0$ complex are tabulated in Table II. The FC value at the central Ga_i atom is 1123×10^{-4} cm^{-1} matched well with an observed Ga_i-B of 1150×10^{-4} cm^{-1}. Although, N is not directly involve in this complex formation, the growth conditions needed to incorporate N on the P sites should lead to a P-poor condition (or another words Ga-rich condition) that also promotes the formation of both constituents, i.e. Ga_i and Ga_P, of the complexes.

Table II. Isotropic hyperfine parameters of Ga_i and selected Ga_i-complexes in GaP.

| Defect	Central			Nearest neighbor			Nearest Neighbor		
	atom	ρ spin/$\mathring{A}^3$	$Ax10^{-4}$ cm^{-1}	atom	ρ spin/$\mathring{A}^3$	$Ax10^{-4}$ cm^{-1}	Atom	ρ spin/$\mathring{A}^3$	$Ax10^{-4}$ cm^{-1}
$Ga_i^{2+}[T_{d,Ga}]$	$Ga_i(1)$	35.40	1876				Ga(4)	1.55	82
$(Ga_i - Al_{Ga})^{2+}$ (unrelaxed)	$Ga_i(1)$	34.07	1805	$Al_{Ga}(1)$	0.36	21	Ga(3)	1.58	84
$Ga_i^{2+}[T_{d,P}]$	$Ga_i(1)$	30.18	1599				P(4)	0.39	35
$(Ga_i - N_P)^{2+}$	$Ga_i(1)$	26.30	1393	$N_P(1)$	0.95	15	P(3)	0.52	47
$(Ga_i - C_P)^{+}$	$Ga_i(1)$	25.95	1375	$C_P(1)$	0.26	15	P(3)	0.53	48
$(Ga_i - Ga_P)^{0}$	$Ga_i(1)$	21.20	1123	$Ga_P(1)$	0.02	1	P(3)	0.29	25
$(Ga_i - Al_P)^{0}$	$Ga_i(1)$	20.76	1101	$Al_P(1)$	0.08	5	P(3)	0.30	27
$(Ga_i - 2Ga_P)^{2-}$	$Ga_i(1)$	17.72	939	$Ga_P(2)$	0.37	19	P(2)	0.26	18
$(Ga_i - 3Ga_P)^{4-}$	$Ga_i(1)$	18.77	995	$Ga_P(3)$	0.31	16	P(1)	0.08	7

To study the cation effects on the FC of $Ga_i - Ga_P$ complex, we replace a Ga antisite (Ga_P) with an Al antisite, creating *Ga_i-Al_P complex*. (Full atomic relaxation has been carried out here.) We found that the effect of replacing the Ga_P by Al_P is small, i.e.,

resulting in a reduction of the central FC by only 22 x 10^{-4} cm^{-1} (see, Table II). This could qualitatively explain the modest variation of the FC (Ga$_i$-B) with Al composition.

Since C impurity is abundant in many growth methods, it might form complexes with Ga$_i$. We, therefore, have investigated *Ga$_i$-C$_P$ complex*. Since here we replace a P atom (group V) with a C atom (group IV), therefore only one electron is missing. In order for the complex to have an unpaired electron occupied Ga$_i$ 4s, we need (1+)-charge state. This complex can also be considered as a of donor-acceptor pair since C$_P$ is a deep acceptor in GaP. We have investigated the formation energy and found that the complex is bound with the binding energy of about 1 eV. The formation energy of each constituent defect and the complex is plotted as a function of the electron Fermi level in Fig 7. We calculated the FC parameters of this complex and tabulated the values in Table II. We found the reduction in the central FC of only 224x10^{-4} cm^{-1} from an isolated Ga$_i$ atom, leading to the FC value of 1375x10^{-4} cm^{-1}. This does not fit well with any observed values. Nevertheless, this result gives a very valuable trend for further study.

We can see that if one starts from an isolated Ga$_i$ on the T_d site surround by 4 P, one can reduce the FC by replacing the neighboring P by other atom, preferably from a different column. Replacing a nearest neighbor P by a group IV (C) atom leads to a reduction in the central FC of ~220x10^{-4} cm^{-1}. Replace a nearest neighbor P by a group III (either Ga or Al) atom leads to reduction in the central FC of ~ 476 x 10^{-4} cm^{-1}, i.e. one gains ~220x10^{-4} cm^{-1} reduction for each column in the periodic table one moves away. If we assume that this trend keeps carry on, then a $(\mathrm{Ga}_i - V_\mathrm{P})^{3-}$ complex should have a central FC of around 700 x 10^{-4} cm^{-1}, hence, in agreement with Ga$_i$-A measurement. However, our calculations show that the *Ga$_i$-V$_P$ complex* is not stable. The Ga$_i$ spontaneously moves to replace the vacancy and form a low-energy Ga$_P$ defect.
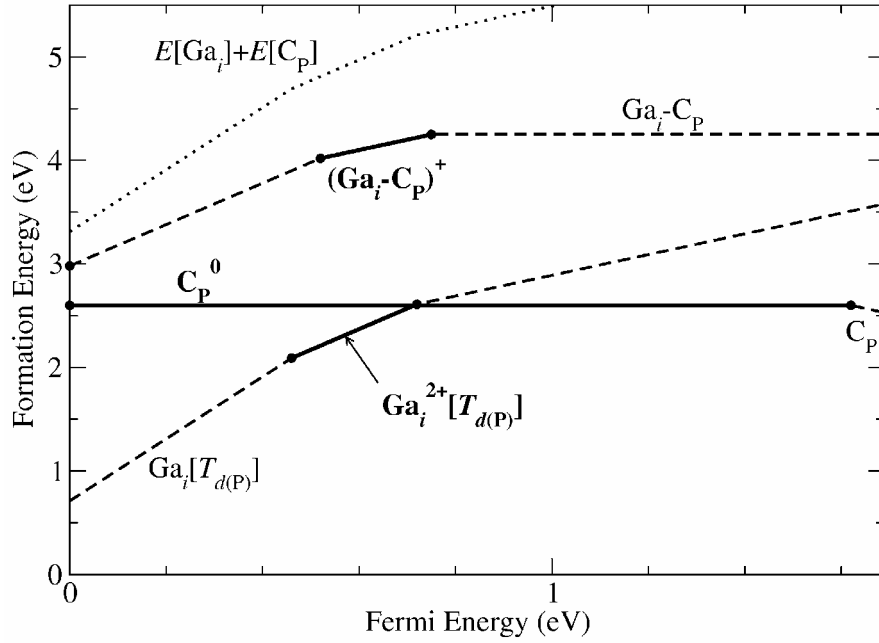
Fig 7. The formation of Ga_i-C_P complex. The charge states with an unpaired electron are plotted with thick solid lines with boldface labeling including the charge state numbers. The dotted lines show the summation of the formation energy of the isolated defects forming the complex. The chemical potential of a C atom is referenced to the diamond phase.

We found that the $Ga_i - Ga_P$ can attract another Ga_P and form a larger *Ga_i-2Ga_P complex*. This complex has a Ga_i in the T_d site originally surrounded by 4 P but has two P atoms replaced by Ga atoms. Substituting two of the group V (P) by group III (Ga) atoms results in a total loss of 4 electrons. Therefore, the charge state of the defect (that leads to an unpaired electron in the Ga_i $4s$ state) changes from 2+ in an isolated Ga_i case to 2− in this $Ga_i - 2Ga_P$ complex. From the energetic viewpoint, we find that an additional Ga_P is "bound" to the $Ga_i - Ga_P$ complex to form $Ga_i - 2Ga_P$ with a binding energy of about 0.5 eV. The formation energy of each constituent defect and the complex is plotted as a function of the electron Fermi level in Fig. 8.
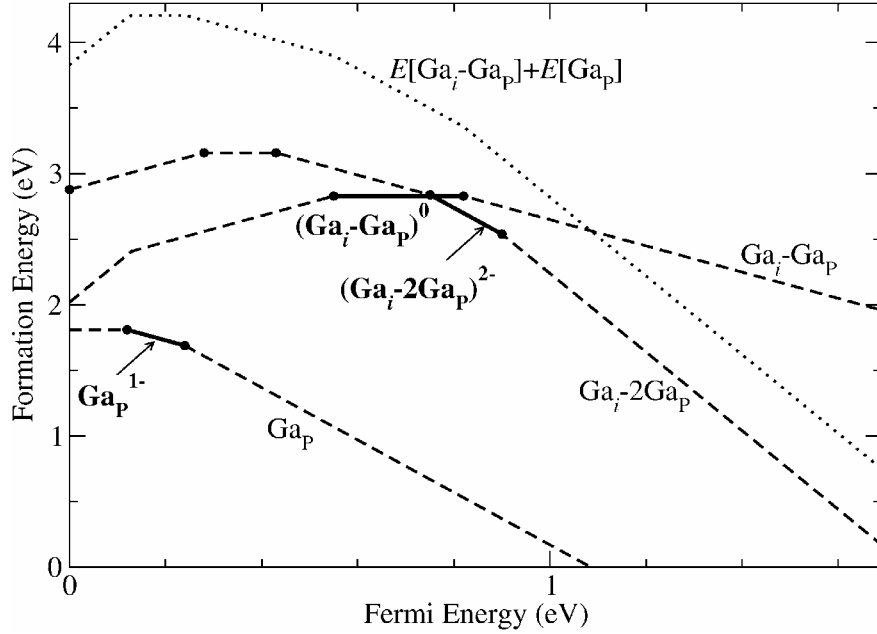
<u>Fig 8</u>. The formation of Ga_i-$2Ga_P$ complex. The charge states with an unpaired electron are plotted with thick solid lines with boldface labeling including the charge state numbers. The dotted lines show the summation of the formation energy of the isolated defects forming the complex.

The calculated FC values of $(Ga_i - 2Ga_P)^{2-}$ complex are tabulated in Table II. The FC value of the central Ga_i atom is 939 x 10^{-4} cm^{-1}, which is reasonably close to the observed Ga_i-A of 770 x 10^{-4} cm^{-1}.

Since the $Ga_i - 2Ga_P$ complex does not lower the FC down enough to match well with the observed Ga_i-A. We further investigate whether if we convert one more P neighbor to be an antisite would help to further lower the FC. It turns out that a *Ga_i-$3Ga_P$ complex* in a (4−)-charge state, which is stable in our calculations and has an unpaired electron in the Ga $4s$ state, have the FC higher than the $Ga_i - 2Ga_P$ complex (see, Table II). This is not at all surprising if we assume that the FC of the complex is reduced from the isolated interstitial because of the result of symmetry breaking. In this view, the $Ga_i - 3Ga_P$ complex has similar symmetry as the $Ga_i - Ga_P$ with the interstitial atom shifted further away from the center - that is why a FC for a $Ga_i - 3Ga_P$ complex is slightly lower than a $Ga_i - Ga_P$ but higher than a $Ga_i - 2Ga_P$ where the symmetry is strongly broken.
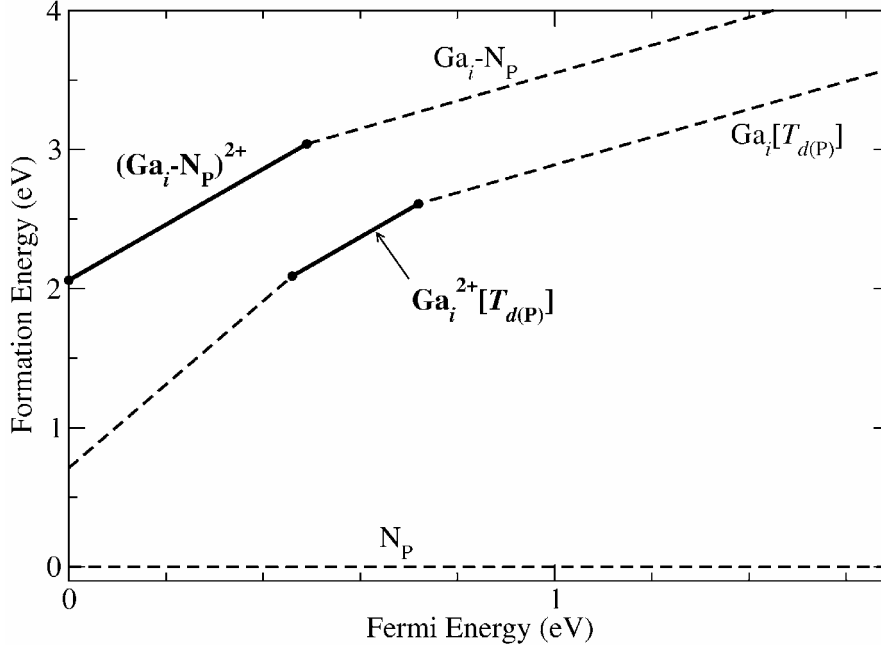
Fig 9. The formation of Ga$_i$-N$_P$ complex. The charge states with an unpaired electron are plotted with thick solid lines with boldface labeling including the charge state numbers. The chemical potential of the N atom is set such that N$_P$ has zero formation energy.

Our experimental collaborators noticed that Ga$_i$-B signal depends rather strongly with a N concentration. We studied effects of replacing an isovalent atom by starting with Ga$_i^{2+}[T_{d,P}]$ defect and replace a nearest neighbor P atom with a N atom. At least, we found that replacing an anion isovalent atom (i.e., replace a P atom with a N atom) has a larger effect on the central FC than replacing a cation isovalent atom (Ga by Al). This is probably due, at least in part, to a large structural relaxation introduced by N atom. FC values are tabulated in Table II.

However, from the energetic point of view, we found the Ga$_i$ do not bind with the N$_P$. The plot of each defect as well as the complex's formation energy as a function of electron Fermi energy is shown in Fig. 9. Here we set the chemical potential of N atom such that the formation energy of N$_P$ is zero. (The binding energy is an absolute quantity which does not depend on the chemical potential of N.) The total formation energy of individual defects is, therefore, just the formation energy of Ga$_i$. It is clear that the complex has higher formation energy by almost 1 eV and should not form.

In conclusion (regarding the Ga_i FC), our calculated FC for an isolated Ga_i^{2+} in GaP is too large to be consistent with the measured values. Our experiment collaborators (Linköpin Univ., Sweden) observed two signatures via ODMR measurements and labeled them, Ga_i-A (Fermi contact = 770×10^{-4} cm^{-1}) and Ga_i-B (1150×10^{-4} cm^{-1}). Our calculated values for isolated Ga interstitials are 1876×10^{-4} cm^{-1} for a Ga_i at a T_d site surrounded by four Ga atoms and 1599×10^{-4} cm^{-1} for a Ga_i at a T_d site surrounded by four P atoms. We proposed that the observed hyperfine spectrum belongs to Ga_i complexes and have investigated some of the probable ones. Indeed, we found that the value of Ga_i FC can be lowered by forming a complex. At this point, we found a $(Ga_i - Ga_P)^0$ complex (FC = 1123×10^{-4} cm^{-1}) and a $(Ga_i - 2Ga_P)^{2-}$ complex (FC = 939×10^{-4} cm^{-1}) to be the most probable models for the observed Ga_i-B and Ga_i-A, respectively. We have published our results together with our experimental collaborators in Phys. Rev. B [P3].

Future Research Activities

Defects and defect complexes in III-V

Summarize the theoretical results on native defects and some complexes in GaP for publication. Complete the study of similar defects in GaAs. In addition, we will study some defect complexes in GaAs that are of current interests, such as nitrogen-carbon dimer complex in GaAs that are recently identified by an IR experiment.

Frenkel pairs and defect complexes in ZnO

1) We will compose a detailed theoretical manuscript that describes in detail the formation of the Zn_i-N_O complex, which is believed to responsible for the observed PL signature by Dr. Look. 2) We will investigate the stability, the formation, and the recombination of Zn_i-V_{Zn} Frenkel pair via first-principle method. This study will involve the calculation of diffusion barrier of Zn_i and/or V_{Zn} in different charge states. 3) Since O_i is proposed to be an important native acceptor that neutralizes the 75-meV donors in the irradiation experiment, we will investigate the electronic properties and formations of the complexes involving O_i and substitution Al and/or Ga.

References

[R1] http://cms.mpi.univie.ac.at/vasp/

[R2] http://www.wien2k.at/

[R3] A.F. Kohan *et al.*, Phys. Rev. B **61**, 15019 (2000)

[R4] F. Oba *et al.*, J. Appl. Phys. **90**, 824 (2001).

[R5] S.B. Zhang, S.-H. Wei, and A. Zunger, Phys. Rev. B **63**, 075205 (2001).

[R6] C.H. Park, S.B. Zhang, and S.-H. Wei, Phys. Rev. B **66**, 073202 (2002).

[R7] C.G. Van de Walle, Phys. Stat. Sol (b) **229**, 221 (2002).

[R8] A.Kamata, H. Mitsuhashi, and H. Fujita, Appl. Phys. Lett. **63**, 3354, (2003).

[R9] S. Limpijumnong and S.B Zhang, Appl. Phys. Lett. **86**, 151910 (2005).

[R10] E.V. Lavrov, J. Weber, F. Börrnert, C.G. Van de Walle, R. Helbig, Phys. Rev. B **66**, 165205 (2002).

[R11] X. Li, B.M. Keyes, S.E. Asher, S.B. Zhang, S.-H. Wei, T.J. Coutts, S. Limpijumnong, and C.G. Van de Walle, Appl. Phys. Letts. **86**, 122107 (2005).

[R12] E.-C. Lee, Y.-S. Kim, Y.-G. Jin, and K.J. Chang, Phys. Rev. B **64**, 085120 (2001).

[R13] B.M. Keyes, L.M. Gedvilas, X. Li, and T.J. Coutts, J. Crystal Growth **281**, 297 (2005).

[R14] C.L. Perkins, S.-H. Lee, X. Li, S.E. Asher, and T.J. Coutts, J. Appl. Phys. **97**, 034907 (2005).

[R15] M. Weyers, M. Sato, and H. Ando, Jpn. J. Appl. Phys. **Part 1 31**, L853 (1992).

[R16] A. Polimeni, G.B.H. von Hogersthal, M. Bissiri, et al., Semicond. Sci. Technol. **17**, 797 (2002).

[R17] F. Jiang, M. Stavola, M. Capizzi, et al., Phys. Rev. B **69**, 041309R (2004).

[R18] U. Kaufmann,J. Schneider, and A. Rauber, Appl. Phys. Lett. **29**, 312 (1976).

Related Activities:

Publications (attached) highly impact journal articles are highlighted by "►"

[P1] ► "Substitutional diatomic molecules NO, NC, CO, N_2, and O_2: Their vibrational frequencies and effects on *p* doping of ZnO", <u>Sukit Limpijumnong</u>, X. Li, S.-H. Wei, and S.B. Zhang, ***Appl. Phys. Lett.*** **86**, 211910 (2005).

[P2] ► "Resolving hydrogen binding sites by pressure - A first-principles prediction for ZnO", <u>Sukit Limpijumnong</u> and S.B. Zhang, ***Appl. Phys. Lett.*** **86**, 151910 (2005).

[P3] ► "Properties of Ga-interstitial defects in $Al_xGa_{1-x}N_yP_{1-y}$", N.Q. Thinh *et al.*, ***Phys. Rev. B*** **71**, 125209 (2005).

[P4] ► "Evidence for native-defect donors in *n*-type ZnO", D. C. Look *et al.*, ***Phys. Rev. Lett.*** **95**, 225 502 (2005).

[P5] "Probing deactivations in Nitrogen doped ZnO by vibrational signatures: A first principles study", <u>Sukit Limpijumnong</u>, X. Li, S.-H. Wei, and S.B. Zhang, ***Physica B*** **376-377**, 686 (2006).

[P6] "Ion relaxation and hydrogen LVM in H-irradiated GaAsN", M.-H. Du, <u>Sukit Limpijumnong</u>, S.B. Zhang, ***Physica B*** **376-377**, 583 (2006).

[P7] "Impurity effects in ZnO and nitrogen-doped ZnO thin films fabricated by MOCVD", X. Li *et al.*, ***J. Cryst. Growth*** **287**, 94 (2006).

Presentations

[C1] <u>Sukit Limpijumnong</u> presented an INVITED TALK at the 8th Asian Workshop on First-principles Electronics Structure Calculations 2005 (AWFPESC 2005), Fudan University, Shanghai, China, entitled: *"First principles study of defects in ZnO"*.

[C2] <u>Sukit Limpijumnong</u> presented a poster at the 23rd International Conference on Defects in Semiconductors at Awaji Island, Hyogo, Japan, July 24-29, 2005, entitled: *"Probing deactivations in Nitrogen doped ZnO by vibrational signatures: A first principles study"*.

Collaborations

1. Drs. Cole Litton and David C. Look (experiment), *Wright-Patterson Air Force Base, Dayton, Ohio, USA*

2. Drs. S.B. Zhang, S-H. Wei and K. Kim (theory), *National Renewable Energy Lab., CO, USA.*

3. Drs. X. Li and T.J. Coutts (experiment), *National Renewable Energy Lab., CO, USA.*

4. Prof. Dr. Weimin Chen (experiment), *Linköpin University, Sweden*.

5. Prof. Dr. W.R.L. Lambrecht (theory), *Case Western Reserve Univ., OH, USA*.

6. Prof. Dr. C.G. Van de Walle (theory), *UC Santa Barbara, CA, USA*.

Honors/Awards

- Sukit Limpijumnong is awarded *" 2005 Thailand Young Scientist Award "* from the The Science Society of Thailand under the Patronage of His Majesty the King

- Sukit Limpijumnong is awarded *" 2005 Corbett Prize for Young Scientists "* from the 23rd International Conf. of Defects in Semiconductors (ICDS-23)

- Sukit Limpijumnong is awarded *" 2004 TWAS Prize for Young Scientists in Thailand "* from the Third Word Academy of Science (TWAS) and the National Research Council of Thailand (NRCT)

- Sukit Limpijumnong has been named *" 2005 TRF Advanced Research Scholar "* by the Thailand Research Fund (TRF)

- Sukit Limpijumnong and Sirichok Jungthawan (student) are awarded *" 2005 NRCT Research Award in mathematics and physical science "* from the National Research Council of Thailand (NRCT)

Appendix

Publications

1. "Substitutional diatomic molecules NO, NC, CO, N_2, and O_2: Their vibrational frequencies and effects on p doping of ZnO", <u>Sukit Limpijumnong</u>, X. Li, S.-H. Wei, and S.B. Zhang, ***Appl. Phys. Lett.*** **86**, 211910 (2005).

2. "Resolving hydrogen binding sites by pressure - A first-principles prediction for ZnO", <u>Sukit Limpijumnong</u> and S.B. Zhang, ***Appl. Phys. Lett.*** **86**, 151910 (2005).

3. "Properties of Ga-interstitial defects in $Al_xGa_{1-x}N_yP_{1-y}$", N.Q. Thinh, I.P. Vorona, I.A. Buyanova, W.M. Chen, <u>Sukit Limpijumnong</u>, S.B. Zhang, Y.G. Hong, H.P. Xin, C.W. Tu, A. Utsumi, Y. Furukawa, S. Moon, A. Wakahara, and H. Yonezu, ***Phys. Rev. B*** **71**, 125 209 (2005).

4. "Evidence for native-defect donors in n-type ZnO", D.C. Look, G. C. Farlow, <u>Pakpoom Reunchan</u>, <u>Sukit Limpijumnong</u>, S.B. Zhang, and K. Nordlund, ***Phys. Rev. Lett.*** **95**, 225 502 (2005).

5. "Probing deactivations in Nitrogen doped ZnO by vibrational signatures: A first principles study", <u>Sukit Limpijumnong</u>, X. Li, S.-H. Wei, and S.B. Zhang, ***Physica B*** **376–377**, 686 (2006).

6. "Ion relaxation and hydrogen LVM in H-irradiated GaAsN", M.-H. Du, <u>Sukit Limpijumnong</u>, S.B. Zhang, ***Physica B*** **376–377**, 583 (2006).

7. "Impurity effects in ZnO and nitrogen-doped ZnO thin films fabricated by MOCVD", X. Li, S.E. Asher, <u>Sukit Limpijumnong</u>, B.M. Keyes, C.L. Perkins, T.M. Barnes, H.R. Moutinho, J.M. Luther, S.B. Zhang, S.-H. Wei, and T.J. Coutts, ***J. Cryst. Growth*** **287**, 94 (2006).

Substitutional diatomic molecules NO, NC, CO, N₂, and O₂: Their vibrational frequencies and effects on *p* doping of ZnO

Sukit Limpijumnong[a)]
National Renewable Energy Laboratory, Golden, Colorado 80401 and School of Physics, Suranaree University of Technology and National Synchrotron Research Center, Nakhon Ratchasima 30000, Thailand

Xiaonan Li, Su-Huai Wei, and S. B. Zhang
National Renewable Energy Laboratory, Golden, Colorado 80401

First-principles calculations show that AB defects substituting on an O site in ZnO where A, B =N, O, or C are an important class of defects whose physical properties cannot be described by the usual split interstitials but rather by substitutional diatomic molecules. The molecular natures of the $(AB)_O$ defects are reflected in their vibrational frequencies which are redshifted from those of the corresponding free molecules but only by about 10%. These calculated results agree with the frequency range recently observed by IR measurement on N-doped ZnO. Moreover, most $(AB)_O$ defects are donors in *p*-type samples. The $(NC)_O$ and $(N_2)_O$ defects have sufficiently low energies to convert substitutional N_O acceptors into donors, thereby hindering the efforts of doping ZnO *p* type. © *2005 American Institute of Physics*. [DOI: 10.1063/1.1931823]

Recent experimental investigations on chemical vapor deposition grown nitrogen-doped ZnO[1–4] revealed that these samples contain not only a large amount of H, but also C, as well as an excess of N in unwanted forms. This, combined with the difficulty of achieving *p*-type ZnO, suggests that these defects may play important roles in compensating or passivating the N acceptors. Moreover, IR absorption measurements on N-doped ZnO showed several peaks in the range of 1800–2000 cm⁻¹, which are surprisingly close to the IR frequencies of free diatomic molecules but significantly higher than the phonon frequencies of the ZnO host. Recent x-ray photoelectron spectroscopy (XPS) experiments found strong signals from the C–N and N–N bonds, which are characteristic of those in free diatomic molecules. In a recent theory work,[5] charge distribution near a substitutional N₂ also showed the sign of a substitutional molecule.

In this work, we investigate systematically first-row C, N, and O impurities in ZnO forming the so-called split interstitials such as $(NC)_O$ and $(N_2)_O$. First-principles calculations show that these complexes have electronic and structural properties, which are inconsistent with the traditional split-interstitials picture[6] but in good agreement with a substitutional diatomic molecule (SDM) picture. In particular, the calculated diatomic bond length, wave functions, and stretch frequencies closely resemble those of free molecules, in qualitative agreement with experiments. The strong tendency of forming such molecules at least in the cases of $(NC)_O$ and $(N_2)_O$ also causes the conversion of the N_O acceptors into unwanted donors that further compensate the remaining acceptors in ZnO.

Our calculations are performed using the density functional theory with the local density approximation (LDA) and ultrasoft pseudopotentials,[7] as implemented in the VASP codes.[8] The Zn 3*d* electrons are treated as valence electrons. The cutoff energy for the plane wave basis set is 300 eV. The calculated heat of formation of 3.58 eV agrees with the ex-

perimental value of 3.60 eV. We use a supercell with 36 atoms for the defect study.[9] Results for $(N_2)_O$ are tested using a 96-atom cell to ensure the convergence to be ±0.2 eV. For charged defects, a jellium background was used. Since LDA severely underestimates the band gap, we have instead examined the electronic properties at the $2 \times 2 \times 2$ Monkhorst-Pack special *k* points, which are used for the Brillouin zone integration. The band gap at the special *k* points is 2.5 eV. All the atoms are relaxed by minimization of force to less than 0.05 eV/Å.

The defect formation energy is defined as[10]

$$\Delta E_f = E_{tot}(D,q) - E_{tot}(0) + \sum \Delta n_X \mu_X + q E_F,$$

where $E_{tot}(D,q)$ is the total energy of the supercell with defect D in charge state q; $E_{tot}(0)$ is the total energy of the supercell without the defect; Δn_X is the number of species X (= Zn, O, N, and C) being removed from a defect-free cell to its respective reservoir with chemical potential μ_X to form the defect cell. The upper limits for μ_{Zn}, μ_O, μ_N, and μ_C are the calculated energies of metallic Zn, gaseous O₂ and N₂, and diamond. For mathematical simplicity, however, we express here the chemical potentials relative to their respective elemental natural phases. This redefines the μ_X so that $\mu_X \leq 0$. To keep ZnO thermodynamically stable, it is also required that $\mu_{Zn} + \mu_O = \mu_{ZnO} = -3.58$ eV. E_F is the electron Fermi level with respect to the valence band maximum (VBM) averaged at the special *k* points, as described in Refs. 11 and 12.

First, let us consider split interstitial in the "traditional" picture: namely, a complex embedded in a local sp^3 environment. For example, the C₂ split interstitial in diamond where each carbon atom is threefold coordinated.[6] One can expect that the pair form single bonds with surrounding host atoms. Alternatively, one can view the complex according to the molecular orbital theory, in which the energy levels of free molecules are $ss\sigma$, $ss\sigma^*$, $pp\pi$ (doublet) $pp\sigma$, $pp\pi^*$ (doublet), and $pp\sigma^*$ in the order of increasing energy. When embedded in ZnO, the $ss\sigma$, $ss\sigma^*$, $pp\pi$, and $pp\sigma$ states are all in the

---
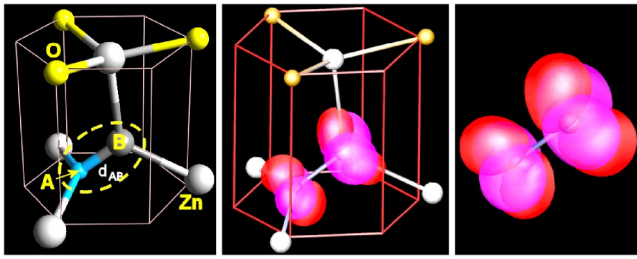[a)]Electronic mail: sukit@sut.ac.th

    86, 211910-1

FIG. 1. (Color online). (a) Atomic structure of an $(AB)_O$ defect, A=N, B =C, where the encircled AB dimer replaces an O atom. Large sphere is Zn and small sphere is O. (b) Charge density of the $pp\pi^*$ states of the $(NC)_O$ defect. The two states should be degenerate in a free dimer as shown in (c) but the degeneracy is lifted by ZnO crystal field.

TABLE I. Calculate bond length, stretch frequencies, and formation energy of the $(AB)_O$ defects at $E_F=0$, $\mu_{Zn}=\mu_N=\mu_C=0$. d_{free} is the bond length of free molecules.

Defect $(AB)_O$	Charge q	$d_{\text{A-B}}$ (Å)	d_{free} (Å)	ω (cm^{-1})	ΔE_f (eV)
$(O_2)_O$	0	1.46	1.23	1051	5.1
$(NO)_O$	2+	1.23		1462	2.5
	1+	1.29		1357	3.1
	0	1.36		1173	4.4
	1−	1.48	1.17	967	6.1
$(CO)_O$	2+	1.16		1894	1.8
	1+	1.22		1652	3.5
	0	1.27	1.14	1373	5.7
$(N_2)_O$	2+	1.14		2108	−1.5
	1+	1.20		1852	0.4
	0	1.28	1.11	1537	2.5
$(NC)_O$	1+	1.18	1.17	1995	0.4

valence band as expected and are hence doubly occupied. If we do an electron counting for $(NC)_O$, for example, we have 5 doubly occupied states with 11 available electrons, 2 from 4 Zn neighbors in Fig. 1(a), 5 from N, and 4 from C. This leaves $(11-10)=1$ electron to occupy the higher $pp\pi^*$ (doublet) states above the VBM as shown in Fig. 2.

The calculated wave functions in Fig. 1(b) are almost copies of the $pp\pi^*$ states for the free dimer in Fig. 1(c). Most strikingly, the charge contour in Fig. 1(b) is for the entire supercell, suggesting that these doublet states are highly localized. Indeed, the dispersion in k space due to cell–cell interaction through the ZnO host is small, only 0.2 eV for these states. Thus, there is little coupling between the $pp\pi^*$ states and the surrounding Zn atoms. This shows clearly that the SDM model is a better description of the $(NC)_O$ complex. Due to the crystal field of ZnO, however, the double degenerate $pp\pi^*$ states of the free molecule is replaced by two nondegenerate, spatially orthogonal states.

The calculated bond lengths compare favorably with those of the corresponding free molecules, also. Note, however, that as a substitutional impurity, each $(AB)_O$ accepts two electrons from its Zn neighbors. Thus, we should compare neutral free molecules with SDMs of $(2+)$ charge state to keep the same orbital occupation. Table I shows that for $(N_2)_O^{2+}$, the bond length, $d_{N-N}=1.14$ Å, is only 3% longer than the triple bond of free N_2 of 1.11 Å. In contrast, the sum of single-bond atomic radii yields 1.50 Å, which is 32% longer. For $(CO)_O^{2+}$, d_{C-O} is longer than that of free CO by only 2%. For $(NO)_O^{2+}$, d_{N-O} is 5% longer. An elongation is generally expected due to the screening of the ZnO host.

To calculate stretch frequencies, we employed the approach used in Ref. 13. Our calculated results for the free molecules are in reasonable agreement with the measured values: 1485(cm^{-1}) versus 1580.2 for O_2, 1819 versus
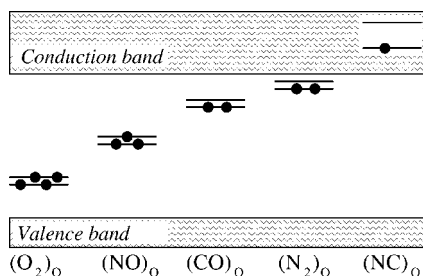

FIG. 2. Calculated energy levels of the $pp\pi^*$ states for charge neutral defects with respect to the band gap of ZnO calculated by the special k-point average. Solid dots show the electron occupations.

1904.2 for NO, 2197 versus 2358.6 for N_2, 2132 versus 2169.8 for CO, and 2052 versus 2068.6 for NC. To calculate the frequency ω for the SDMs in ZnO, in principle, one should solve the dynamic matrix with coupling to at least a few shells of neighboring atoms. However, we found that the coupling to the ZnO host is very weak, which is a reminiscence of the substitutional molecules: for example for $(N_2)_O$, the coupling results in a shift in ω less than 2 cm^{-1}. Because of this, in the calculation we keep the host atoms fixed, which allows us to include also the anharmonic effect. Table I, column 5 shows ω scaled by the ratio between experiment and theory for free molecules (given by the previous results) to reduce systematic errors in the results. The frequencies of the SDMs are reasonably close to those of the free molecules.

Because the $pp\pi^*$ molecular orbitals are antibonding orbitals, its occupation will lead to an increase in the AB bond length. We can see from Table I that adding electrons to the $pp\pi^*$ states always causes an increase in the AB bond length, resulting in weaker bonds and a reduction in ω. For example for $(N_2)_O$, the bondlength increases from 1.14 Å for $q=2+$, to 1.20 Å for $q=+$, and to 1.28 Å for $q=0$. Accordingly, the frequency decreases from 2108, to 1852, and eventually to 1537 cm^{-1}. Because of the Coulomb repulsion between electrons, energy levels in Fig. 2 will shift when occupation changes. For example, in the case of $(O_2)_O$, the removal of any electron from the gap state in Fig. 2 would lower the level to below the VBM, thus making the neutral state the only stable state.

The formation energies of the SDM impurities (ΔE_f) are tabulated in Table I. Figure 3 shows the E_F dependence of ΔE_f for $(CO)_O$, $(NC)_O$, $(NO)_O$, $(N_2)_O$, and N_O. Our results for N_O agree to within 0.2 eV with those in Refs. 5, 14, and 15. For $(N_2)_O$, our results agree to within 0.3 eV with Ref. 15. Isolated interstitial N_i and C_i are unstable against spontaneous formation of $(NO)_O$ and $(CO)_O$ so they are ignored. In the presence of N_O, $(NO)_O$, and $(CO)_O$ are also unstable against the formation of $(N_2)_O$ and $(NC)_O$. On the other hand, both $(N_2)_O$ and $(NC)_O$ have lower formation energy than that of isolated N_O in p-type ZnO. Hence, their formation will severely reduce the concentration of N_O acceptors.
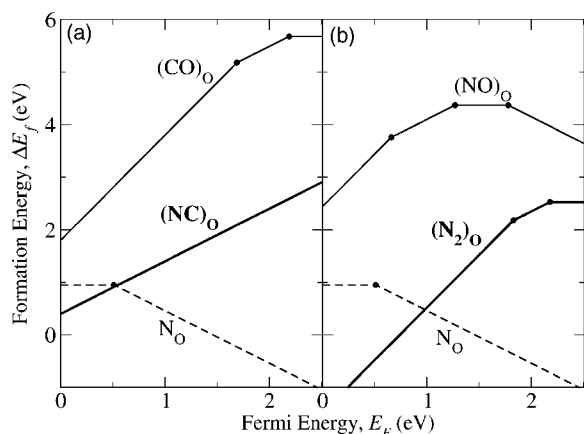
FIG. 3. Formation of (a) $(NC)_O$ from isolated NO and $(CO)_O$ and (b) $(N_2)_O$ from N_O and $(NO)_O$. The chemical potentials are set at $\mu_{Zn}=\mu_N=\mu_C=0$.

Also, the SDMs are donors, therefore compensating any remaining N_O acceptors.

The situation could be more severe when higher N concentration, [N], than the equilibrium value is incorporated via nonequilibrium growth methods because high [N] implies higher chemical potential μ_N. Note that the formation energy of the $(N_2)_O$ complex decreases twice as fast as that of N_O when one raises μ_N. However, because the formation of $(N_2)_O$ from $N_O+(NO)_O$ involves the breakup of one SDM, the diffusion of N_i, and the formation of another SDM, one might be able to control the growth temperature to be low enough to suppress $(N_2)_O$. Also, one should be cautioned about carbon impurities in p-type ZnO. Carbon can form not only double donor C_{Zn}, by substituting Zn, but also single donor $(NC)_O$, which has low formation energy when E_F is low. Hence, beside controlling the concentration of $(N_2)_O$ by kinetic means, one also has to suppress C_{Zn} and $(NC)_O$ in order to get high enough hole concentrations.

Recent XPS experiment has found strong signals of N–N and C–N bonds with similar characteristics to those of free diatomic molecules.[4] These observations strongly suggest the existence of $(N_2)_O$ and $(NC)_O$ in these samples. The calculated frequencies for $(N_2)_O^{2+}$ and $(NC)_O^{2+}$, which are the most stable form for these complexes in p-type ZnO, are 2108 and 1995 cm^{-1}, respectively. These frequencies fall within 200 cm^{-1} of the experimentally observed ones.[2] Also, the calculated frequency of 1894 cm^{-1} for $(CO)_O^{2+}$ is consistent with experiment but the calculated formation energy is higher than $(NC)_O$. Although we do not have a definitive answer why $(CO)_O$ should coexist with $(NC)_O$, we realize that the probability for an interstitial C_i to find an O site should be significantly larger than to find an N_O site.

In conclusion, first principles total energy calculations show that first-row impurities, C, N, and O, can form substitutional diatomic molecules on the oxygen site in ZnO. Both the electronic and structural properties of the SDMs are consistent with those of free molecules but in contrast to those of conventional split interstitials. The calculated vibrational frequencies are in qualitative agreement with recent IR experiment. Our calculations further show that all these SDMs are donors in p-type ZnO. In particular, $(NC)_O$ and $(N_2)_O$ could have low formation energies. These results should shed new lights on how to improve the fabrication of high quality p-type ZnO by nitrogen.

[1] S. J. Pearton, D. P. Norton, K. Ip, Y. W. Heo, and T. Steiner, J. Vac. Sci. Technol. B **22**, 932 (2004).

[2] B. M. Keyes, L. M. Gedvilas, X. Li, and T. J. Coutts, J. Cryst. Growth (submitted).

[3] X. Li, B. M. Keyes, S. E. Asher, S. B. Zhang, S.-H. Wei, T. J. Coutts, S. Limpijumnong, and C. G. Van de Walle, Appl. Phys. Lett. **86**, 122107 (2005).

[4] C. L. Perkins, S.-H. Lee, X. Li, S. E. Asher, and T. J. Coutts, J. Appl. Phys. **97**, 034907 (2005).

[5] E.-C. Lee, Y.-S. Kim, Y.-G. Jin, and K. J. Chang, Phys. Rev. B **64**, 085120 (2001).

[6] S. Uhlmann, T. Frauenheim, and U. Stephan, Phys. Rev. B **51**, 4541 (1995).

[7] D. Vanderbilt, Phys. Rev. B **41**, 7892 (1990).

[8] G. Kresse and J. Furthmüller, Comput. Mater. Sci. **6**, 15 (1996).

[9] S. B. Zhang, S.-H. Wei, and A. Zunger, Phys. Rev. B **63**, 075205 (2001).

[10] S. B. Zhang and J. E. Northrup, Phys. Rev. Lett. **67**, 2339 (1991).

[11] S. B. Zhang, J. Phys.: Condens. Matter **14**, R881 (2002).

[12] S.-H. Wei, Comput. Mater. Sci. **30**, 337 (2004).

[13] S. Limpijumnong, J. E. Northrup, and C. G. Van de Walle, Phys. Rev. B **68**, 075206 (2003).

[14] L. G. Wang and A. Zunger, Phys. Rev. Lett. **90**, 256401 (2003).

[15] Y. Yan, S. B. Zhang, and S. T. Pantelides, Phys. Rev. Lett. **86**, 5723 (2001).

Resolving hydrogen binding sites by pressure—A first-principles prediction for ZnO

Sukit Limpijumnong[a]
School of Physics, Institute of Science, Suranaree University of Technology, Nakhon Ratchasima 30000, Thailand and National Synchrotron Research Center, Suranaree University of Technology, Nakhon Ratchasima 30000, Thailand

S. B. Zhang
National Renewable Energy Laboratory, Golden, Colorado 80401

The binding sites and vibrational frequencies ω of H in ZnO are studied by first-principles total-energy calculations. In the past, different experiments have observed different primary H vibrational modes, making the comparison with theory, and hence the identification of the most favorable H site, difficult. Here, we show that by applying a hydrostatic pressure, one should be able to make an unambiguous distinction, in particular, between the bond center sites and antibonding sites. This is because ω should *increase* with pressure for the former but *decrease* for the latter with the magnitude of calculated slopes about 4 cm^{-1}/GPa, which should be large enough to measure. © *2005 American Institute of Physics.* [DOI: 10.1063/1.1900935]

Recently, ZnO has attracted a lot of attention due to its potential for blue light optoelectronics. If reasonably good *p*-type conductivity can be achieved, ZnO could eventually emerge as a superior alternative to GaN. Hydrogen is one of the most common impurities in semiconductors. It is abundant in air, used in the various growth techniques, and generally has a rather high diffusivity inside semiconductors. Usually, H is an amphoteric impurity, namely, acting either as a donor or an acceptor depending on the Fermi level. However, ZnO is an exception[1] for which isolated interstitial is predicted to be the predominant form of H (Ref. 2), and H acts only as a shallow donor.[1–5] Both first-principles calculations and local vibration measurements indicate that hydrogen prefers to bond with oxygen. However, what is the most favorable geometry is still under intensive debate.[2–8]

In a tetrahedrally coordinated semiconductor, a hydrogen atom can bind to an anion atom predominantly in two ways: in the bond center (BC) site or in the antibonding (AB) site. Due to the low symmetry of the ZnO wurtzite crystal, however, there are two types of orientations ($\parallel$ and $\perp$) for each site above, as shown in Fig. 1(a). First-principles calculations suggested that all four sites have relatively low energies with the global-minimum BC$_\parallel$ site lower than the AB$_O$ sites by less than 0.2 eV. The occupation of the BC sites by an H atom requires large displacements of the host atoms, which may rarely happen due to their relatively large masses with respect to that of H. Therefore, from a kinetic point of view, the H atom might occupy the AB$_O$ sites, instead, despite their slightly higher energies. In cases like this, often, a calculation of the local vibrational modes (LVMs) could differentiate among the structures. Indeed, the calculated H stretch frequencies for the BC and AB$_O$ sites differ by about 300 cm^{-1}. However, the measured *primary* frequencies for interstitial H by different groups also differ by this amount. This makes the assignment difficult because assigning the modes to different sites would contradict energetic argument in favor of kinetic argument. Therefore, it is highly desirable

to have another experimental means to independently confirm the assignment.

In this letter, we predict, based on first-principles calculations, that an experiment on the LVMs (e.g., IR, Raman, or inelastic neutron scattering) under pressure should independently provide the critical test of the H binding sites, differentiating between BC and AB$_O$. The reason is because the O-H bond length for the BC sites decreases under pressure, resulting in an increase in the LVM frequencies. In contrast, the O-H bond length for the AB$_O$ sites increases under pressure, resulting in a decrease in the LVM frequencies. Frequency shifts ($\Delta\omega$), as much as ± 35 cm^{-1}, are predicted over a pressure range of 8 GPa, at which phase transition takes place.[9] These shifts should be large enough to be readily detected by experiments.

We used the density-functional theory, within the local-density approximation (LDA), and the Vanderbilt-type ultrasoft pseudopotentials,[10] as implemented in the VASP code.[11] Zinc 3d states are treated as valence states. The cutoff energy for the plane-wave expansion is 400 eV, with additional tests carried out at 515 eV. The calculated equilibrium lattice constant of ZnO is only 1.4% shorter than experiment. We used a supercell approach with a Monkhorst-Pack k-point mesh
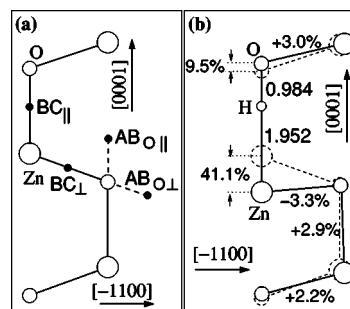

FIG. 1. (a) Schematic representation of the four H sites in ZnO and (b) calculated atomic positions for H$^+$ at the BC$_\parallel$ site, in the (11–20) plane. The dashed circles and dashed lines indicate bulk atomic positions and bonds, respectively. Distances are given in unit of Å and percentage changes are with respect to the bond length of bulk ZnO.

[a]Electronic mail: sukit@sut.ac.th

TABLE I. Calculated formation energy with respect to that of $BC_\parallel$ and the O-H bond length for H^+ in ZnO.

Site	ΔE (eV)			$d_{O\text{-}H}$ (Å)	
	Present	Ref. 2	Ref. 6	Present	Ref. 6
$BC_\parallel$	0.00	0.00	0.0	0.986	0.990
$BC_\perp$	0.15	−0.02	0.1	0.982	
$AB_{O\parallel}$	0.17	0.23	0.1	1.003	1.006
$AB_{O\perp}$	0.14	0.04	0.1	1.003	

for Brillouin-zone integration ($2 \times 2 \times 2$ for the 36-atom cell and $1 \times 1 \times 1$ for the 96-atom cell). For charged H, we use a jellium background. All atoms in the supercell are allowed to relax in the structural optimizations. A test using the 96-atom cell shows that the energy difference between the two BC configurations in the 36-atom calculations are converged to within 0.01 eV. The smaller supercell is used for extracting the energy difference needed for LVM calculation.

We simulate the stretch frequency by tracing the potential energy curve of the vibration. This has been carried out by calculating the energy as a function of H displacement in both compression (toward O) and extension (away from O) directions. Because (1) H is much lighter than the host atoms and (2) the LVM of the O-H bond (around 3000 cm^{-1}) is much higher than the crystal phonon modes, the displacement of the host atoms during the vibration can thus be neglected. A previous study[12] has explicitly compared the LVMs obtained by freezing host atoms and the LVMs obtained from dynamic matrix approach. A good agreement was found provided that the reduced mass of the anion-H pair is used. Due to the light mass of the H atom, anharmonic contribution ($\widetilde{\omega}_{AC}$) could also be important.[13] We include $\widetilde{\omega}_{AC}$ in our calculation by fitting the calculated energy curve as a function of the H displacement with a fourth-degree polynomial, i.e.,

$$V(x) = \frac{k}{2}x^2 + \alpha x^3 + \beta x^4. \tag{1}$$

To solve the Schrödinger equation with such a potential, we used a perturbation theory[14] to obtain an approximate analytical solution, which reads

$$\widetilde{\omega} = \widetilde{\omega}_{Har} + \widetilde{\omega}_{AC} = \sqrt{\frac{k}{\mu}} - 3\frac{\hbar}{\mu}\left(\frac{5\alpha^2}{2k^2} - \frac{\beta}{k}\right). \tag{2}$$

Table I shows the calculated energy for the four H sites and the corresponding O-H bond lengths. It suggests that $BC_\parallel$ is the most stable H configuration, in agreement with the recent results by Lavrov et al.[6] Figure 1(b) shows the atomic geometry of the fully relaxed $BC_\parallel$. We see that, with respect to ideal ZnO, the Zn atom adjacent to the H atom has relaxed away from the H through the basal plain defined by the three remaining oxygen atoms by as much as 41.1%. As a result, the three remaining Zn-O bonds are compressed by 3.3%. Our calculated O-H bondlengths ($d_{O\text{-}H}$) agree with those in Ref. 6 to within 0.005 Å.

Table II shows the calculated LVM frequencies, $\widetilde{\omega}_{Har}$, $\widetilde{\omega}_{AC}$, and $\widetilde{\omega}$, as defined in Eq. (2). The anharmonic contribution $\widetilde{\omega}_{AC}$, for example, −282 cm^{-1} for $BC_\parallel$ and −352 cm^{-1} for $AB_{O\parallel}$, is typically 8–10 % of the corresponding harmonic contribution $\widetilde{\omega}_{Har}$, 3659, and 3370 cm^{-1}, respectively, and the two have opposite signs. It appears that the difference in $\widetilde{\omega}$ between the $\parallel$ and $\perp$ modes are relatively small, typically 40 cm^{-1}, with the latter being slightly larger. We may expect some errors in our calculated $\widetilde{\omega}$'s, as $\widetilde{\omega}$ for the free water molecule in Table II is lower than experiment[15] by $\omega_{ER} = 98$ cm^{-1}. The error is most likely systematic because the calculated O-H bond lengths are consistently longer than experiment by about 2%. We have therefore corrected the errors for all the $\widetilde{\omega}$'s by adding ω_{ER} to obtain ω. The same procedure, but with $\omega_{ER} = 51$ cm^{-1}, is applied to the calculated results in Ref. 6. After the correction, the average values for the BC and AB_O modes are $\omega(BC) = 3497$ and $\omega(AB_O) = 3135$ cm^{-1}, respectively. These can be compared with the corrected values in Table II for Ref. 6, $\omega(BC) = 3551$ and $\omega(AB_O) = 3259$ cm^{-1}. Thus, theories agree to within $3551 - 3497 = 54$ cm^{-1} for $\omega(BC)$ and $3259 - 3135 = 124$ cm^{-1} for $\omega(AB_O)$. These differences, 54 and 124 cm^{-1}, are significantly smaller than the calculated splitting between the BC and AB_O modes: 362 (present) and 292 cm^{-1} (Ref. 6). It comes to our attention that the measured LVM frequencies in Refs. 6,8 differ by 285 cm^{-1}, suggesting that one of them could be the BC mode whereas the other is the AB_O mode.

More definitive identification of the experimental LVMs may be obtained by pressure measurement. This is possible because the neighboring atoms of the BC and AB_O sites are different, which could result in different responses to external pressure. To simulate the pressure effect, we need the total energy as a function of volume, from which the

TABLE II. Stretch modes for interstitial H^+ in ZnO, in units of cm^{-1}. $\widetilde{\omega}_{Har}$, $\widetilde{\omega}_{AC}$, and $\widetilde{\omega}$ are described in Eq. (2), whereas the calculated ω's (columns 4 and 5) include the systematic error correction, as described in the text.

Site	Present			Ref. 6 $\omega(\widetilde{\omega})$	Measured ω
	$\widetilde{\omega}_{Har}$	$\widetilde{\omega}_{AC}$	$\omega(\widetilde{\omega})$		
$BC_\parallel$	3659	−282	3475 (3377)	3551 (3500)	3611[a]
$BC_\perp$	3706	−285	3519 (3421)		
$AB_{O\parallel}$	3370	−352	3116 (3018)	3259 (3208)	3326[b]
$AB_{O\perp}$	3379	−323	3154 (3056)		
H_2O	3815	−257	3657 (3559)	3657 (3606[d])	3657[c]

[a]Reference 6.
[b]Reference 8.
[c]Reference 15.
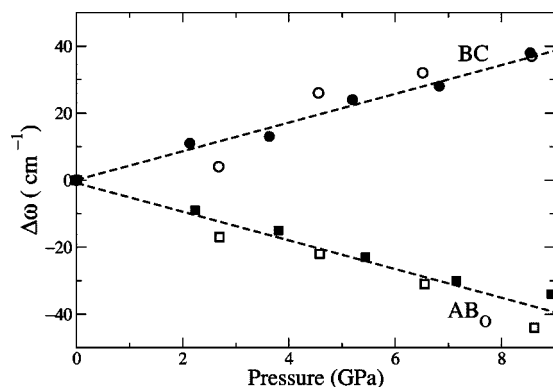[d]Calculated using FHI98 codes.

FIG. 2. The shifts in the stretch mode frequencies of the O-H bonds for the four H sites in Fig. 1, as a function of the external pressure. Two possible orientations of the O-H bonds in the crystal are coded with solid ($\parallel$) and open ($\perp$) symbols. The lines are least-square fits to the calculated data.

pressure $P(V)$ as a function of V is obtained through $P(V)=-dE(V)/dV$. Next, we need the frequency as a function of volume, $\omega(V)$. From $\omega(V)$ and $P(V)$, we can deduce $\omega(P)$. The above calculation should be straightforward if we use very large supercells. In practice, we use a finite-size 36-atom supercell, which might introduce errors both in $P(V)$ and $\omega(V)$. To minimize the error in $P(V)$, we calculate instead $dE(V)/dV$ using a primitive cell for the reasons that P is an intensive quantity and that in the dilute limit the effect of the defect should diminish. To minimize the error in $\omega(V)$, we did selectively 96-atom cell calculations to adjust the 36-atom cell results. The correction on ω was found to be rather small, whose main role was to eliminate the artificial small splitting between the $\parallel$ and $\perp$ modes due to the specific shape of the 36-atom cell. Figure 2 shows the calculated ω for the four H binding sites, as a function of P. We see clearly the qualitative difference between the LVMs for the BC and AB_O sites: while $\omega(BC)$ increases with pressure, $\omega(AB_O)$ decreases, instead. In spite of that, $\omega(BC)$ and $\omega(AB_O)$ have, fortuitously, a similar magnitude of slope around 4.2 cm^{-1}/GPa.

The distinct pressure dependences in Fig. 2 may be qualitatively understood by the change of the O-H bond length (d_{O-H}) under pressure, namely, a decrease in d_{O-H} would correspond to an increase in ω, as demonstrated in Ref. 13. Here, d_{O-H} for AB_O monotonically increases with P, which explains why ω decreases in Fig. 2, e.g., at $P=5.4$ GPa, $\Delta d_{O-H}=0.0013$ Å whereas $\Delta \omega=-23$ cm^{-1} for $AB_{O\parallel}$. On the other hand, d_{O-H} for BC monotonically decreases with P, which explains why ω increases in Fig. 2: at $P=5.2$ GPa, $\Delta d_{O-H}=-0.0021$ Å whereas $\Delta \omega=+22$ cm^{-1} for BC$_\parallel$. We speculate that the change in d_{O-H} for AB_O under pressure is because of the compression of the neighboring Zn-O bonds. To test this hypothesis, we have calculated an acetylene molecule (H-C-C-H) and found that indeed if we compress the C-C bond by 0.02 Å, both of the C-H bonds will increase, as expected, by about 0.001 Å. Concerning the change in d_{O-H} for BC under pressure, we note that the H atom sits between an O and a Zn atom. When the O-Zn distance is reduced due to the external pressure, the O-H distance (d_{O-H}) is also reduced.

A recent experiment showed that the 3326 cm^{-1} frequency corresponds to an H mode in the $\perp$ direction, whose frequency changes with pressure by a negative slope,

−1.5 cm^{-1}/GPa (Ref. 16). This mode has also been assigned to hydrogen on the $AB_{O\perp}$ sites. In fact, this assignment agrees with our present calculation where the $AB_{O\perp}$ site should have a negative pressure slope, as well as a slightly lower formation energy than that of the $AB_{O\parallel}$ site (see Table I). Even the measured slope, −1.5 cm^{-1}/GPa, is within a factor of 3 of the calculated one, −4.2 cm^{-1}/GPa. Note that to calculate the small changes in ω accurate to within 10 cm^{-1} requires a very high convergence to at least within 0.001 Å in the atomic positions and 1 meV in energy. Hence, such a deviation from experiment is not at all surprising. Also, while both the measured 3326 and 3611 cm^{-1} modes in Table II have been previously assigned to interstitial H, there is always the concern whether they belong to some hydrogen/(unknown)-defect complexes, instead. We believe that the pressure dependence of the LVMs should not depend very sensitively on the complex formation. In other words, the pressure coefficient should still be positive if the H in a complex can be described as a bond-center H, but negative if the H can be described as an antibonding H.

In conclusion, first-principles studies predict that hydrostatic-pressure experiments could be an important tool for making unambiguous identification of interstitial H in ZnO; in particular, showing a clear, qualitative difference between the bond center and antibonding sites. The frequency ω for the former should increase with pressure, but ω for the latter should decrease, with a slope of 4.2 cm^{-1}/GPa. The magnitude of the calculated slopes qualitatively agrees with the only known experiment.

[1] C. G. Van de Walle and J. Neugebauer, Nature (London) **423**, 626 (2003).
[2] C. G. Van de Walle, Phys. Rev. Lett. **85**, 1012 (2000).
[3] S. F. J. Cox, E. A. Davis, S. P. Cottrell, P. J. C. King, J. S. Lord, J. M. Gil, H. V. Alberto, R. C. Vilão, J. Piroto Duarte, N. Ayres de Campos, A. Weidinger, R. L. Lichti, and S. J. C. Irvine, Phys. Rev. Lett. **86**, 2601 (2001).
[4] D. M. Hofmann, A. Hofstaetter, F. Leiter, H. Zhou, F. Henecker, B. K. Meyer, S. B. Orlinskii, J. Schmidt, and P. G. Baranov, Phys. Rev. Lett. **88**, 045504 (2002).
[5] K. Shimomura, K. Nishiyama, and R. Kadono, Phys. Rev. Lett. **89**, 255505 (2002).
[6] E. V. Lavrov, J. Weber, F. Börrnert, C. G. Van de Walle, and R. Helbig, Phys. Rev. B **66**, 165205 (2002).
[7] C. H. Seager and S. M. Myers, J. Appl. Phys. **94**, 2888 (2003).
[8] M. D. McCluskey, S. J. Jokela, K. K. Zhuravlev, P. J. Simpson, and K. G. Lynn, Appl. Phys. Lett. **81**, 3807 (2002).
[9] S. Limpijumnong and S. Jungthawan, Phys. Rev. B **70**, 054104 (2004).
[10] D. Vanderbilt, Phys. Rev. B **41**, 7892 (1990).
[11] G. Kresse and J. Furthmüller, Comput. Mater. Sci. **6**, 15 (1996).
[12] S. Limpijumnong and C. G. Van de Walle, Mater. Res. Soc. Symp. Proc. **639**, G4.3 (2001).
[13] S. Limpijumnong, J. E. Northrup, and C. G. Van de Walle, Phys. Rev. B **68**, 075206 (2003).
[14] L. D. Landau and E. M. Lifshitz, *Quantum Mechanics*, 3rd ed. (Pergamon, Oxford, 1977), p. 136.
[15] E. McCartney, *Absorption and Emission by Atmospheric Gases: The Physical Processes* (Wiley, New York, 1983).
[16] M. D. McCluskey and S. J. Jokela, in *Proceedings of the NATO Advanced Research Workshop on Zinc Oxide*, edited by N. Nickel and E. Terukov, NATO Science Series II (2005), Vol. 194.

Properties of Ga-interstitial defects in Al$_x$Ga$_{1-x}$N$_y$P$_{1-y}$

N. Q. Thinh, I. P. Vorona,* I. A. Buyanova, and W. M. Chen[†]

Department of Physics and Measurement Technology, Linköping University, 58183 Linköping, Sweden

Sukit Limpijumnong

School of Physics, Institute of Science, Suranaree University of Technology, Nakhon Ratchasima 30000, Thailand

S. B. Zhang

National Renewable Energy Laboratory, Golden, Colorado 80401, USA

Y. G. Hong, H. P. Xin, and C. W. Tu

Department of Electrical and Computer Engineering, University of California, La Jolla, California 92093-0407, USA

A. Utsumi, Y. Furukawa, S. Moon, A. Wakahara, and H. Yonezu

Department of Electrical and Electronic Engineering, Toyohashi University of Technology, Toyohashi, Aichi, 441-8580, Japan

A detailed account of the experimental results from optically detected magnetic resonance (ODMR) studies of grown-in defects in (Al)GaNP alloys, prepared by molecular beam epitaxy, is presented. The experimental procedure and an in-depth analysis by a spin Hamiltonian lead to the identification of two Ga$_i$ defects (Ga$_i$-A and Ga$_i$-B). New information on the electronic properties of these defects and the recombination processes leading to the observation of the ODMR signals will be provided. These defects are deep-level defects. In conditions when the defect is directly involved in radiative recombination of the near-infrared photoluminescence band, the energy level of the Ga$_i$-B defect was estimated to be deeper than $\sim$1.2 eV from either the conduction or valence band edge. In most cases, however, these defects act as nonradiative recombination centers, reducing the efficiency of light emission from the alloys. They can thus undermine the performance of potential photonic devices. High thermal stability is observed for these defects.

I. INTRODUCTION

One of the most important aspects in the physics and technology of semiconductors is to understand and control defects, which are known to often produce deep levels in the forbidden energy gap. Intrinsic defects such as self-interstitials, vacancies, and antisites have been found to be commonly occurring defects in semiconductor crystals grown under nonoptimized, nonequilibrium conditions, or subject to high-energy particle bombardment. They are fundamental building blocks for defect complexes and in some cases nucleation sites for the formation of clusters and extended defects. Intrinsic defects and their complexes are known to play a crucial role in determining the electronic and optical properties of semiconductors. In some cases when their properties are well understood and controlled, they can be used to tailor the physical properties of semiconductors such as carrier lifetime, Fermi level position, and doping [e.g., the antisite-related defects in GaAs (Refs. 1 and 2) and P$_{In}$ antisite in InP (Refs. 3 and 4)]. In most cases, however, defects are known to severely degrade device performance and can hinder a semiconductor from practical applications. In any case, a good understanding of the defect properties is vital, especially concerning a positive identification of their chemical nature and their role in altering material properties. Up to now only very few experimental techniques have been proven successful in meeting the demand. Among them, magnetic resonance techniques have been

shown to be the most powerful of the ones that have successfully identified many intrinsic defects in semiconductors.[5–7] When the conventional electron spin resonance (ESR) technique fails to provide the required sensitivity to reveal defects in semiconductor thin films and quantum structures grown by modern epitaxy techniques, its advanced variant—namely, the optically detected magnetic resonance (ODMR) technique—has shown to be successful.[8–11]

The aim of the present work is to reveal important grown-in defects in (Al)GaNP alloys by employing the ODMR technique. (Al)GaNP represents a class of newly emerging dilute nitrides, which have recently attracted great attention. These materials exhibit unusual and fascinating new physical properties, such as a giant band-gap bowing that allows widely extended band-structure engineering.[12–19] One can also vary the lattice constant of the alloy materials over a wide range by varying the N content. For example, adding about 1.8% of N into GaP can make the parent material lattice matched to Si, opening the possibility for optoelectronic integrated circuits[19,20] and multijunction III-V solar cells fabricated on Si wafers. A crossover from an indirect to a direct band gap induced by incorporation of >0.4% N (Refs. 15–18) promises high radiative efficiency. Due to the large mismatch in size and electronegativity between N and the replaced P atom, however, successful growth of (Al)GaNP has to be undertaken under nonequilibrium conditions.[21,22] The nonequilibrium growth conditions, together with the disparity between N and P atoms resulting in

a strong local potential and strain field, lead to the formation of various point defects and clusters. The efficiency of visible light emissions in (Al)GaNP has been shown to deteriorate with increasing N and Al compositions. Up to now, band-to-band transitions have not been observed in this material despite the crossover to a direct band gap, due predominantly to nonradiative recombination at the defects. Currently, there is a great need in identifying important grown-in defects in this dilute nitride and in assessing their exact roles in carrier recombination.

In this work, we were able to identify Ga_i interstitial defects by ODMR as the dominant grown-in intrinsic defects in (Al)GaNP, prepared by molecular beam epitaxy (MBE). We obtained detailed information on the electronic properties of the defects and their role in carrier recombination. Preliminary results were briefly presented in a recent Rapid Communication.[23] In this paper, we shall present in details our experimental procedure and an in-depth analysis by a spin Hamiltonian that led to the identification of the two Ga_i defects. New information on the electronic properties of these defects and the recombination processes leading to the observation of the ODMR signals will be provided. A discussion about the formation mechanism of the defects will not be included here, but can be found elsewhere.[24] The paper is organized as follows: In Sec. II, we shall describe the samples under study, the details of the ODMR, and related photoluminescence (PL) experiments. In Sec. III, we shall present a detailed account of the ODMR results including temperature, angular, and spectral dependences. An analysis of the ODMR results by a spin Hamiltonian and a discussion of the microscopic structures of the defects and the involved recombination processes will be presented in Sec. IV. The main conclusions of the present study will be summarized in Sec. V.

II. EXPERIMENT

A. Samples

Three types of (Al)GaNP samples were studied in this work, varying by their chemical compositions and substrate materials. The first two types were grown at 520 °C on GaP substrates by gas-source molecular beam epitaxy (GS-MBE) and have a typical thickness between 0.75 and 0.9 μm. They are (1) quaternary $Al_xGa_{1-x}N_yP_{1-y}$ with a fixed value $y=0.012$ and varied x values, $x=0.00$, 0.01, 0.02, and 0.30; (2) Al-free GaN_yP_{1-y} with varied y values, $y=0.013$, 0.023, and 0.031. They will be referred below as AlGaNP/GaP and GaNP/GaP, respectively. The third type (denoted as GaNP/Si below) is $GaN_{0.018}P_{0.982}$ with a thickness of 0.15 μm grown at 590 °C on a Si (100) substrate, by solid-source MBE. Rapid thermal annealing (RTA) was performed for 30 sec at the temperature range 700–900 °C with halogen lamps in a flowing N_2 ambient.

B. Experimental procedure

The ODMR measurements were performed at two microwave frequencies on a modified Bruker ER-200 D X-band ($\sim$9.3 GHz) setup with a flow cryostat and a W-band
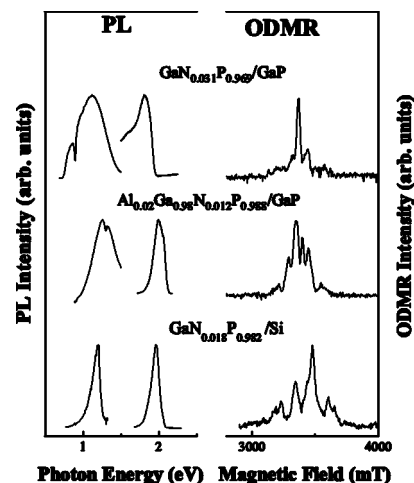

FIG. 1. Representative PL and ODMR spectra from three types of (Al)GaNP samples studied in this work. The PL spectra were measured at 2 K. The ODMR spectra were measured at 5 K and at the W band (94.8 GHz), by monitoring the NIR PL emissions. The sign of the ODMR signals is negative for GaNP/GaP and AlGaNP/GaP, but positive for GaNP/Si. They are all shown as positive for easy viewing.

($\sim$95 GHz) setup with an Oxford superconducting split-coil magnet (0–5 T) cryostat. A solid-state laser with 532-nm wavelength was used as an excitation source in the ODMR measurements. The PL signal was detected through proper optical filters by a cooled Ge detector and a GaAs photodiode for the near-infrared (NIR) and visible spectral range, respectively. The ODMR signals were detected by the lock-in technique as spin-resonance-induced changes of PL intensity, in phase with an amplitude modulation (0.5–20 kHz) of the microwave radiation. The typical microwave power employed was 170–200 mW. The measurements were performed in the temperature range of 2–40 K.

III. RESULTS

A. PL and ODMR

Upon above-band-gap optical excitation, all three types of the samples studied exhibit PL emissions in the visible spectral range (see Fig. 1) that are known to arise from N-related localized states.[25] They also give rise to defect-related deep PL emissions within the NIR spectral range whose origins are still largely unknown (see the PL bands at the lower energies in Fig. 1). Judging from their energy positions and their shifts with N and Al compositions, as well as different signs of the ODMR signals (to be presented below), we believe that the deep emissions from the three types of samples are of different origins. Representative PL spectra from the three types of samples are given in Fig. 1, together with typical ODMR spectra obtained by monitoring these PL emissions. The ODMR spectra show the following two distinct features originated from different defects. The first one is a single strong line situated in the middle of the ODMR spectra from the AlGaNP/GaP and GaNP/GaP samples, with a g value close to 2. Due to a lack of hyperfine (HF) structure, unfortunately, the chemical nature of the corre-
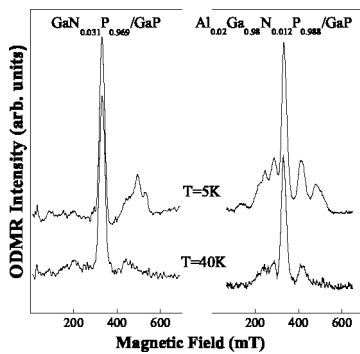
FIG. 2. ODMR spectra taken at two different temperatures, 5 and 40 K, from $GaN_{0.031}P_{0.969}/GaP$ and $Al_{0.02}Ga_{0.98}N_{0.018}P_{0.982}/GaP$. The X-band microwave frequency was 9.31 GHz.

FIG. 3. ODMR spectra of the three types of (Al)GaNP samples obtained at 5 K and when the external magnetic field was oriented along the three main crystallographic axes. The $Al_{0.02}Ga_{0.98}N_{0.018}P_{0.982}/GaP$ sample was measured at the X band, while the other two samples were measured at the W band.

sponding defect cannot be identified. Below we shall simply refer to it as the "$g=2$" defect. The second feature of the ODMR spectra consists of a complicated pattern of lines spreading over a wide field range. Such multiple ODMR lines can arise from a high-electron-spin state exhibiting a zero-field splitting due to a defect crystal field, from an HF interaction involving a high nuclear spin, or from several overlapping ODMR signals due to different defects. To resolve this issue, the temperature and angular dependences of the ODMR spectra were investigated.

B. Temperature dependence of the ODMR

To examine if the second feature of the ODMR spectra originates from a single or more than one defect, temperature dependence studies were performed. This is because the temperature dependence of spin-lattice relaxation is often different, such that relative intensity of the ODMR signals from different defects may be altered by the measurement temperature. ODMR spectra from AlGaNP/GaP and GaNP/GaP at 5 K and 40 K (Fig. 2) clearly show that about half of the multiple ODMR lines undergo thermal quenching in intensity. This finding provides strong evidence that the multiline feature of the ODMR spectra in fact consists of two groups of lines from two different defects (denoted as Ga$_i$-A and Ga$_i$-B), of which Ga$_i$-B loses signal strength at elevated temperatures and vanishes at $T \geq 40$ K (see Fig. 2).

C. Angular dependence of the ODMR

Both Ga$_i$-A and Ga$_i$-B give rise to multiple ODMR lines, which can arise either from a high-electron-spin state exhibiting a zero-field splitting caused by a defect crystal field or from an HF interaction involving a high nuclear spin. The former should give rise to an anisotropic ODMR spectrum reflecting the symmetry of the defect, whereas the latter may or may not do so. To identify the origin of the multiple ODMR lines, angular dependence studies were carried out by rotating the external magnetic field in a {110} crystallographic plane. Typical ODMR spectra are displayed in Fig. 3 when the direction of the external magnetic field is oriented along the three main crystallographic axes, as examples. The ODMR spectra are shown to be isotropic, within the experi-
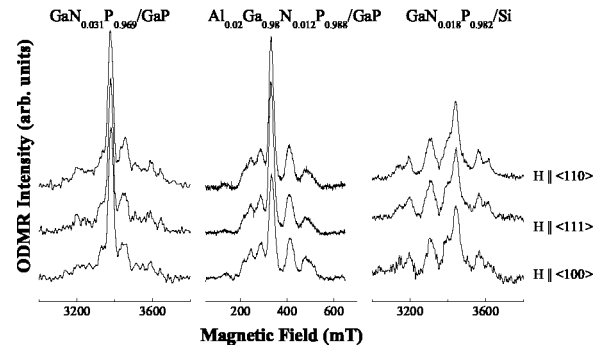
mental error. This finding supports the assignment that the multiple ODMR lines for each defect should be due to an HF structure, which will be shown below to arise from a strong interaction between an unpaired electron spin ($S=1/2$) and the nuclear spin ($I=3/2$) of a Ga atom.

D. Spectral dependence of the ODMR

In the AlGaNP/GaP and GaNP/GaP samples, all defects—i.e., the "$g=2$" defect, the Ga$_i$-A, and the Ga$_i$-B—give rise to negative ODMR signals that correspond to a decrease upon spin resonance in the intensity of the monitored PL emissions over the entire visible and NIR spectral range. (The ODMR signals are displayed as positive ones throughout the paper merely for easy viewing.) The only exception occurs for the $Al_xGa_{1-x}N_yP_{1-y}$ sample series when $x=0.00$ and $y=0.012$, where the sign of the ODMR signals turns to positive by monitoring the NIR PL emissions. A possible reason for this sign change will be discussed in Sec. IV E. In the GaNP/Si samples, however, the ODMR signals (shown in Figs. 1 and 3) correspond to a spin-resonance-induced increase in the monitored NIR PL emission—i.e., a positive sign of ODMR. On the other hand, in the visible spectral range, the ODMR signal strength was too weak to be detected.

E. Effect of RTA on the ODMR

In Fig. 4, we show representative ODMR spectra from the AlGaNP alloys before and after post-growth RTA treatments. All the defects under study exhibit high thermal stability up to 900 °C and can only be partially removed by RTA. It should be noted that the RTA causes a larger reduction of the "$g=2$" defect than the two Ga$_i$ defects.

IV. DISCUSSION

A. Spin Hamiltonian analysis

The left panels of Figs. 5–7 show that the ODMR spectra at the X band are rather irregular, which makes it very difficult to assign them to a specific nuclear spin state. For this reason, the ODMR was also performed at the W band in a
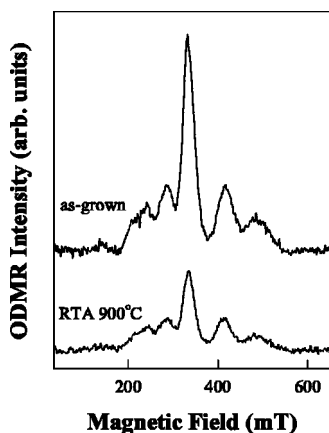
FIG. 4. ODMR spectra from the as-grown and RTA treated $Al_{0.02}Ga_{0.98}N_{0.018}P_{0.982}$/GaP samples, obtained at 5 K for the X band. The RTA treatment was done at 900 °C.

higher magnetic field, which usually avoids a strong nonlinear Zeeman effect due to level repelling at low fields. The ODMR spectra at the W band show a clear pattern with two groups of lines from Ga_i-A and Ga_i-B with distinctly different intensities. Each defect shows grossly four lines with additional features (a shoulder or a splitting). A close inspection reveals that each defect in fact gives rise to two sets of four lines with a fixed intensity ratio of 40/60 and a fixed ratio of line spacing=1.3. The most plausible explanation for these experimental findings is that the ODMR lines from each defect should originate from the HF structure related to an atom with the following properties: (i) it has two isotopes, of which both have a nuclear spin $I=3/2$ to account for the two sets of four lines; (ii) the ratio of the natural abundances of the two isotopes should be near 40/60 to account for the ratio of the corresponding ODMR intensity; (iii) the ratio of the nuclear magnetic moments of the two isotopes should be near 1.3 to account for the ratio of the line spacing.

To confirm the assignment and to obtain information on the physical properties of the defects, a detailed analysis of the experimental data was performed using the following spin Hamiltonian:
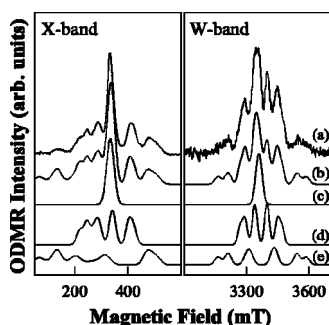

FIG. 5. (a) Experimental ODMR spectra from $Al_{0.02}Ga_{0.98}N_{0.018}P_{0.982}$/GaP, taken at 5 K for both the X (9.31 GHz) and W (94.8 GHz) bands. (b) The simulated ODMR spectra including contributions from (c)–(e) below. (c) The simulated ODMR spectrum for the "$g=2$" defect. A fitting value of g =2.017 was used. (d) and (e) The simulated ODMR spectra for Ga_i-A and Ga_i-B, respectively, by using the spin Hamiltonian parameters given in Table I.
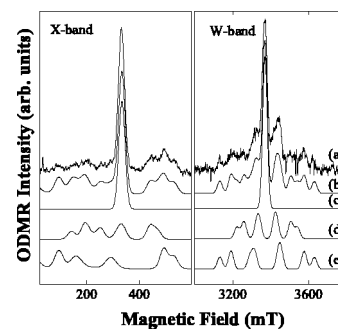

FIG. 6. (a) Experimental ODMR spectra from $GaN_{0.031}P_{0.969}$/GaP, taken at 5 K at both the X (9.31 GHz) and W (94.8 GHz) bands. (b)–(e) have the same meaning as in Fig. 5.

$$H = \mu_B \mathbf{B} \cdot \mathbf{g} \cdot \mathbf{S} + \mathbf{S} \cdot \mathbf{A} \cdot \mathbf{I}. \qquad (1)$$

Here the first and second terms describe electron Zeeman and central HF interactions, respectively; μ_B is the Bohr magneton, $\mathbf{B}$ is the external magnetic field, $\mathbf{g}$ is the Zeeman splitting tensor, and $\mathbf{A}$ is the central HF interaction tensor for each isotope. The effective electron spin is $S=1/2$ and the nuclear spin is $I=3/2$. By fitting the spin Hamiltonian to the experimental data, the spin Hamiltonian parameters were determined for both Ga_i-A and Ga_i-B in all samples and are given in Table I. Both $\mathbf{g}$ and $\mathbf{A}$ tensors are deduced to be isotropic, within the experimental accuracy, and are reduced to the scalars g and A. This finding, together with the rather strong HF interaction, points to A_1 symmetry (s like) for the electron wave function localized at the defects. For example, Figs. 5–7 show the simulated ODMR curves for $Al_{0.02}Ga_{0.98}N_{0.012}P_{0.988}$/GaP, $GaN_{0.031}P_{0.969}$/GaP, and $GaN_{0.018}P_{0.982}$/Si, assuming a Gaussian line shape for each ODMR line. It is apparent that the agreement between the simulations and the experimental results is very good for both X- and W-band spectra.

The intensity of the low-field X-band ODMR lines appears to be weaker in experiment than in simulation. This can be attributed to the fact that the simulations only take into account magnetic-dipole-allowed electron spin resonance transitions but not the difference in recombination rates of the spin sublevels.[10,11] At lower fields when the electronic Zeeman term becomes comparable or weaker than the
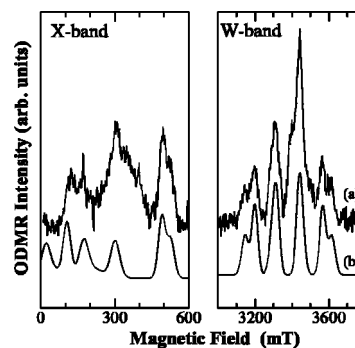

FIG. 7. (a) Experimental ODMR spectra from $GaN_{0.018}P_{0.982}$/Si, taken at 5 K at both the X (9.31 GHz) and W (94.8 GHz) bands. (b) The simulated ODMR spectra for Ga_i-B.

TABLE I. Spin Hamiltonian parameters determined by fitting Eq. (1) to experimental data for the Ga_i-A and Ga_i-B defects in the three types of samples. Spin density η^2 at Ga_i is also shown and is deduced from our calculated $4s$ electron density, $|\psi_{4s}(0)|^2 = 72.7 \times 10^{24}$ cm^{-3}. Note that for the $GaN_{0.018}P_{0.982}$/Si and $Al_xGa_{1-x}N_yP_{1-y}$/GaP ($x=0$ and $y=0.012$) samples, the ODMR signal of Ga_i-A, if existing, is obscured by the presence of the much stronger ODMR signals from other defects and thus its HF interaction parameter cannot be reliably determined. No ODMR signals from Ga_i-A and Ga_i-B were observed in the $GaN_{0.013}P_{0.987}$/GaP sample within the detection limit of our ODMR experiments.

Samples	GaN_yP_{1-y}/GaP				GaN_yP_{1-y}/Si	$Al_xGa_{1-x}N_yP_{1-y}$/GaP						
x	0				0	0	0.01		0.02		0.3	
y	0.031		0.023		0.018	0.012						
Defect	Ga_i-A	Ga_i-B	Ga_i-A	Ga_i-B	Ga_i-B	Ga_i-B	Ga_i-A	Ga_i-B	Ga_i-A	Ga_i-B	Ga_i-A	Ga_i-B
S	1/2	1/2	1/2	1/2	1/2	1/2	1/2	1/2	1/2	1/2	1/2	1/2
I	3/2	3/2	3/2	3/2	3/2	3/2	3/2	3/2	3/2	3/2	3/2	3/2
g	2.001	2.003	2.001	2.003	2.001	2.005	2.01	2.005	2.01	2.005	2.01	2.005
$A(^{69}Ga) \times 10^{-4}$ cm^{-1}	770	1150	770	1150	1145	1150	490	1030	490	1030	450	980
$A(^{71}Ga) \times 10^{-4}$ cm^{-1}	1000	1480	1000	1480	1477	1480	630	1320	630	1320	580	1260
$\eta_2(Ga_i)$	0.20	0.30	0.20	0.30	0.30	0.30	0.13	0.27	0.13	0.27	0.12	0.25

HF interaction [see Eq. (1)], the spin sublevels undergo strong admixing due to the HF interaction, which reduces the difference in the recombination rates. As the ODMR intensity is proportional[10,11] to the product of the microwave-induced spin transition probability and the difference in the recombination rates, a reduction of the latter should thus lead to a decrease in the actual ODMR intensity.

It should also be noted that the fitting of the ODMR spectra from the GaNP/Si samples in Fig. 7 is less satisfactory by considering Ga_i-B alone, due to a contribution from a broad background close to the middle of the spectra. Though a contribution from Ga_i-A to the background is possible, it cannot be definitely concluded since the characteristic HF structure was not resolved in this case. Even assuming the contribution from Ga_i-A, additional contributions from other unknown defect(s) are still apparent. A similar situation occurs in the Al-free sample in the AlGaNP/GaP series—i.e., the only other sample that also exhibits positive ODMR signals. In both cases, the strong ODMR line related to the "$g=2$" defect, which dominates the ODMR spectra in the rest of the samples, is absent.

B. Defect identification

The above analysis proves that both Ga_i-A and Ga_i-B involve an atom with well-defined natural abundances of the two isotopes and their respective nuclear spin numbers and magnetic moments. Among all elements, only Ga meets all these specifications. Ga has two naturally abundant isotopes: ^{69}Ga (60.4% abundant) and ^{71}Ga (39.6% abundant). The ratio of their nuclear magnetic moments is $\mu(^{71}Ga)/\mu(^{69}Ga) = 1.27$. Our ODMR results thus provide compelling evidence for the involvement of a Ga atom in the core of both Ga_i-A and Ga_i-B defects.

Now let us turn to the location of the Ga atom in Ga_i-A and Ga_i-B that gives rise to the observed HF structure. A Ga atom, instead of residing in its designated lattice site, can reside either on a site of the group-V sublattice forming a cation antisite or on an interstitial position leading to Ga self-interstitials. A Ga-related cation antisite was predicted by earlier[26] and our present theoretical calculations to possess an electron wave function of T_2 symmetry, which will yield a very weak and anisotropic HF interaction at the defect center. This is clearly inconsistent with our experimental observation of the strong isotropic HF interaction and can therefore be ruled out as a candidate for the model of Ga_i-A and Ga_i-B under study. Our theoretical calculations also estimate that the HF interaction of a neutral Ga_i should be weaker than 100×10^{-4} cm^{-1}, which cannot explain the observed strong HF interaction. A Ga_i in its Ga_i^{2+} charge state, on the other hand, is predicted to possess a strongly localized electron wave function of A_1 symmetry in agreement with the experimental results. Therefore we can conclude that the Ga atom in the Ga_i-A and Ga_i-B defects is a Ga_i^{2+} interstitial.

The next question is whether both Ga_i-A and Ga_i-B are just simple, isolated Ga_i residing on different Ga_i sites or Ga_i-related complexes. For that we calculated for each microscopic configuration the HF interaction A from the interaction between the spin density of the electron and the nuclear spins. Using state-of-the-art first-principles supercell calculations as implemented in the WIEN2k code,[27] we calculated the electron spin distribution topology that was then used to calculate the HF tensor. The calculations were based on generalized gradient approximations (GGA's) within the framework of density functional theory (DFT), using the all-electron full-potential linearized augmented-plane-wave (FPLAPW) method. The relativistic effects were included through a scalar relativistic treatment for valence electrons. All atoms in the supercell are allowed to relax. The atomic geometry optimization has been performed using the first-principles ultrasoft pseudopotential plane-wave method with GGA as implemented in the VASP code.[28] Our test calculations of a well-established signature, Zn_i in ZnSe,[29] yielded the central HF parameter in good agreement with the experiment to within 10%. A supercell containing 32 atoms, which was sufficient to provide converged HF parameters,[30] was used. The electron density of a free atom was calculated by

placing the atom in a large cubic supercell ($10 \times 10 \times 10$ Å^3) to reduce the intercell interactions. Our theoretical calculations predict strong HF interactions for isolated Ga$_i$ in GaP: i.e., $A(^{69}\text{Ga}) = 1876 \times 10^{-4}$ cm^{-1} for Ga$_i$ at the T_d site surrounded by four Ga atoms and $A(^{69}\text{Ga}) = 1599 \times 10^{-4}$ cm^{-1} for Ga$_i$ at the T_d site surrounded by four P atoms. These values are much larger ($>30\%$) than the experimental values determined for Ga$_i$-A and Ga$_i$-B. A reduced HF interaction is commonly regarded as evidence for a complex due to charge transfer or redistribution of the electron wave function from Ga$_i$ to the other partner(s) of the complex. This conclusion is supported by recent experimental ODMR studies in wurtzite GaN that have convincingly shown that isolated Ga self-interstitials are unstable at temperatures well below room temperature and readily form complexes.[31–33] Considering the more dilute crystal lattice of the GaNP and AlGaNP alloys that makes Ga$_i$ easier to migrate, the isolated Ga self-interstitials in these alloys are more likely to be unstable at the growth temperatures, leading to the formation of complexes. Such complexes usually possess larger binding energies, which are consistent with the observed high thermal stability of the Ga$_i$-A and Ga$_i$-B defects.

C. Localization of electron wave functions at the defects

The degree of localization of the electron wave functions at the defect can be estimated using a one-electron linear combination of atomic orbital (LCAO) scheme.[34] The wave function for the unpaired electron can be constructed as a LCAO centered on the atoms surrounding the defect:

$$\Psi = \sum_i \eta_i \psi_i. \tag{2}$$

The wave function on the ith site can be approximated as a hybrid of the ns, np orbitals:

$$\psi_i = \alpha_i (\psi_{ns})_i + \beta_i (\psi_{np})_i, \tag{3}$$

where $n = 4$ for Ga. The normalization, ignoring the overlap, requires

$$\alpha_i^2 + \beta_i^2 = 1, \quad \sum_i \eta_i^2 = 1. \tag{4}$$

Generally, with an axially symmetric A tensor, the principal values can be described as

$$A_\parallel^i = a_i + 2b_i, \tag{5}$$

$$A_\perp^i = a_i - b_i, \tag{6}$$

where

$$a_i = \frac{8}{3} \pi g_0 g_N \mu_B \mu_N \alpha_i^2 \eta_i^2 |\psi_{4s}(0)|_i^2, \tag{7}$$

$$b_i = \frac{2}{5} g_0 g_N \mu_B \mu_N \beta_i^2 \eta_i^2 \langle r_{3p}^{-3} \rangle_i. \tag{8}$$

Here g_0 and g_N denote electron and nuclear g values. In our case, the HF tensor of the Ga$_i$ site is shown to be isotropic—

i.e., $A_\parallel^{\text{Ga}} = A_\perp^{\text{Ga}}$ and thus $\alpha_{\text{Ga}}^2 = 1$ and $\beta_{\text{Ga}}^2 = 0$. The wave function of the unpaired electron at the Ga$_i$-A and Ga$_i$-B defects can then be approximated as being constructed from the s orbital only.

For a free neutral Ga atom, we calculated the charge density of the $4s$ electron using the relativistic GGA-FP-LAPW method described in Sec. IV B and found $|\psi_{4s}(0)|^2 = 72.7 \times 10^{24}$ cm^{-3}. Based on this, we estimate the localization of the unpaired electron at the Ga$_i$ to be in the range of 12%–30% (Table I). The rather strong localization confirms that these are deep-level defects.

D. Local surrounding of the defects

In a tetrahedral semiconductor like GaNP or AlGaNP, self-interstitials can occupy three high-symmetry positions in which two of them have T_d symmetry surrounded by group-III or group-V atoms, respectively, and the third has hexagonal symmetry (D_{3d}) surrounded by both group-III and group-V sublattices. In order to provide information on the specific Ga$_i$ site and the sublattice immediately surrounding the Ga$_i$ in Ga$_i$-A and Ga$_i$-B, the chemical compositions of each sublattice were varied experimentally by varying Al and N compositions. The results are summarized in Table I. It can be seen that a rather strong reduction (about 10% for Ga$_i$-B) of the HF interaction was observed when the Al composition is raised from $x = 0.00$ to as low as $x = 0.01$. With a further increase in Al composition, however, the rate of decrease in the HF interaction is drastically reduced to about 5% from $x = 0.01$ to $x = 0.30$. This observation indicates that Al directly affects the Ga$_i$-A and Ga$_i$-B defects. The nonlinear dependence also indicates that the presence of Al near the defects may not necessarily follow the statistic distribution expected for random alloy formation.[24] This suggestion is further supported by the fact that the ODMR intensity increases significantly upon incorporation of Al in the alloy. We should point out that the incorporation of Al in GaAs was also required to introduce the Ga$_i$ defect in AlGaAs.[35,36] Moreover, the strength of the HF interaction in the (Al,Ga)As-based structures[35–38] is very close to that of Ga$_i$-A in the Al-containing AlGaNP studied in this work. Assuming that a similar Ga$_i$ defect complex is involved, the correlation between these two alloy systems seems to suggest that the Ga$_i$ in Ga$_i$-A is surrounded by the group-III sublattice as the group-V sublattice is made of completely different atoms between AlGaAs and AlGaNP. In the previous studies of Ga$_i$ in AlGaAs,[35] it was suggested that Ga$_i$ is not very near the group-III sublattice based on the experimental observation that the ODMR spectrum is insensitive to the change of Al composition from 20% to 50%. Our finding of the nonlinear dependence of the HF interaction on Al compositions, which exhibits a much-reduced variation for high Al compositions, questions this earlier suggestion.

In contrast to the dependence on Al composition, the HF interaction of both Ga$_i$-A and Ga$_i$-B defects in GaNP was found in this work to be insensitive to N compositions up to 3%. On the other hand, the incorporation of N is essential for the observation of the Ga$_i$-A and Ga$_i$-B defects in

GaNP. This indicates that either N is directly involved as part of the defect or the required nonequilibrium growth conditions or possible ion bombardment during the incorporation of N in GaNP facilitates the formation of the Ga_i-A and Ga_i-B defects. It is interesting to note that the strength of the HF interaction of Ga_i-A in GaNP, $A(^{69}Ga) = 770 \times 10^{-4}$ cm^{-1}, is very close to 741×10^{-4} cm^{-1} observed for the Ga_i in its parent GaP.[39] The same applies to Ga_i-A in AlGaNP; i.e., $A(^{69}Ga) = (450$–$490) \times 10^{-4}$ cm^{-1} is very close to 500×10^{-4} cm^{-1} observed in the AlGaAs-based alloys.[35–38] In contrast, Ga_i-B was never observed in N-free GaP and AlGaAs-based alloys. This may indicate that N could be directly involved in the structure of the Ga_i-B defect.

E. Recombination processes

The ODMR signals were detected as changes of the PL intensity induced by the spin resonance. The sign of the ODMR signals can thus provide us with useful information about the role of the involved defects in carrier recombination processes.

In the GaNP/GaP series of samples, in Figs. 1 and 6, the ODMR signals correspond to a decrease upon spin resonance in the intensity of all monitored PL emissions over the entire spectral range. Such a negative and emission-insensitive ODMR signal has often been taken as a signature of a nonradiative defect,[10,39] which is not directly related to the monitored PL emissions. The reason why a nonradiative defect can be detected via a radiative recombination process lies on their competition in recombination of photogenerated free carriers. Figure 8(a) shows schematically the recombination processes leading to the observation of the negative ODMR signals. Spin-resonance-enhanced recombination via a nonradiative defect leads to a reduction of free carriers available for radiative recombination and thus to a decrease in the intensity of PL emissions.[10,11,25,40] Such nonradiative recombination can occur via a single defect or via intercenter charge transfer[41] between two defects—e.g., between the "$g=2$" defect and Ga_i-A (or Ga_i-B). The latter scenario is quite likely in the present case, judging from the simultaneous appearance of these two defects for each sample under various measurement conditions. Therefore it can be concluded that Ga_i-A, Ga_i-B, and the "$g=2$" defect act as nonradiative recombination channels, reducing the radiative efficiency of the alloys. This is confirmed by an anticorrelation between the intensities of the visible PL emissions and the ODMR signals, in Fig. 9. For example, a significant increase in the ODMR intensity of the Ga_i-A and Ga_i-B defects (and also the "$g=2$" defect) can be observed with increasing N composition, which is accompanied by a substantial decrease of the visible PL emissions. These defects can undermine performance of potential photonic and optoelectronic devices and therefore should be addressed adequately. The observed increase of the NIR PL in Fig. 9, on the other hand, can be explained by the fact that the NIR PL originates from defects that were introduced by the incorporation of N.
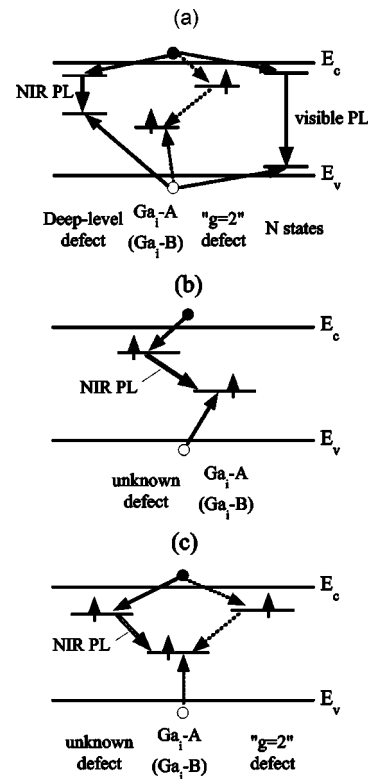
FIG. 8. (a) A schematic diagram of the carrier recombination processes leading to the observation of negative ODMR signals in GaNP/GaP. The spin resonance induces an increase in the nonradiative recombination (indicated by the dashed arrows) via the "$g=2$" and Ga_i-A (or Ga_i-B) defects and a decrease in the radiative recombination process monitored by the PL in both the visible and NIR spectral ranges. (b) A schematic diagram of the carrier recombination process leading to the observation of positive ODMR signals in GaNP/Si; i.e., the spin-resonance-induced increase in the radiative recombination via the unknown defect and Ga_i-A (or Ga_i-B) is directly monitored by the NIR PL. (c) A schematic diagram of the competitive carrier recombination processes leading to the observation of positive and negative ODMR signals in the AlGaNP/GaP series of samples.

In the $GaN_{0.018}P_{0.982}$/Si samples, the ODMR signals were found to be positive by monitoring the NIR PL emissions (Figs. 1 and 7). This can be explained as follows: The monitored PL emission is directly related to the defects—e.g., intercenter charge transfer between an unknown defect and the Ga_i-A (or Ga_i-B) defect [see Fig. 8(b)]. The spin-resonance-enhanced radiative recombination between them leads to an intensity increase of the corresponding PL. It should be pointed out that the "$g=2$" defect is absent in this case. Instead, a broad background ODMR was detected, as shown in Fig. 7, of which the origin of the corresponding defect is still unknown. It is denoted as "unknown defect" in Fig. 8(b). The energy of the related PL emission can usually be employed to estimate the energy position of the defect level if the recombination process is fully understood. Since the spin-dependent recombination processes involving the Ga_i defects are likely to be of an intercenter charge transfer origin and the energy position of the other partner is unknown, at present we are not able
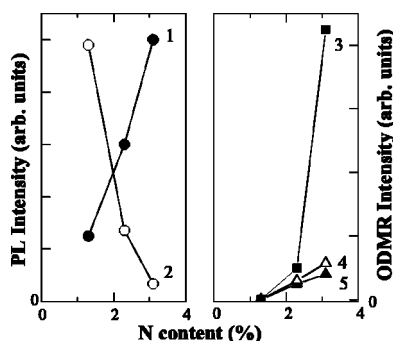
FIG. 9. Relative intensities of the PL emissions and the ODMR signals as a function of the N composition, obtained from the GaNP/GaP series of samples. The open and solid circles denote the intensities of the visible and NIR PL emissions, respectively. The solid and open triangles represent the intensities of the Ga_i-A and Ga_i-B ODMR signals, respectively. The solid squares denote the ODMR intensity of the "$g=2$" defect.

to precisely deduce the energy level positions of the Ga_i defects. However, a rough estimate of the energy position for the Ga_i-B defect can be made to be at least >1.2 eV away from either the conduction or valence band edge.

In the AlGaNP/GaP series of samples, on the other hand, both positive and negative ODMR signals have been observed, depending on the Al compositions and the monitored PL. In the Al-free sample, positive ODMR signals similar to that from the $GaN_{0.018}P_{0.982}$/Si sample were detected by monitoring the NIR PL. The recombination process can thus be described in a similar fashion as discussed above and shown in Fig. 8(b). In the Al-containing AlGaNP, however, the ODMR signals switch sign to become negative. This is accompanied by the appearance of the "$g=2$" defect and a simultaneous disappearance of the "unknown defect" in the ODMR spectra, as shown in Fig. 5. This sign change can be understood, as schematically shown in Fig. 8(c), by the following competing intercenter charge transfer and recombination processes between these defects: (1) the nonradiative recombination between the "$g=2$" and Ga_i-A (or Ga_i-B) defects, which gives rise to negative ODMR signals, and (2) the radiative recombination between the "unknown defect" and the Ga_i-A (or Ga_i-B) defect, which gives rise to positive ODMR signals. In principle, both processes coexist and the sign of the combined ODMR signals depends on their relative importance. The change of the signal sign from positive in the Al-free sample to negative in the Al-containing samples as soon as Al is incorporated suggests that process (1) becomes dominant over process (2). With increasing Al composition, the intensity of the negative ODMR signals in Fig. 10 increases, signifying the importance of the nonradiative recombination between the "$g=2$" and Ga_i-A (or Ga_i-B) defects. With a further increase of the Al composition to 30%, however, the ODMR intensity decreases for all defects. This is a sign that other nonradiative defects become important and overshadow the above defects.

It should be pointed out that, although the intercenter charge transfer is shown in Fig. 8 only from the "$g=2$" de-
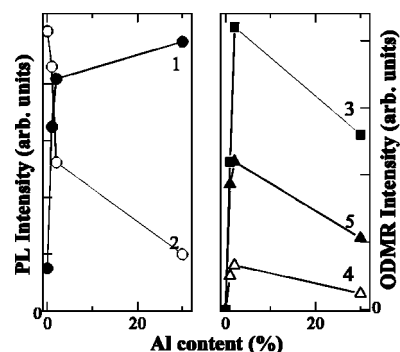
FIG. 10. Relative intensities of the PL emissions and the ODMR signals as a function of the Al composition, obtained from the AlGaNP/GaP series of samples. The legends are the same as in Fig. 9.

fect (or the "unknown defect") to the Ga_i-A (or Ga_i-B) defect, the reverse process is also possible if their energy order is reversed. This possibility holds as long as the paramagnetic charge state of Ga_i in the Ga_i-A (or Ga_i-B) defect, before the charge transfer, is $2+$.

V. CONCLUSIONS

In summary, we have studied and identified two different Ga_i defects in dilute nitride AlGaNP by ODMR. The assignment of Ga_i to both defects is concluded from its unique HF interaction. Both defects are complexes involving a Ga_i^{2+}. The redistribution of the electron wave function leads to a reduction of the HF interaction. The HF interaction also strongly depends on the presence of Al, indicating that the defects may be surrounded by group-III atoms. The incorporation of both Al and N is shown to play an important role in the formation of the defects, indicative of the involvement of N in Ga_i-B. The defects are found to introduce energy levels deep inside the band gap—e.g., ~ 1.2 eV from the conduction (or valence) band edge for the Ga_i-B defect. In most cases, these defects act as nonradiative recombination centers reducing the efficiency of light emissions from the alloys. They can thus undermine the performance of photonic devices based on these materials. In view of the high thermal stability (at up to 900 °C) of the defects, post-growth RTA was found to be inadequate to remove the defects. Future studies are needed to control their formation during the growth, in order to improve radiative efficiency. The present studies also shed new light on Ga self-interstitials in III-V's in general.

*Permanent address: Institute of Semiconductor Physics, Pr. Nauky 45, Kiev 03028, Ukraine.

†Corresponding author: wmc@ifm.liu.se

[1] G. M. Martin and S. Makram-Ebeid, in *Deep Centers in Semiconductors*, edited by S. Pantelides (Gordon and Breach, New York, 1986), p. 389.

[2] X. Liu, A. Prasad, W. M. Chen, A. Kurpiewski, A. Stoschek, Z. Liliental-Weber, and E. R. Weber, Appl. Phys. Lett. **65**, 3002 (1994).

[3] W. M. Chen, I. A. Buyanova, A. Buyanov, T. Lundström, W. G. Bi, and C. W. Tu, Phys. Rev. Lett. **77**, 2734 (1996).

[4] W. M. Chen, P. Dreszer, A. Prasad, A. Kurpiewski, W. Walukiewicz, E. R. Weber, E. Sörman, B. Monemar, B. W. Liang, and C. W. Tu, J. Appl. Phys. **76**, 600 (1994).

[5] G. D. Watkins, Semicond. Semimetals **51A**, 1 (1998).

[6] J.-M. Spaeth, J. R. Niklas, and R. H. Bartram, *Structural Analysis of Point Defects in Solids* (Springer-Verlag, New York, 1992).

[7] U. Kaufmann and J. Schneider, Festkoerperprobleme **20**, 87 (1980).

[8] B. C. Cavenett, Adv. Phys. **30**, 475 (1981).

[9] T. A. Kennedy and E. R. Glaser, Semicond. Semimetals **51A**, 93 (1998).

[10] W. M. Chen, Thin Solid Films **364**, 45 (2000).

[11] W. M. Chen, in *EPR of Free Radicals in Solids*, edited by A. Lund and M. Shiotani (Kluwer Academic, Dordrecht, 2003), p. 601.

[12] J. N. Baillargeon, K. Y. Cheng, G. E. Hofler, P. J. Pearah, and K. C. Hsieh, Appl. Phys. Lett. **60**, 2540 (1992).

[13] X. Liu, S. G. Bishop, J. N. Baillargeon, and K. Y. Cheng, Appl. Phys. Lett. **63**, 208 (1993).

[14] S. Miyoshi, H. Yaguchi, K. Onabe, and R. Ito, Appl. Phys. Lett. **63**, 3606 (1993).

[15] L. Bellaiche, Su-Huai Wei, and Alex Zunger, Phys. Rev. B **56**, 10 233 (1997).

[16] W. Shan, W. Walukiewicz, K. M. Yu, J. Wu, J. W. Ager III, E. E. Haller, H. P. Xin, and C. W. Tu, Appl. Phys. Lett. **76**, 3251 (2000).

[17] H. P. Xin, C. W. Tu, Yong Zhang, and A. Mascarenhas, Appl. Phys. Lett. **76**, 1267 (2000).

[18] I. A. Buyanova, G. Pozina, J. P. Bergman, W. M. Chen, H. P. Xin, and C. W. Tu, Appl. Phys. Lett. **81**, 52 (2002).

[19] H. Yonezu, Semicond. Sci. Technol. **17**, 762 (2002).

[20] K. Momose, H. Yonezu, Y. Fujimoto, Y. Furukawa, Y. Motomura,

and K. Aiki, Appl. Phys. Lett. **79**, 4151 (2001).

[21] I. Suemune, K. Uesugi, and T.-Y. Seong, Semicond. Sci. Technol. **17**, 755 (2002).

[22] K. Onabe, in *III-V Nitrides*, edited by F. A. Ponce, T. D. Monstakas, I. Akasaki, and B. A. Monemar, Mater. Res. Soc. Symp. Proc. No. 449 (Materials Research Society, Pittsburgh, 1997), p. 23.

[23] N. Q. Thinh, I. P. Vorona, I. A. Buyanova, W. M. Chen, S. Limpijumnong, S. B. Zhang, Y. G. Hong, H. P. Xin, C. W. Tu, A. Utsumi, Y. Furukawa, S. Moon, A. Wakahara, and H. Yonezu, Phys. Rev. B **70**, 121201(R) (2004).

[24] N. Q. Thinh, I. P. Vorona, M. Izadifard, I. A. Buyanova, W. M. Chen, Y. G. Hong, H. P. Xin, and C. W. Tu, Appl. Phys. Lett. **85**, 2827 (2004).

[25] I. A. Buyanova, G. Yu. Rudko, W. M. Chen, H. P. Xin, and C. W. Tu, Appl. Phys. Lett. **80**, 1740 (2002).

[26] G. A. Baraff and M. Schluter, Phys. Rev. Lett. **55**, 1327 (1985).

[27] P. Blaha, K. Schwarz, G. K. H. Madsen, D. Kvasnicka, and J. Luitz, computer code WIEN2K, An Augmented Plane Wave + Local Orbitals Program for Calculating Crystal Properties, Karlheinz Schwarz, Technical Universität Wien, Austria, 2001.

[28] G. Kresse and J. Furthmüller, Comput. Mater. Sci. **6**, 15 (1996).

[29] F. Rong and G. D. Watkins, Phys. Rev. Lett. **58**, 1486 (1987).

[30] C. G. Van de Walle and P. E. Blöchl, Phys. Rev. B **47**, 4244 (1993).

[31] M. Linde, S. J. Uftring, G. D. Watkins, V. Härle, and F. Scholz, Phys. Rev. B **55**, R10 177 (1997).

[32] C. Bozdog *et al.*, Phys. Rev. B **59**, 12 479 (1999).

[33] K. H. Chow and G. D. Watkins, Phys. Rev. Lett. **85**, 2761 (2000).

[34] G. D. Watkins and J. W. Corbett, Phys. Rev. **121**, 1001 (1961).

[35] T. A. Kennedy and M. G. Spencer, Phys. Rev. Lett. **57**, 2690 (1986).

[36] T. A. Kennedy, R. Magno, and M. G. Spencer, Phys. Rev. B **37**, 6325 (1981).

[37] J. M. Trombetta, T. A. Kennedy, W. Tseng, and D. Gammon, Phys. Rev. B **43**, 2458 (1991).

[38] T. Wimbauer *et al.*, Phys. Rev. B **58**, 4892 (1998).

[39] K. M. Lee, in *Defects in Electronic Materials*, edited by M. Stavola *et al.*, Mater. Res. Soc. Symp. Proc. No. 104 (Material Research Society, Pittsburgh, 1988), p. 449.

[40] W. M. Chen and B. Monemar, Phys. Rev. B **40**, 1365 (1989).

[41] W. M. Chen, B. Monemar, E. Janzén, and J. L. Lindström, Phys. Rev. Lett. **67**, 1914 (1991).

PHYSICAL REVIEW LETTERS

Evidence for Native-Defect Donors in *n*-Type ZnO

D. C. Look,[1,2] G. C. Farlow,[1] Pakpoom Reunchan,[3] Sukit Limpijumnong,[3,4] S. B. Zhang,[4] and K. Nordlund[5]

[1]*Semiconductor Research Center, Wright State University, Dayton, Ohio 45435, USA*
[2]*Materials and Manufacturing Directorate, Air Force Research Laboratory, Wright-Patterson Air Force Base, Ohio 45433, USA*
[3]*School of Physics, Suranaree University of Technology and National Synchrotron Research Center, Nakhon Ratchasima, Thailand*
[4]*National Renewal Energy Laboratory, Golden, Colorado 80401, USA*
[5]*Accelerator Laboratory, University of Helsinki, FIN-00014, Helsinki, Finland*

Recent theory has found that native defects such as the O vacancy V_O and Zn interstitial Zn_I have high formation energies in *n*-type ZnO and, thus, are not important donors, especially in comparison to impurities such as H. In contrast, we use both theory and experiment to show that, under N ambient, the complex Zn_I-N_O is a stronger candidate than H or any other known impurity for a 30 meV donor commonly found in bulk ZnO grown from the vapor phase. Since the Zn vacancy is also the dominant acceptor in such material, we must conclude that native defects are important donors and acceptors in ZnO.

PACS numbers: 61.72.Ji, 71.55.Gs, 72.20.Fr, 78.55.Et

Semiconducting ZnO has generated great interest in the past decade because of advances in bulk and epitaxial growth that have opened the door for new photonic and electronic applications, such as UV light emitting diodes and transparent transistors [1,2]. Previous research had established that ZnO was always *n*-type and that the dominant donors were usually shallow with activation energies of between 30 and 60 meV [3,4]. Because it was also known that the crystal growth was typically Zn-rich, the dominant donor was almost always identified as either the O vacancy V_O or the Zn interstitial Zn_I [5,6]. This model was strongly challenged in the year 2000 when Kohan *et al.* showed theoretically that both V_O and Zn_I have high formation energies in *n*-type ZnO and that, furthermore, both are deep, not shallow, donors [7]. More recent theory has concluded that Zn_I is actually a shallow donor, rather than deep [8,9], as has also been suggested by electron-irradiation experiments [6]; however, its high formation energy would still limit its participation in the conductivity of *n*-type material. Also in the year 2000, the defect-donor model was further challenged by Van de Walle's theoretical result that H is always a donor in ZnO, that it is easily ionized, and that it has a low enough formation energy to be abundant; thus, Van de Walle suggested that it was likely to be a dominant background donor in ZnO materials that were exposed to H during growth [10]. This proposal has been amenable to testing, because H-containing, high-quality, bulk ZnO, grown by a seeded chemical vapor transport (SCVT) technology, has been commercially available for the past few years. For the most part, these tests have confirmed that a shallow donor due to H exists in SCVT ZnO and can contribute significantly to the conductivity [11–16]. This fact, coupled with the theoretical evidence of high formation energies for the native donors [7], has led to a prevailing opinion that native donors do not play a significant role in the conductivity of as-grown ZnO. In contrast, we will offer evidence here that native donors

can contribute significantly to conduction in ZnO but as complexes, rather than isolated elements.

The main sample used in this study was a 5 mm × 5 mm × 0.42 mm piece cut from a wafer grown by the SCVT technique at ZN Technology, Inc. [17]. Material of this type is of very high quality, with peak electron mobility >2000 cm^2/V s, 300 K carrier concentration in the 10^{16} cm^{-3} range, and photoluminescence (PL) linewidths under 0.5 meV, as shown in Figs. 1 and 2 [4]. The sample was first annealed at 715 °C, in order to release most of the H [14,15], then was irradiated with high-energy electrons to create point defects, and finally was annealed again at temperatures from 200–500 °C, in order to investigate the annihilation of the point defects. As seen in Fig. 1, several sharp PL lines appear in the region 3.357–3.365 eV, and these spectral features are usually assigned to transitions of excitons bound to neutral donors (D^0X transitions), in which the donor remains in its ground state ($n = 1$) during the transition. Some of these lines have been tentatively identified; for example, the lines at 3.35964 eV (I_8 or I_{8a} in
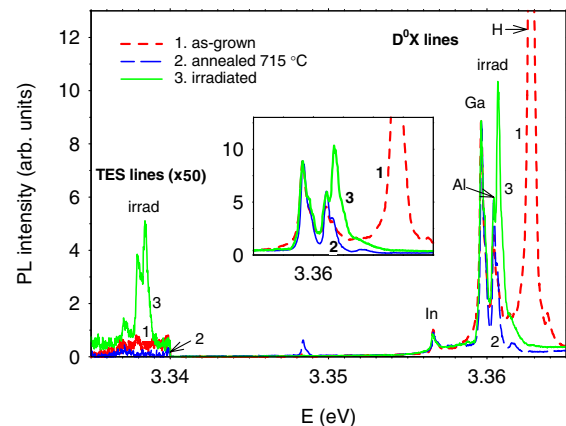

FIG. 1 (color online). 4-K photoluminescence spectra for ZnO sample. The inset shows the D^0X lines in greater detail.

the literature) and 3.36042 eV (I_6 or I_{6a}) have been assigned to Ga_{Zn} and Al_{Gn}, respectively. (See Ref. [18] for an excellent review of PL in ZnO.) All of the spectra presented in this work are normalized to the I_8 line, because it is relatively isolated and also not expected to change significantly as a result of annealing or irradiation treatments. However, the most dominant PL line in this particular sample before annealing is the D^0X line at 3.36270 eV (I_4), now almost universally assigned to interstitial H [16,18]. This identification results at least partially from annealing experiments, because I_4 disappears for anneals above 600 °C, in good correlation with the effusion of H from the sample [14–16,19]. Our sample behaves in the same way, as evidenced by the strong reduction of I_4 after an anneal of 715 °C (curve 2 in Fig. 1). Not shown in Fig. 1 is a two-electron satellite (TES) replica of I_4, appearing at 3.32961 eV. A TES transition is one in which the donor is left in an excited $n = 2$ state after the collapse of the exciton. If the donor associated with I_4 follows a hydrogenic model, then the ground-state ($n = 1$) energy of this donor should be given by $4/3(3.36270 - 3.32961) = 44.1$ meV. Other TES transitions, also not shown, are seen near 3.32 eV and may be associated with I_6 and I_8 [18]. If so, then the hydrogenic model would predict -ground-state energies of 53–55 meV for these donors, presumably associated with Ga_{Zn} and Al_{Zn}. Thus, the donors identified from PL are H, at 44 meV, and Ga_{Zn} and Al_{Zn}, at about 55 meV.

To create point defects, we have used the Van de Graaff electron accelerator at Wright State University. The sample was irradiated on the Zn face (0001) with 1 MeV electrons three separate times, making a total fluence of 3×10^{17} cm^{-2}. The PL spectrum after the third irradiation is presented as curve 3 in Fig. 1. A new sharp defect line at 3.36070 eV, which we will designate as I_D, is generated by the irradiation. Concomitantly, a triplet feature, comprised of energies 3.33711, 3.33793, and 3.33840 eV, is also generated. These we will designate $I_{D,TES1}$, $I_{D,TES2}$, and $I_{D,TES3}$. This triplet has an intensity about 100 times less than that of I_D, and this reduction is about the same as that observed for the TES line of H compared with its parent line, I_4. Thus, the defect triplet at 3.338 eV clearly is related to I_D, and, if the hydrogenic model holds, the associated energy is $4/3(3.3607 - 3.3379) \approx 30.4$ meV. This value is less than that predicted from an empirical version of Haynes' rule presented in Ref. [18]. However, that version was developed for simple, isolated impurities, Al, Ga, In, and H, and there is no reason to expect that it should hold for a defect-related complex. Both I_D and its TES triplet are greatly reduced for anneals greater than 500 °C (not shown), evidently due to defect recombination. It is important to note at this point that the as-grown sample, represented by curve 1 in Fig. 1, has two small lines at the energies of $I_{D,TES1}$ and $I_{D,TES2}$, respectively, and possibly also a line in the I_D region, although obscured by I_6. This is our first indication that the *as-grown* sample contains defect-related donors.

We next discuss the temperature-dependent mobility μ and carrier concentration n, shown in Fig. 2. To avoid clutter, we show curves representing only four stages in the evolution of this sample: (1) as-grown; (2) annealed at 715 °C for 1/2 hour in flowing N_2 gas; (3) irradiated with 1 MeV electrons, in three equal stages up to a total fluence of 3×10^{17} cm^{-2}; and (4) annealed at 400 °C, following previous anneals beginning at 200 °C. It should be noted that a final anneal at 500 °C (not shown) eliminated almost all of the irradiation damage and basically returned the μ and n curves to those of stage 2. [Note that a return to the μ and n curves of stage 1 (as-grown) is of course impossible, because the H content was lost in stage 2, the first 715 °C anneal.]

The mobility data (inset in Fig. 2) were fitted to an accurate charge-carrier scattering theory, described elsewhere [20], and the only fitting parameter was the acceptor concentration N_A. The carrier concentration data of Fig. 2 were then fitted to the charge-balance equation:

$$n + N_A = \sum_i \frac{N_{Di}}{1 + n/\phi_{Di}}, \tag{1}$$

where the subscript i denotes a particular donor and where ϕ_{Di} is a function of T and E_{Di}, the donor energy [cf. Eq. (8) of Ref. [20]]. The fitting parameters in Eq. (1) are the donor concentrations (N_{Di}'s), donor energies (E_{Di}'s), and acceptor concentration N_A. Excellent fits to the n vs $1/T$ data in Fig. 2 were obtained by also including a degenerate surface layer in the analysis [20,21].

The PL results discussed above determined the energies of three different donors, calculated from their respective TES lines: 55 meV, possibly associated with Ga_{Zn} and/or Al_{Zn}; 44 meV, associated with H; and 30 meV, produced by irradiation and thus associated with a defect. Indeed, the 30 and 44 meV energies turn out to be good fitting parameters for two of the three donors required to fit our Hall-effect data, but the third donor is best fitted with about 75 meV, rather than 55 meV. The carrier concentration fits are
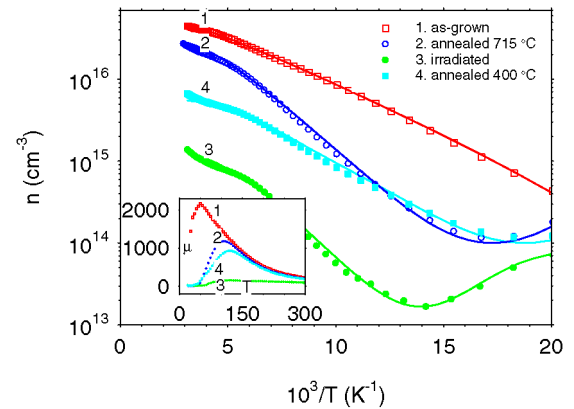

FIG. 2 (color online). Temperature-dependent carrier concentration for ZnO sample. The solid lines are theoretical fits. The inset shows the experimental mobility curves after the same four treatments.

shown as solid lines in Fig. 2, and the fitting parameters are given in Table I. Two major conclusions are evident from the results: (1) the 44 meV H level essentially disappears during the 715 °C anneal, in agreement with the PL data; and (2) a 30 meV level is produced by irradiation but also exists in the as-grown sample and the sample annealed at 715 °C. It should be emphasized that the choice of 30 meV as a Hall fitting parameter is not dependent on the fact that the PL analysis also found a donor at 30 meV. Indeed, a donor of this energy has been found previously by a number of groups to give good fits to ZnO Hall-effect data [3,4,6]. To help identify this 30 meV donor, we appeal to theory.

First of all, we calculate the expected 1 MeV-electron-bombardment production rates of Zn and O Frenkel pairs from molecular dynamics simulations [22]. The threshold energies were calculated by giving a randomly chosen O or Zn atom a recoil energy in a random direction in an experimentally controlled angular window of 15 degrees around the desired (0001) direction. The interatomic interaction model for the ZnO system will be published elsewhere [23], but the potential development principles are described in Ref. [24]. To account for the experimental situation with a beam acceptance angle, the threshold was determined as the average over the direction-specific thresholds obtained within the 15° angular window.

For Zn-face (0001) irradiation at 300 K, the threshold for O displacement is 44 eV, and that for Zn displacement, 34 eV. We then apply the McKinley-Feshbach relativistic cross-section formula [25] to give effective production rates of 0.18 cm^{-1} for O displacement and 0.30 cm^{-1} for Zn displacement. Thus, we would expect that our fluence of 3×10^{17} cm^{-2} would produce O_I and V_O concentrations of about 5×10^{16} cm^{-3} and Zn_I and V_{Zn} concentrations of about 9×10^{16} cm^{-3}. Either of these numbers is consistent with the observed 30 meV donor concentration of about 2×10^{17} cm^{-3} in the irradiated sample (see Table I), because the value 2×10^{17} cm^{-3} is actually an upper limit. That is, the mobility after such a heavy irradiation is almost certainly reduced by electrical inhomogeneity, and, thus, it is artificially low, leading to artificially high donor and acceptor concentrations. However, the concentration of Zn_I should still be about twice that of V_O, and, moreover, there is abundant evidence that V_O is a deep, not shallow, donor [7–9,26]. Thus, Zn_I is a much better candidate for the irradiation donor than V_O. However, there also is evidence that isolated Zn_I is mobile

at room temperature, so that it likely has to form a complex to be stable [27,28].

A search for potential complexing partners for Zn_I immediately suggests N, which easily substitutes for O in the ZnO lattice and which indeed has a concentration of about 10^{17} cm^{-3} in ZnO material of the type we are using [29]. Thus, we have examined the formation energy, binding energy, and $(0/+)$ transition energy of the complex Zn_I-N_O using first principles calculations. We applied density functional theory (DFT) within the local density approximation (LDA) and used Vanderbilt-type ultrasoft pseudopotentials, as implemented in the VASP code [30]. To obtain defect formation energies, defined elsewhere [31,32], a supercell approach was used, with a ZnO supercell size of 96 atoms. The main result of the calculation is that the binding energy of the Zn_I-N_O complex is about 0.9 eV; thus, the complex should be stable at room temperature. The formation energies of the N_O, Zn_I, and Zn_I-N_O species in ZnO depend on the Fermi energy and the partial pressures of the elements or, in other words, the chemical potentials of the elements, during growth. The secondary-ion mass-spectroscopy measurements [29] found a N concentration [N] of about 1×10^{17} cm^{-3}. Based on our calculated formation energies of N_O, Zn_I, and Zn_I-N_O, together with the measured N concentration ([N] = [N_O] + [Zn_I-N_O]), we estimate a N chemical potential of 0.92 eV below the N_2 precipitation limit (assuming Zn-rich and charge-neutral growth conditions and a growth temperature of 950 °C). The calculated formation energy [33] shows that, during growth, N_O^- acts as the dominant acceptor and Zn_I^{2+} as the dominant donor, with the Fermi energy pinned at about 1.0 eV above the valence band where the two defects have approximately the same energy, about 1.4 eV. The corresponding defect concentrations are on the order of 10^{17} cm^{-3}. The concentration of the Zn_I-N_O complex is about 2 orders of magnitude lower, as determined from the reaction $N_O + Zn_I \rightarrow Zn_I$-$N_O$ + 0.9 eV and the associated detailed-balance relationship $[N_O][Zn_I]/N_{site}[Zn_I$-$N_O] = \exp(-E_b/kT)$. Here we use $N_{site}(ZnO) = 4.28 \times 10^{22}$ cm^{-3} and $E_b = 0.9$ eV. At $T = 950$ °C, we get $[Zn_I$-$N_O]/[Zn_I] = 0.012$, which means that only about 1/100 of the Zn_I ions take part in formation of the complex. However, during cooldown, it is expected that the formation of the complex will accelerate, assuming a sufficiently low Zn_I diffusion barrier. As the temperature cools to about 500 °C, the quantity $[Zn_I$-$N_O]/[Zn_I]$ approaches unity, which means that about half of the Zn_I are already bound in the com-

TABLE I. Fitting parameters for mobility and carrier concentration data.

	E_{D1} (meV)	N_{D1} (10^{16} cm^{-3})	E_{D2} (meV)	N_{D2} (10^{16}cm^{-3})	E_{D3} (meV)	N_{D3} (10^{16}cm^{-3})	N_A (10^{16}cm^{-3})
As-grown	30	0.45	44	3.0	75	2.0	0.13
715 °C	30	0.74			75	3.2	0.7
Irradiated	30	~20			75	0.13	~20
400 °C	30	1.35			75	0.4	1.2

plexes. At room temperature, $[Zn_I\text{-}N_O]/[Zn_I] \approx 10^9$, so that nearly 100% of the Zn_I are in complexes. With other impurities (such as H_I) in the sample, the above balance conditions would vary somewhat, but the main conclusions should remain the same.

The electronic transition energy of $Zn_I\text{-}N_O$ is somewhat uncertain, due to the well-known LDA gap error. However, our calculations show that the donor level of $Zn_I\text{-}N_O$ is shallower than that of isolated Zn_I, which itself is argued to be a shallow donor [8,9]. In addition, a wave function analysis of Zn_I shows delocalization, which is characteristic of a shallow level. In short, although the $(0/+)$ transition energy of $Zn_I\text{-}N_O$ cannot be accurately calculated, it is entirely consistent with the observed value of 30 meV. Further details of these calculations will be published elsewhere.

It is also interesting to compare the 0.9 eV binding energy with the activation energy for irradiation-defect annealing in ZnO, measured previously as 1.7 eV [34]. The difference between these two energies, 0.8 eV, should be the motional energy for Zn_I and is a reasonable value for an interstitial.

Other evidence for a $Zn_I\text{-}N_O$ complex comes from optically detected magnetic resonance experiments in epitaxial N-doped ZnO [35]. An observed spin-$1/2$ center was consistent with a Zn interstitial, possibly in association with an N atom, since it was not observed in a sample with lower N content. Besides Zn_I, other donors, such as H, are also believed to associate with N [14,36]. However, H-N would be neutral, whereas Zn_I-N has a shallow-donor level.

Finally, other Zn_I-acceptor complexes that behave as shallow donors are also predicted to be stable. For example, very recently Wardle *et al.* [37] have used DFT to show that $Zn_I\text{-}Li_{Zn}$ is bound by 0.7 eV and has a shallow-donor transition. This result further strengthens and generalizes our assertion that Zn_I-related shallow donors can exist and be important in as-grown ZnO.

In summary, we have carried out extensive low-temperature photoluminescence and temperature-dependent Hall-effect measurements on irradiated ZnO and have identified a defect-related donor at about 30 meV, which also exists in as-grown ZnO. We have further carried out molecular dynamics simulations, to show that the expected production rate of Zn_I is consistent with the concentrations of the 30 meV donor after irradiation, and density functional calculations to show that the $Zn_I\text{-}N_O$ defect complex is a shallow donor with a sufficient binding energy to explain the annealing data. Thus, the conclusion is that native-defect-related donors can exist in n-type ZnO and contribute to its conductance.

[1] D. C. Look, Mater. Sci. Eng. B **80**, 383 (2001).
[2] S. J. Pearton *et al.*, Prog. Mater. Sci. **50**, 293 (2005).
[3] P. Wagner and R. Helbig, J. Phys. Chem. Solids **35**, 327 (1974).
[4] D. C. Look *et al.*, Solid State Commun. **105**, 399 (1998).
[5] F. A. Kröger, *The Chemistry of Imperfect Crystals* (North-Holland, Amsterdam, 1964).
[6] D. C. Look, J. W. Hemsky, and J. R. Sizelove, Phys. Rev. Lett. **82**, 2552 (1999).
[7] A. F. Kohan *et al.*, Phys. Rev. B **61**, 15 019 (2000).
[8] F. Oba *et al.*, J. Appl. Phys. **90**, 824 (2001).
[9] S. B. Zhang, S.-H. Wei, and A. Zunger, Phys. Rev. B **63**, 075205 (2001).
[10] C. G. Van de Walle, Phys. Rev. Lett. **85**, 1012 (2000).
[11] S. F. J. Cox *et al.*, Phys. Rev. Lett. **86**, 2601 (2001).
[12] D. M. Hofmann *et al.*, Phys. Rev. Lett. **88**, 045504 (2002).
[13] K. Shimomura, K. Nishiyama, and R. Kadono, Phys. Rev. Lett. **89**, 255505 (2002).
[14] N. H. Nickel and K. Fleischer, Phys. Rev. Lett. **90**, 197402 (2003).
[15] K. Ip *et al.*, Appl. Phys. Lett. **82**, 385 (2003).
[16] Y. M. Strzhemechny *et al.*, Appl. Phys. Lett. **84**, 2545 (2004).
[17] ZN Technology, 910 Columbia Street, Brea, CA 92821, USA.
[18] B. K. Meyer *et al.*, Phys. Status Solidi B **241**, 231 (2004).
[19] D. C. Look *et al.*, Phys. Status Solidi A **195**, 171 (2003).
[20] D. C. Look, Semicond. Sci. Technol. **20**, S55 (2005).
[21] D. C. Look and R. J. Molnar, Appl. Phys. Lett. **70**, 3377 (1997).
[22] J. Nord, K. Nordlund, and J. Keinonen, Phys. Rev. B **68**, 184104 (2003).
[23] P. Erhart, K. Albe, N. Juslin, and K. Nordlund (to be published).
[24] J. Nord *et al.*, J. Phys. Condens. Matter **15**, 5649 (2003).
[25] F. Agullo-Lopez, C. R. A. Catlow, and P. D. Townsend, *Point Defects in Materials* (Academic, New York, 1988).
[26] P. Kasai, Phys. Rev. **130**, 989 (1963).
[27] Yu. V. Gorelkinskii and G. D. Watkins, Phys. Rev. B **69**, 115212 (2004).
[28] C. Coşkun *et al.*, Semicond. Sci. Technol. **19**, 752 (2004).
[29] D. C. Look *et al.*, Appl. Phys. Lett. **81**, 1830 (2002).
[30] G. Kresse and J. Furthmüller, Comput. Mater. Sci. **6**, 15 (1996).
[31] S. B. Zhang and J. E. Northrup, Phys. Rev. Lett. **67**, 2339 (1991).
[32] S. Limpijumnong *et al.*, Phys. Rev. Lett. **92**, 155504 (2004).
[33] See EPAPS Document No. E-PRLTAO-030548 for the calculated defect formation energy. This document can be reached via a direct link in the online article's HTML reference section or via the EPAPS homepage (http://www.aip.org/pubservs/epaps.html).
[34] D. C. Look *et al.*, Appl. Phys. Lett. **75**, 811 (1999).
[35] G. N. Aliev *et al.*, Phys. Rev. B **70**, 115206 (2004).
[36] N. Ohashi *et al.*, J. Appl. Phys. **93**, 6386 (2003).
[37] M. G. Wardle, J. P. Goss, and P. R. Briddon, Phys. Rev. B **71**, 155205 (2005).

ELSEVIER

Probing deactivations in Nitrogen doped ZnO by vibrational signatures: A first principles study

Sukit Limpijumnong[a,b,*], Xiaonan Li[c], Su-Huai Wei[c], S.B. Zhang[c]

[a]*National Synchrotron Research Center, Nakhon Ratchasima, Thailand*
[b]*School of Physics, Suranaree University of Technology, Nakhon Ratchasima, Thailand*
[c]*National Renewable Energy Laboratory, Golden, CO, USA*

Abstract

Based on first principles calculations, we investigate two probable types of deactivation mechanisms that hinder current efforts of doping ZnO p-type. (i) Passivation by Hydrogen. H prefers to bind with N_O at the anti-bonding site and form N_O–H complexes with a binding energy of about 1 eV. (ii) Passivation by the formation of substitutional diatomic molecules (SDM). Carbon impurities and excess N strongly prefer to passivate N_O and form low-energy SDM on the Oxygen site, $(NC)_O$ or $(N_2)_O$, both of which are donors with several-eV binding energies. Our calculated vibrational frequencies of N_O–H complexes and SDMs are consistent with the frequencies recently observed by IR measurement on N-doped ZnO, which is not p-type.
© 2005 Elsevier B.V. All rights reserved.

1. Introduction

Recent SIMs results on nitrogen-doped ZnO grown by chemical vapor deposition technique show a substantial amount of H, C and N in unwanted forms [1–4]. These impurities are likely to play important roles in compensating or passivating N acceptors, making it difficult to dope ZnO p-type. Recent IR measurements on N-doped ZnO, which is not p-type, revealed several peaks associated with H, including a peak at $3020\,\mathrm{cm}^{-1}$ which is consistent with the N–H stretch vibration frequency. In addition, the spectrum in the lower frequency range contains several peaks in the range of $1800–2000\,\mathrm{cm}^{-1}$, which are close to the frequencies of diatomic molecules.

Based on first principles calculations, we found two types of defect complexes that are likely to form. While isolated H is predicted to exclusively be a donor in ZnO [5,6], it can also passivate N_O acceptors and form an electrically inactive N_O–H complex (Fig. 1) [3]. For the second type of complex, C impurities and excess N atoms prefer to passivate N_O acceptors and form a "substitutional diatomic molecule" (SDM), which is a strongly bound NC or N_2 molecule substituted on an oxygen site [$(NC)_O$ or $(N_2)_O$] (Fig. 2) [7,8]. The $(NC)_O$ or $(N_2)_O$ SDMs are single and double donors, respectively. These SDMs have electronic and structural properties similar to free diatomic molecules. The calculated local vibrational modes (LVM) of these defects are in good agreement with the peaks recently observed by FTIR measurement on N-doped ZnO. These results suggest that, in addition to H, one should be careful with a C impurity that can turn an existing N acceptor (N_O) into an $(NC)_O$ SDM, which is a donor. In addition, excessive N incorporation could lead to an unwanted $(N_2)_O$ SDM, which is a double donor, instead of the desired N_O.

*Corresponding author. School of Physics, Suranaree University of Technology, Nakhon Ratchasima 30000, Thailand. Tel.: +66 44 22 4319; fax: +66 44 22 4185.
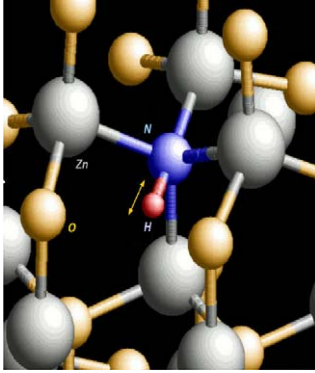
E-mail address: sukit@sut.ac.th (S. Limpijumnong).

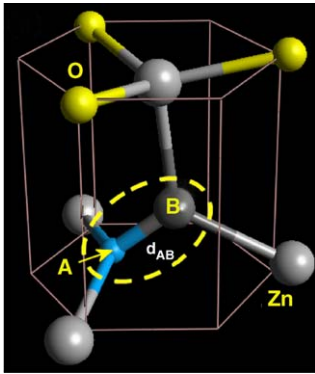Fig. 1. Atomic structure of the N_O–H complex. Large sphere is Zn and small sphere is O. Impurities N and H are labeled.

Fig. 2. Atomic structure of the substitutional diatomic molecule, where the encircled AB dimer replaces an O atom in ZnO. For $(N_2)_O$ SDM, $A = B = N$. For $(NC)_O$ SDM, $A = N$ and $B = C$. The large sphere is Zn and the small sphere is O.

2. Theoretical approach

2.1. Total-energy and formation energy calculations

Our first principles calculations are based on the pseudopotential planewave method with density-functional theory in the local-density approximation. The Vanderbilt-type ultra-soft pseudopotential [9], as implemented in the VASP codes [10], is used. The use of ultrasoft versions of the pseudopotentials allows relatively low energy cutoffs (300 eV) to be used for the planewave basis set. The Zn 3d electrons are treated as valence electrons. The calculated heat of formation for ZnO of 3.58 eV agrees with the experimental value of 3.60 eV.

To study defects, we use a supercell approach with a supercell containing at least 36 atoms. Test calculations for the $(N_2)_O$ and N_O–H complexes are performed with a larger 96-atom cell to ensure that the convergence is within ± 0.2 eV. For charged defects, a jellium background was used. Since LDA substantially underestimates the ZnO band gap, we have instead examined the electronic properties at the $2 \times 2 \times 2$ Monkhorst-Pack special k

points, which are also used for the Brillouin zone integration. The band gap at the special k points is 2.5 eV. All atoms in the cell are allowed to relax until the magnitude of the residue force on each atom is <0.05 eV/Å. The defect formation energy (ΔH_f) which has been described in detail elsewhere (for example, Refs. [11,12]), can be defined as

$$\Delta H_f = E_{tot}(D, q) - E_{tot}(0) + \Delta n_{Zn}\mu_{Zn} + \Delta n_O\mu_O + \Delta n_X\mu_X + qE_F, \quad (1)$$

where $E_{tot}(D,q)$ and $E_{tot}(0)$ are the total energies from first principles calculations of the supercell with and without the defect, D, and $X (= H, N, C)$ represents impurity elements. Quantities Δn_A and μ_A are the number of species $A (= Zn, O, H, N, C)$ removed from a defect-free cell to its respective reservoir to form the defect cell and the corresponding reservoir chemical potential. The chemical potentials μ_{Zn}, μ_O, μ_H, μ_N and μ_C have upper limits at their respective natural phases, i.e. the energies of metallic Zn, gaseous O_2, H_2, N_2 and solid-state C, which are offset to zero in the present study. To keep the ZnO thermodynamically stable, it is also required that $\mu_{Zn} + \mu_O = \mu_{ZnO,calc} = -3.58$ eV. This imposes an additional constraint that μ_O be in the range -3.58 eV $\leqslant \mu_O \leqslant 0$ and redefines $\mu_{Zn} = -3.58$ eV$-\mu_O$. Unless noted otherwise, all calculations in this paper are done in the Zn-rich limit, i.e. $\mu_{Zn} = 0$. In Eq. (1), q and E_F are the defect charge state and Fermi level with respect to the VBM.

2.2. Vibration frequency calculations

We use the so-called frozen phonon calculation approach. After the defect is relaxed to the lowest energy configuration, we dislocate the vibrating atom (for example H atom in the N–H LVM case) along the vibrating direction in a small step at a time (typical step is 0.05 Å). For each step, the calculated total energy is recorded. The potential energy curve is constructed from the plot of total energy versus the vibrating distance.

In the case of N_O–H complex, it is a good approximation to dislocate only the H atom to construct the potential energy curve. This is because H is much lighter than other atoms. However, when calculating the N–H stretch frequency the reduced mass of N and H atoms must be used. Due to its light mass, the H atom vibrates with a large amplitude, i.e. ~10% of the bond distance in the ground state and 20% in the first excited state. Therefore, it is important to include anharmonic effects in the LVM calculation [13,14].

In the case of SDMs, the situation is somewhat different. N and C have a comparable mass that is over ten times heavier than H, leading to a much smaller zero-point vibration amplitude. Since the amplitude of the vibration is small, the anharmonicity in N–C and N–N vibrations are much smaller than that of the H–N vibration. For example, including anharmonicity in the calculation only leads to a

change in the LVM of a free N_2 molecule by $< 20\,cm^{-1}$ out of a total frequency of about $2000\,cm^{-1}$ [14]. In calculating the LVM of SDMs, both atoms in the dimer are simultaneously dislocated with the same amplitude in opposite directions. Other atoms in the supercell are fixed.

3. Results and discussions

3.1. Passivation by hydrogen

Using the definition of the formation energy given above, we calculated the formation energies of an isolated interstitial H, a nitrogen acceptor N_O, and a N_O–H complex in ZnO. An isolated interstitial H is exclusively a donor in ZnO and always exists in the form of H^+. For an isolated H^+ location, there are four low-energy sites surrounding an O atom with the so-called $BC_\parallel$ site being the site with the lowest energy [6,15]. The other three sites have slightly higher energies (approximately within 0.2 eV). An isolated N_O is an acceptor. Currently the exact location of the ionization energy of N_O is still under debate [3]. Over almost the entire Fermi energy range, the isolated N_O is stable in a $(1-)$-charge state whereas an isolated interstitial H atom is always stable in a $(1+)$-charge state. The two defects, therefore, have a Coulomb attraction and have a strong tendency to form a N_O–H defect complex. The formation energy of H^+ (at $BC_\parallel$ site) and N_O are plotted (dashed lines) as a function of Fermi level in Fig. 3 with the sum of the two formation energies shown as dotted lines. In the same figure, we also plot the formation energy of the N_O–H complex (thick solid line). The binding energy of the N_O–H complex is 0.95 eV, i.e. the difference in energy between the dotted and solid line. For the N_O–H defect complex, the $AB_{N\perp}$ configuration (Fig. 1) has the lowest

Fig. 3. Formation energy of an interstitial H, N_O (dashed lines) and a N_O–H complex (solid line) in ZnO as a function of electron Fermi energy. The dotted line shows the sum of the formation energies of an isolated interstitial hydrogen and an isolated N_O. The Zn-rich condition, N_2 and H_2 phase precipitation limits were assumed. The energy difference between the dotted line and the solid line is the binding energy of the N_O–H complex.

formation energy. The AB_N configurations are energetically more stable than the BC by about 0.2–0.3 eV, making the likelihood of forming BC configurations negligible. The difference in formation energy between the two AB_N configurations is within the computational error bar. Both AB_N configurations have a similar N–H stretch mode frequency, with an average value of $2927\,cm^{-1}$. The anharmonic contributions are rather large, i.e. approximately 8%. Both BC configurations also have a similar N–H stretch mode frequency, with an average value of $3319\,cm^{-1}$, which is clearly higher than those of the AB_N configurations. The anharmonic contributions are less than half of those for the AB_N cases. The smaller anharmonic contribution in BC in comparison with AB_N agrees with the usual trend found for an isolated H in ZnO [6] as well as in the GaN system [13]. To estimate the systematic error of our calculation, we calculated the known stretch-mode frequency of a free ammonia (NH_3) molecule. We obtained the symmetric stretch LVM of $3194\,cm^{-1}$ which is $143\,cm^{-1}$ smaller than the known experimental value ($3337\,cm^{-1}$). Assuming that our calculated LVM of the N–H bond in ZnO is underestimated by similar amount, our adjusted value for AB_N of $2927 + 143 = 3070\,cm^{-1}$ is in reasonable agreement with the recently observed peak at $3020\,cm^{-1}$ [3].

3.2. Passivation by the formation of substitutional diatomic molecules

The diatomic molecule is one of the most common forms for first row elements, namely, C, N, and O, because these small atoms tend to form strong triple bonds with each other. Recently, similar complexes, such as N_2 and NC inclusions in GaAs have been studied both theoretically and experimentally [16,17]. In the case of ZnO, the $(N_2)_O$ and $(NC)_O$ SDM are found to have bonding and anti-bonding characteristics very similar to their free molecules confirmed by the detailed investigation of the electronic wavefunctions [7,8]. Here, we will focus only on the energetic and the LVM of the complexes.

Fig. 4 shows the E_F dependence of the formation energy (ΔH_f) in the Zn-rich, N-rich, and C-rich conditions ($\mu_{Zn} = \mu_N = \mu_C = 0$) for $(CO)_O$, $(NC)_O$, $(NO)_O$, and $(N_2)_O$. Since the isolated interstitials N_i and C_i have very high formation energies, they tend to immediately bind with the closest lattice O, forming $(NO)_O$ and $(CO)_O$. However, in the presence of N_O, $(NO)_O$ and $(CO)_O$ are unstable against the formation of $(N_2)_O$ and $(NC)_O$. The binding energies are typically several eV due in part to Coulomb attraction between oppositely charged impurities and in part to the combination of two impurities into one. This can significantly reduce the formation energy because, for example, when $N_O + (NO)_O \rightarrow (N_2)_O + O_O$, one less oxygen site is disturbed by the impurities after the reaction. In the right panel of Fig. 4, the formation energy of N_O and $(NO)_O$ are shown as the dashed line and the thin solid line with the sum of the two as the dotted line. The sum is to be
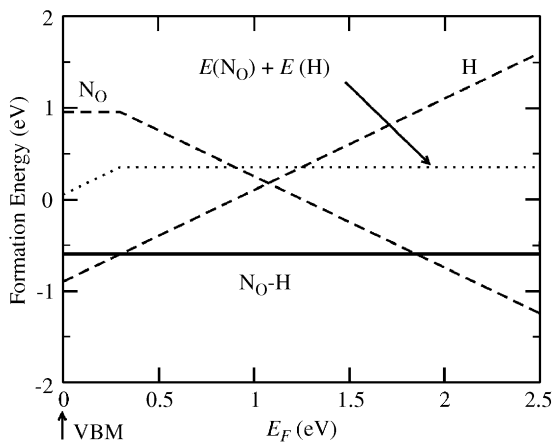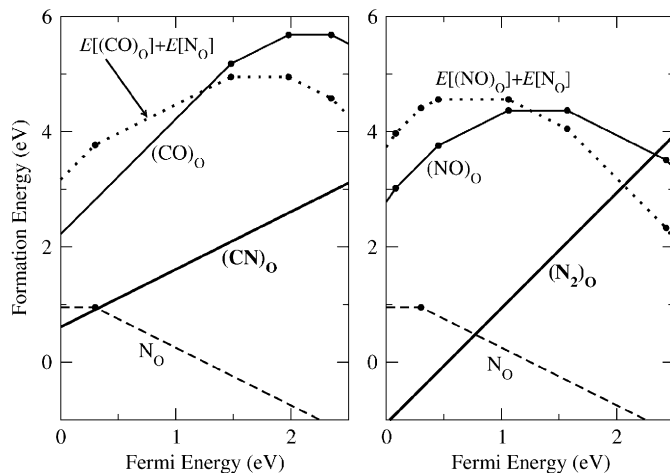
Fig. 4. Formation of (left panel) $(NC)_O$ from isolated N_O and $(CO)_O$ and (right panel) $(N_2)_O$ from N_O and $(NO)_O$. The Zn-rich condition, N_2 and diamond phase precipitation limits were assumed.

compared with the thick solid line, which is the formation energy of $(N_2)_O$ defect. We can immediately see that the binding energy, which is the difference between the dotted line and the thick solid line, depends somewhat on the Fermi energy, but has a typical value of several eV. The binding energy is of similar magnitude for the case of $(NC)_O$, as shown in the left panel. This is especially true in the case of p-type ZnO, for which the binding energies are large enough to make both $(N_2)_O$ and $(NC)_O$ lower in energy than isolated N_O. It is therefore expected that the formation of $(N_2)_O$ and $(NC)_O$ will compete with the formation of N_O acceptors. Since these SDMs are donors in p-type samples, their formation further hinders p-type doping by compensating the already lowered N_O acceptors.

The situation could be worse when one tries to increase N concentration, [N], above the equilibrium value via non-equilibrium growth methods. Effectively, this is similar to increasing the nitrogen chemical potential μ_N. Although the formation energy of N_O decreases as one raises μ_N, the formation energy of the $(N_2)_O$ complex decreases twice as fast. In thermal equilibrium, this would end up increasing the concentration of the donor $(N_2)_O$ complex instead of the acceptor N_O. However, because the formation of $(N_2)_O$ from $N_O + (NO)_O$ involves the breakup of one SDM, the diffusion of N_i, and the formation of another SDM, one might be able to adjust the growth temperature to be low enough that $(N_2)_O$ is suppressed.

The calculated frequencies for $(N_2)_O^{2+}$ and $(NC)_O^+$, which are the most stable form for these complexes in p-type ZnO, are 2108 and 1995 cm^{-1}, respectively. These frequencies fall within 200 cm^{-1} of the experimentally observed values [2]. Moreover, recent XPS experiments have found strong signals of N–N and C–N bonds with similar characteristics to those of free diatomic molecules [4]. These observations strongly suggest the existence of $(N_2)_O$ and $(NC)_O$ in these samples.

4. Conclusion

First principles total energy calculations show that H, C, and N can passivate N_O acceptors in ZnO. H can passivate N_O and form N_O–H complexes with the binding energy of approximately 1 eV. C and excess N can passivate N_O and form low energy $(NC)_O$ and $(N_2)_O$ substitutional diatomic molecules (SDM) on the oxygen site in ZnO. The calculated vibrational frequencies are in qualitative agreement with recent IR experiments. Our calculations also show that both $(NC)_O$ and $(N_2)_O$ are donors in p-type ZnO. These results should shed new light on efforts to improve the fabrication of high quality p-type ZnO by nitrogen.

References

[1] S.J. Pearton, D.P. Norton, K. Ip, Y.W. Heo, T. Steiner, J. Vac. Sci. Technol. B 22 (2004) 932.
[2] B.M. Keyes, L.M. Gedvilas, X. Li, T.J. Coutts, J. Cryst. Growth 281 (2005) 297.
[3] X. Li, B.M. Keyes, S.E. Asher, S.B. Zhang, S.-H. Wei, T.J. Coutts, S. Limpijumnong, C.G. Van de Walle, Appl. Phys. Lett. 86 (2005) 122107.
[4] C.L. Perkins, S.-H. Lee, X. Li, S.E. Asher, T.J. Coutts, J. Appl. Phys. 97 (2005) 034907.
[5] C.G. Van de Walle, Phys. Rev. Lett. 85 (2000) 1012.
[6] S. Limpijumnong, S.B. Zhang, Appl. Phys. Lett. 86 (2005) 151910.
[7] S. Limpijumnong, X. Li, S.-H. Wei, S.B. Zhang, Appl. Phys. Lett. 86 (2005) 211910.
[8] E.-C. Lee, Y.-S. Kim, Y.-G. Jin, K.J. Chang, Phys. Rev. B 64 (2001) 085120.
[9] D. Vanderbilt, Phys. Rev. B 41 (1990) 7892.
[10] G. Kresse, J. Furthmüller, Comput. Mater. Sci. 6 (1996) 15.
[11] S.B. Zhang, J.E. Northrup, Phys. Rev. Lett. 67 (1991) 2339.
[12] C.G. Van de Walle, S. Limpijumnong, J. Neugebauer, Phys. Rev. B 63 (2001) 245205.
[13] S. Limpijumnong, J.E. Northrup, C.G. Van de Walle, Phys. Rev. B 68 (2003) 075206.
[14] S. Limpijumnong, in: N.H. Nickel, M.D. McCluskey, S.B. Zhang (Eds.), Hydrogen in Semiconductors, MRS Symp. Proc. No. 813, Materials Research Society, Pittsburgh, 2004, p. H3.6.
[15] E.V. Lavrov, J. Weber, F. Börrnert, C.G. Van de Walle, R. Helbig, Phys. Rev. B 66 (2002) 165205.
[16] W. Ulrici, B. Clerjaud, Phys. Rev. B 72 (2005) 045203.
[17] P. Carrier, S.-H. Wei, S.B. Zhang, S. Kurtz, Phys. Rev. B 71 (2005) 165212.

Ion relaxation and hydrogen LVM in H-irradiated GaAsN

Mao-Hua Du[a],*, Sukit Limpijumnong[a,b], S.B. Zhang[a]

[a]National Renewable Energy Laboratory, Golden, Colorado 80401, USA
[b]National Synchrotron Research Center and School of Physics, Suranaree University of Technology, Nakhon Ratchasima, Thailand

Abstract

First-principles calculations show that the hydrogen configurations in GaAsN depend on how hydrogen is introduced into the sample. Since proton and neutral H have different ground states, the proton injected into the sample by H-irradiation follows a unique energy pathway to form a charged dihydride, instead of the charge-neutral H_2^* monohydride. The subsequent charge neutralization causes the spontaneous canting of the dihydrides. The resulting canted N–2H structure explains the recent puzzling IR observation, the recoveries of the GaAs band gap and lattice parameter, and the dihydride symmetry determined by the XANES experiment. It may also have broad implications for ion implantation studies in other solids.
© 2006 Elsevier B.V. All rights reserved.

PACS: 61.72.Vv; 63.20.Pw; 61.72.Ji; 61.72.Bb

Keywords: Ion implantation; Dilute III–V nitrides; Hydrogen; IR modes

1. Introduction

Large size-mismatched dilute alloys such as GaAsN [1] and ZnSeO [2,3] are promising alloy semiconductors with unique physical properties. For example, with only an atomic percent of N incorporated into GaAs, the band gap decreases by several hundred meV [4]. On the other hand, H irradiation causes a nearly full recovery of the GaAs band gap [5] and lattice parameter [5] from those of GaAsN. The formed H complexes after H irradiation should be charge neutral due to their large concentration ($>10^{20}\,cm^{-3}$). First-principles total energy calculations suggested that the lowest-energy charge-neutral H complex is the α-H_2^*(N) complex with characteristic Ga–H and N–H monohydride bonds (Fig. 1a), and that this complex can explain the above experimental observations [6,7]. However, a recent infrared experiment [8] on H-irradiated samples did not observe any Ga–H modes. Instead, two N–H stretch modes were observed at 3195 and 2967 cm^{-1}, as shown in Table 1. Hence, both modes here belong to the N–H bonds. In D-irradiated samples, the two stretch

modes shift to 2216 and 2376 cm^{-1}, respectively. In H/D co-irradiated samples, however, two *additional* D-stretch modes, at 2221 and 2366 cm^{-1} (see Fig. 2a), and one *additional* H-stretch mode, were observed. A second H mode is also expected, but was not observed, which was due possibly to contamination. The observation of the two (instead of one) additional D modes indicates that the H complexes must contain two inequivalent H atoms strongly coupled to each other. A recent XANES study [9] further reveals that the symmetry of the 2 H complexes should be C_{2v}-like, thus further undermining the validity of the C_{3v}-based H_2^* model.

The disagreement between theory and experiment on H configurations in GaAsN suggests that the observed H-complex may not be the ground-state configuration. During H-irradiation, the equilibrium between the injected protons and the electron reservoir of energy E_F is not maintained. Therefore, one cannot assume that protons will take the theoretically predicted ground-state structure for neutral H.

In contrast to the conventional view of H irradiation as simply another convenient mean to enhance H concentration [H] in the solid, in this paper, we will show that the final H configurations can be altered by how the H is

*Corresponding author. Tel.: +1 303 384 6294; fax: +1 303 384 6432.
E-mail address: mao_hua_du@nrel.gov (M.-H. Du).

introduced into the solid. For H irradiation of GaAsN, the relaxation pathway for proton must be considered instead of the neutral H, because H irradiation in large quantity causes the accumulation of positive charges that cannot be easily dissipated. As a result, the injected protons enter the sample and get trapped in the proton-ground-state structure, $N-2H_{BC}^{2+}$, rather than the neutral-H-ground-state structure, $\alpha-H_2^*$. The subsequent charge neutralization results in the formation of metastable canted N–2H complex, which cannot be converted easily to the ground-state structure, $\alpha-H_2^*(N)$, due to a kinetic barrier. The canted N–2H model explains all experimental observations, including IR modes (both in frequency and relative amplitude), dihydride symmetry, and the bandgap and lattice parameter recovery. The good agreement between theory and experiments establishes a new direction to examine ion implantations in semiconductors and solids in general.

2. Method

Our calculations are based on the density functional theory within the local density approximation (LDA). The electron–ion interactions are described by the ultra-soft pseudopotentials [10], as implemented in the VASP codes [11]. The valence wavefunctions are expanded in a plane-wave basis with a cutoff energy of 348 eV. All calculations were performed using a 64-atom supercell. The vibrational frequencies were calculated based on the dynamical matrix approach [12]. We used the special k-points scheme for Brillouin zone summation and relaxed all the atoms until the forces were less than 0.02 eV/Å.
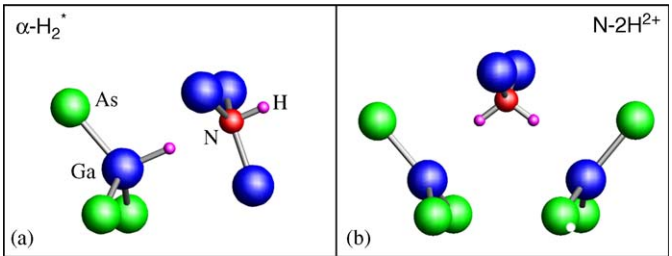

Fig. 1. Ball-stick models for (a) $\alpha-H_2^*$ and (b) $N-2H^{2+}$.

3. Results

Once protons enter the sample, they are unlikely to be neutralized, because the $(+/0)$ level for the diffusing H is near the conduction band minimum of GaAs, which is well above that of GaAsN. It therefore makes sense to study the H^+ instead of H^0 traps in H-irradiated GaAsN.

The most likely proton traps in GaAsN are the N-centered di-proton complexes, among which we found that neither the $\alpha-H_2^{*2+}$ nor the interstitial H_2^{2+}(Ga) (namely, a charged molecule at the tetrahedral interstitial site next to a Ga) is a good candidate for the proton trap, because a positive charge completely destabilizes the respective atomic structure. Instead, the $N-2H_{BC}^{2+}$ complex is found to be the ground-state for a di-proton complex (see Fig. 1b). Charge neutral $\alpha-H_2^*$ and interstitial H_2(Ga) may occasionally form by simultaneously creating *two* holes near the valence band maximum. Even if this happens, however, our calculation shows that the resulting $\alpha-H_2^{*0}(N) + 2h^+$ and $H_{2,int}^0(Ga) + 2h^+ + N_{As}$ are significantly less stable than the $N-2H_{BC}^{2+}$ (by 0.47 and 0.80 eV/H, respectively). On the other hand, the trapping of two H^+ to form $N-2H_{BC}^{2+}$ lowers the energy by 0.48 eV/H [13]. Each trapped H forms a strong bond with the N (see Fig. 1b) by passing the positive charge to a nearby threefold-coordinated Ga in the $N-2H_{BC}^{2+}$ complex. This could be an important initial step to separate holes from the dihydrides for charge neutralization.
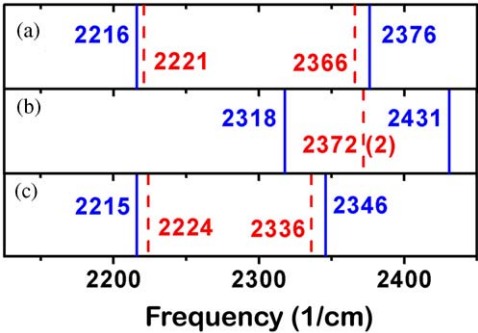

Fig 2. The various D stretch-modes for (a) experiment, (b) $N-2H^{2+}$, and (c) canted N–2H. Solid lines indicate D stretch-modes in fully deuterated samples, whereas dashed lines indicate additional D stretch-modes in H/D flux.

Table 1
Stretch and wag mode frequencies in units of cm^{-1}. N/A stands for not available

	Experiment			$\alpha-H_2^*$		$N-2H^{2+}$			Canted N–2H		
	Stretch		wag	Stretch	wag	Stretch		wag	Stretch		wag
H-modes (H-flux)	3195	2967	1447	3140	944	3305	3209	1328	3207	3052	1417
D-modes (D-flux)	2376	2216	1076	2290	687	2431	2318	974	2346	2215	1037
Additional Modes (H/D flux)	3192	N/A	N/A	None		3260		1164	3204	3056	1257
	2366	2221	N/A			2372		1164	2336	2224	1238

Bonapasta et al. proposed that the $N–2H_{BC}^{2+}$ complex accounts for the measured H-modes [14]. However, a sample cannot host a few atomic percent of positively charged H complexes and also the $N–2H_{BC}^{2+}$ complex does not agree with experimental observation of two inequivalent N–H bonds. Thus, the $N–2H_{BC}^{2+}$ complex cannot be the final H configuration after H irradiation. The charge neutralization of the $N–2H_{BC}^{2+}$ must take place as the sample is grounded, but at a later time. This could happen, for example, by capturing electrons (injected from ground by the electrostatic potential between sample and ground) in the conduction band.

Upon the $N–2H_{BC}^{2+}$ neutralization, two important things happen spontaneously to $N–2H_{BC}^{2+}$: (1) the formation of the Ga–Ga bond in Fig. 3a and (2) the canting of the dihydride in Fig. 3b. The former eliminates electronic states from within the original GaAs band gap in agreement with the gap recovery experiment. The latter qualitatively alters the H/D vibrational properties. Because of its importance, we have calculated not only the initial and final positions of canting, but also four intermediate ones along the pathway. The smoothness of the curve in Fig. 3 suggests that the results are numerically highly accurate. We note that such a canting occurs only when the weak Ga–Ga bond forms due to the Coulomb attraction between the electron-rich Ga–Ga bond and the electron-depleted H bonded to N.

Table 1 tabulates the calculated H and D frequencies. When compared with experiment, the dihydride $N–2H_{BC}^{2+}$ and canted N–2H models produce better results for the H wag mode, 1328 and 1417 cm^{-1}, respectively, than the monohydride α-H_2^* model does, 944 cm^{-1}. This is another indication that the defect responsible for the IR signals cannot be a monohydride. Because the two additional D modes in the mixed H/D flux are key IR results, they are examined in greater details in Fig. 2: The canting of the dihydride leads to two additional modes versus one

additional mode of the uncanted $N–2H_{BC}^{2+}$. Only the former agrees with the IR experiment. The canting of the dihydride also results in two equivalent minima in the energy landscape, which become vibrationally different when one H is replaced by D. The barrier in Fig. 3 is only 50 meV. Hence, we expect that, at low T, each N-DH complex should be trapped to one of the minima and contributes only to one of the additional D modes. At higher T, however, there will be no such trapping so that each N–DH complex contributes to both additional D modes, possibly in a 1:1 ratio.

We have also calculated the relative IR intensities (I) for the D modes in Fig. 2c. The ratio of IR intensities originated from the same defect can be approximated to the first-order by the ratio of $|d\mathbf{p}/dQ_i|$ [2,15,16], where $\mathbf{p}$ is the dipole moment of the system and Q_i is the ith normal-mode coordinate. We calculated the dipole moment change $\Delta\mathbf{p}$ for each mode after taking same distance ($|\Delta Q|$) of atomic displacements along each normal-mode coordinate (Q_i). Then the ratio of any two IR intensities here is simply the ratio of $|\Delta\mathbf{p}|^2$ resulted from atomic displacement of same $|\Delta Q|$ in two normal-mode coordinates. This yields $I_{2215}:I_{2224}:I_{2336}:I_{2346} = 1:0.84:0.44:0.21$, where the subscripts are the mode frequencies (cm^{-1}). These results can be compared to the measured IR intensities, estimated from reading Fig. 2 in Ref. [8], $I_{2216}:I_{2221}:I_{2366}:I_{2376} \approx 1:0.43:0.33:0.29$. By reproducing the qualitative experimental trend, these calculations provide further support to the canted N–2H model.

Once the H atoms are trapped in a neutral canted N–2H complex, they may not escape easily to form α-H_2^*, despite that the latter is 0.2 eV/H lower in energy. The minimum-energy barrier for converting a canted N–2H to α-H_2^* is calculated to be 0.8 eV. In addition, because of the large mass differences between H and Ga and between H and N, the actual barrier to convert a canted N–2H to α-H_2* could be significantly higher than the calculated 0.8 eV [17]. Note that the kinetic energy carried by proton should not help the N–2H overcome the energy barrier to become α-H_2^*, because it dissipates quickly after protons enter the sample by a distance of only a few nm [18], which is two orders of magnitudes smaller than GaAsN film thickness of 300 nm studied in Ref. [8]. Also, a GaAs capping layer of 100-nm thickness is usually applied to eliminate direct damages by the energetic protons [19,20]. Hence, protons enter most of GaAsN layer by thermal diffusion. Thus, one can safely ignore any effect of energetic protons and local heating on the relaxation of the metastable H complexes.

Despite the kinetic barrier, there is a finite probability that α-H_2^*(N) may form. However, even if this happens, the H at α-H_2^*(N) can be etched away by diffusing protons. Our calculations show that, an H$^+$(As), which has roughly a 0.2-eV diffusion barrier in GaAsN, can spontaneously transform any α-H_2^*(N) into an interstitial H$_2$(Ga) plus an H$^+$(N). This reaction is not only exothermic with energy lowering by 0.61 and 0.48 eV for H^0 and H$^+$, respectively, but also barrierless other than the diffusion one. These,
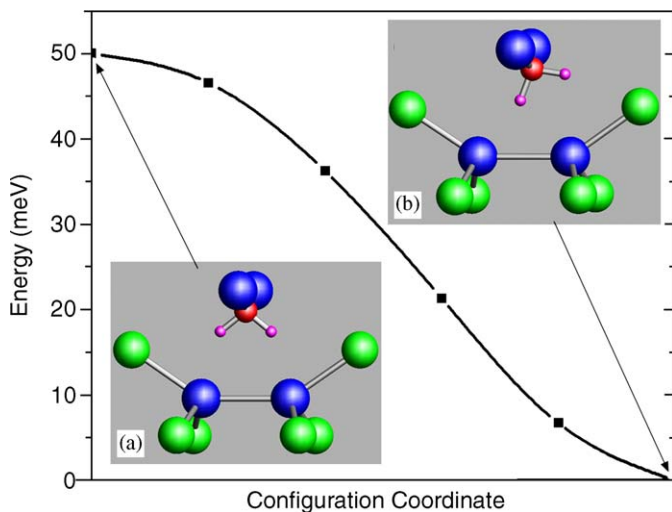

Fig 3. Calculated canting pathway, indicating that the uncanted N–2H is unstable against the canting. The structures of uncanted and canted N–2H complexes are shown in insets (a) and (b), respectively.

combined with the proposed proton relaxation pathway, explain why a metastable dihydride C_{2v} symmetry was observed by the recent XANES study, instead of the global minimum-energy monohydride C_{3v} symmetry.

Finally, we studied the recovery of the GaAs lattice parameter upon H irradiation. To mimic the epitaxial growth, we fixed the planar lattice parameters to that of bulk GaAs, but allowed the third one along [0 0 1] to relax. Assuming the lattice parameter of bulk GaAs is 100%, we obtain 98.69% for N_{As}, 98.81% for $H_{BC}^{+}(N)$, 99.59% for α-$H_2^*(N)$, and 100.23% for $H_2(Ga)$. The canted N–2H may take two distinct orientations with respect to the [0 0 1] direction with degeneracy of 2 and 4, respectively. The corresponding lattice parameters are 100.55% and 99.37%, so the weighted average is 99.76%. This result is slightly better than that of α-H_2^*, but could be expected, because for H_2^*, two H atoms cut only one strained N–Ga bond, whereas for canted N–2H, the two H atoms cut two N–Ga bonds, instead, leaving more rooms for the lattice recovery.

4. Summary

In summary, we have developed a model for ion relaxation following the initial implantation. The theory is qualitatively different from the ordinary equilibrium defect theory and may have implications for a broad range of ion implantation experiments. Application of this theory to GaAsN:H reveals a canted N–2H complex, which simultaneously accounts for all major experimental observations including the puzzling IR frequencies and amplitudes, the dihydride symmetry by XANES, the recovery of the GaAs band gap by optical measurement, and the recovery of the GaAs lattice parameter by X-ray diffraction.

Acknowledgements

References

[1] I.A. Buyanova, W.M. Chen (Eds.), Physics and Applications of Dilute Nitride, Taylor & Francis, New York, 2004.

[2] A. Polimeni, M. Capizzi, Y. Nabetani, et al., Appl. Phys. Lett. 84 (2004) 3304.

[3] W. Shan, W. Walukiewicz, J.W. Ager, et al., Phys. Status Solidi B 241 (2004) 603.

[4] M. Weyers, M. Sato, H. Ando, Jpn. J. Appl. Phys. Part 1 31 (1992) L853.

[5] A. Polimeni, G.B.H. von Hogersthal, M. Bissiri, et al., Semicond. Sci. Technol. 17 (2002) 797.

[6] A. Polimeni, G. Ciatto, L. Ortega, et al., Phys. Rev. B 68 (2003) 085204.

[7] A. Janotti, S.B. Zhang, S. -H. Wei, C.G. Van de Walle, Phys. Rev. Lett. 89 (2002) 086403.

[8] F. Jiang, M. Stavola, M. Capizzi, et al., Phys. Rev. B 69 (2004) 041309(R).

[9] G. Ciatto, F. Boscherini, A.A. Bonapasta, F. Filippone, A. Polimeni, M. Capzzi, Phys. Rev. B 71 (2005) 201301.

[10] D. Vanderbilt, Phys. Rev. B 41 (1990) R7892.

[11] G. Kresse, J. Furthmuller, Phys. Rev. B 54 (1996) 11169.

[12] J.E. Northrup, Phys. Rev. B 39 (1989) R1434. The anharmonic effect (AE) consistently shifts the H-stretch frequencies downward by $\sim100\,cm^{-1}$. The AE also makes the calculated H-stretch modes for NH_3 lower than the experimental values by about the same amount. A correction for systematic error thus wipes out nearly all the AE.

[13] Here, we compare the energy with $H^+(N) + H^+(As)$, because in these H-irradiation experiments, [H] is greater than [N].

[14] A. Amore Bonapasta, F. Filippone, P. Giannozzi, Phys. Rev. B 68 (2003) 115202.

[15] E.B. Wilson, J.C. Decious, P.C. Cross, Molecular Vibrations, McGraw-Hill, New York, 1955.

[16] D. Porezag, M.R. Pederson, Phys. Rev. B 54 (1996) 7830.

[17] Our calculation assumes that each atom responds instantaneously to the movement of all other atoms. However, as much heavier atoms, Ga ($m = 69$) and N ($m = 14$) cannot move in harmony with the light H ($m = 1$). The result of this effect is that the system cannot take the lowest-energy path.

[18] M. Capizzi, private communication.

[19] A. Polimeni, G. Baldassarri H. v. H., M. Bissiri, M. Capizzi, M. Fischer, M. Reinhardt, A. Forchel, Phys. Rev. B 63 (2001) R201304.

[20] G. Baldassarri H. v. H., M. Bissiri, A. Polimeni, M. Capizzi, M. Fischer, M. Reinhardt, A. Forchel, Appl. Phys. Lett. 78 (2001) 3472.

Impurity effects in ZnO and nitrogen-doped ZnO thin films fabricated by MOCVD

Xiaonan Li[a],*, Sally E. Asher[a], Sukit Limpijumnong[b], Brian M. Keyes[a], Craig L. Perkins[a], Teresa M. Barnes[a], Helio R. Moutinho[a], Joseph M. Luther[a], S.B. Zhang[a], Su-Huai Wei[a], Timothy J. Coutts[a]

[a]*National Renewable Energy Laboratory, 1617 Cole Boulevard, Golden, CO 80401, USA*
[b]*School of Physics, Suranaree University of Technology and National Synchrotron Research Center, Nakhon Ratchasima, Thailand*

Abstract

We studied the role of impurities in nitrogen-doped ZnO thin film to understand the difficulty of producing p-type ZnO via nitrogen doping. The ZnO:N films were fabricated by low-pressure metal-organic chemical vapor deposition (MOCVD) using diethylzinc (DEZ) and nitric oxide (NO) precursors. Although very high levels of nitrogen incorporation were observed ($\sim 10^{21}\,cm^{-3}$), acceptor concentrations were typically low (10^{14}–$10^{17}\,cm^{-3}$). The investigation suggests that the low carrier concentrations are possibly due to compensation and passivation effects by hydrogen and carbon impurities unintentionally incorporated into the films from the metal-organic precursor. X-ray photoelectron spectroscopy (XPS) demonstrated that carbon was a bulk impurity in MOCVD-grown films. Secondary-ion mass spectrometry (SIMS) analysis confirmed the presence of carbon and indicated that hydrogen was also a bulk impurity. The concentration of carbon contaminant was found to increase with nitrogen doping. Both XPS and Fourier transform infrared spectroscopy (FTIR) data indicated that defect complexes (CH_x, NH_x, and NC_x) are likely present in MOCVD-grown ZnO films. First-principles calculations predict that the N_O–H and $(NC)_O$ defect complexes are neutral and 1^+ charge state; therefore, the existing carbon and hydrogen passivate the nitrogen acceptor species. Thus, we believe a low hole concentration in MOCVD-fabricated ZnO:N films are partially due to inadvertent passivation by hydrogen and carbon.
© 2005 Elsevier B.V. All rights reserved.

1. Introduction

ZnO is a wide-band gap ($\sim 3.37\,eV$) semiconductor that has been used extensively in surface acoustic wave devices and solar cells [1,2]. It has typically been used as an n-type semiconductor because it is straightforward to prepare the material as n-type with or without extrinsic doping. In recent years, the international research community has devoted significant effort to fabricate p-ZnO because manufacturable p-type material would allow applications such as ultraviolet (UV) light-emitting diodes and lasers.

To date, there is substantial evidence that p-type ZnO has been achieved by a number of groups [3–10]. However, it has typically been difficult to prepare high-quality p-type ZnO material reproducibly; the p-type ZnO is usually characterized by relatively low-hole concentration, low-hole mobility, and instability [3,6,7,9,11]. Especially under the ultraviolet photoelectron illumination, the p-type ZnO film appears as n-type [12].

Efforts to make p-ZnO thin films have involved several deposition methods (e.g., CVD, sputtering, spray deposition, diffusion, oxidation of Zn_3N_2) and several different dopants (e.g., nitrogen, phosphorus, arsenic, antimony, and lithium). A carrier concentration as high as $1.7 \times 10^{19}\,cm^{-3}$ has been reported for phosphorus-doped

---

*Corresponding author. Tel.: +1 303 384 6428; fax: +1 303 384 6430.
  E-mail address: xiaonan_li@nrel.gov (X. Li).

p-type ZnO [13]. In the case of nitrogen, co-doping with aluminum, gallium and indium has been reported with varied degrees of success [4,14–16]. In many cases, the window of the deposition parameters for achieving p-type material was narrow [6,14,17]. Post-deposition annealing was used in some cases to realize p-type conduction [3].

Nitrogen has been regarded as the most-promising acceptor dopant because of its low ionization energy, suitable ionic radius, ease of handling, low material toxicity, and abundance. Much effort has been devoted to nitrogen-related doping and co-doping, but low-resistivity p-type ZnO:N has yet to be obtained. For ZnO:N film grown by CVD, the typical carrier concentrations are only 10^{15}–10^{18}, despite nitrogen concentrations in the range of $10^{21}\,cm^{-3}$ [6,18]. The reasons for the low electrical activity of incorporated nitrogen are still under debate, but it is well known that films grown via MOCVD can contain hydrocarbon impurities that originate from the metal-organic precursors and that such impurities can affect the action of dopants such as nitrogen. In this paper, we report on the results of an in-depth study of carbon and hydrogen impurities in ZnO:N thin films fabricated by MOCVD and discuss the possibility of the compensation of the p-type nitrogen doping by various hydrogen- and carbon-related defect complexes.

2. Methods

Nitrogen-doped ZnO thin films were fabricated by low-pressure MOCVD. The precursors were DEZ ($C_2H_5)_2Zn$), oxygen, and dilute NO gas (2 wt% NO/Ar). The carrier gas for all the precursors was N_2 gas. The deposition temperature was varied between 200 and 550 °C. Undoped ZnO samples were grown using the reaction between DEZ and O_2 gas. The nitrogen-doped ZnO samples were grown using DEZ and NO. Two types of substrates, Si and Corning 1737 glass, were used. The Si substrate was suitable for subsequence FTIR analysis, whereas the glass substrate was suitable for other characterization techniques such as X-ray diffraction (XRD), XPS, SIMS, and optical and electronic property analyses.

Atomic force microscopy (AFM) (Dimension 3100 with Nanoscope IIIa controller, using Si cantilevers) was used to assess the topography of the thin films. Crystal properties were assessed using XRD (Sintag Model PTS). A Cary 5G spectrophotometer with an integrating-sphere detector was used to measure total transmittance and reflectance spectrum in the wavelength ranging from 350 to 2000 nm. Electrical properties were studied by Hall measurement (BioRad Model HL5500) and capacitance–voltage (C–V) analysis (double-Schottky surface-contact mercury probe, MSI Electronics Hg-2C-5). The nitrogen, hydrogen, and carbon concentrations were analyzed using SIMS (Cameca IMS 5f) and XPS (Physical Electronics Model 5600). Details of the XPS analysis can be found in a previous publication [12]. The N–H bond signatures were studied by room-temperature FTIR transmittance with ZnO films

grown on parallelogram-shaped single-crystal silicon substrates and mounted in an attenuated total-reflectance (ATR) accessory attached to a Nicolet Magna-IR 550 spectrometer [19].

We performed first-principles calculations based on density functional theory (DFT) within the local density approximation (LDA) and ultrasoft pseudopotentials; As implemented in the Vienna ab-initio simulation package (VASP) codes. Zn 3d states were included in the valence, the cutoff energy for the plane-wave expansion is 300 eV. We used a supercell approach and monkhorst-pack k-point mesh for brillouin zone integrations. Wurtzite supercells containing 36 atoms were used with the k-point mesh of $2 \times 2 \times 2$. Test calculations of up to a 96-atom cell have shown that this is adequate for well-localized defects being studied here. For defects with non-zero charge; a jellium background is used to prevent the divergence of the madelung sum. The definition of formation energy of a defect from first-principles calculations can be found elsewhere (e.g., Refs. [20,21]).

3. Results and discussions

3.1. General properties of N-doped ZnO

Nitrogen is a group-V element; hence, it should be possible to use as a p-type dopant by substituting it for O in ZnO. An O-poor growth ambient is generally required for p-type doping by nitrogen [22]. In our experiments, if oxygen is used as an oxidizer and NO gas is used as a dopant, the resulting ZnO film contains no detectable nitrogen doping [23]. Using NO gas for both oxidizer and dopant, nitrogen concentrations as high as $2.60 \times 10^{21}\,cm^{-3}$ were achieved. This high concentration of nitrogen can be achieved in a wide processing range. Nevertheless, the growth window for a successful fabrication of p-type film is very narrow. The p-type ZnO:N films are achieved only in a growth temperature range of 400–440 °C [6].

A typical topography of the MOCVD-formed ZnO:N films on a glass substrate is illustrated in Fig. 1. The figure clearly shows that the film is polycrystalline with the grain size smaller than 100 nm, and an average surface roughness of around 10–20 nm. XRD analysis indicated that the ZnO:N films maintained the Wurtzite structure of undoped ZnO. However, compared with the strong (0 0 2) orientation preference in undoped ZnO film, ZnO:N deposited on glass lost the (0 0 2) orientation preference and became randomly oriented, as shown in Fig. 2. The transmittances of undoped ZnO and ZnO:N films are shown in Fig. 3. Because of the wide fundamental optical bandgap, undoped ZnO is colorless and highly transparent. The increased absorption near the band edge made the nitrogen-doped ZnO film yellowish.

Results of Hall probe analysis on several typical ZnO samples are shown in Table 1. Undoped ZnO is n-type with a carrier concentration in the range of 10^{16}–$10^{18}\,cm^{-3}$. The

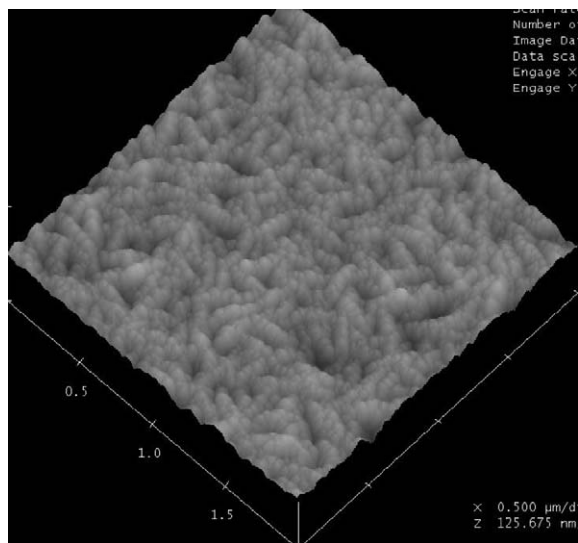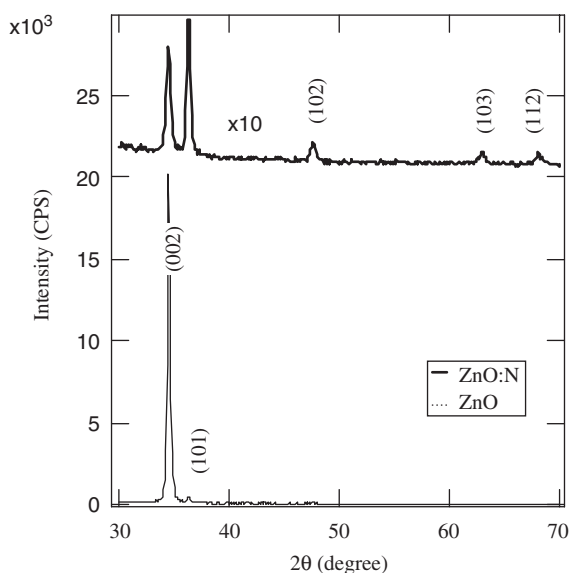Fig. 1. The topography of a 0.74-μm-thick ZnO:N film grown on a glass substrate at 400 °C.

Fig. 2. X-ray diffraction data of ZnO and ZnO:N films. Both films were deposited on glass substrate at 400 °C.

Fig. 3. Optical transmittance of ZnO and ZnO:N films. Both films were deposited on glass substrate at 400 °C.

nitrogen-doped ZnO samples are no longer n-type, but are either semi-insulating or weak p-type with the carrier concentration of around 10^{13}–10^{18} cm^{-3}. A double-Schottky surface-contact C–V technique was used to confirm the Hall results. The Hg probe contact makes it possible to contact both p- and n-type samples. In this method, the conductivity type of the samples is determined from the response of the depletion-layer width against the polarity of the bias applied to the inner main electrode. A ZnO:N sample measured by Hall with a p-type carrier concentration of 6.6×10^{13} cm^{-3} was analyzed by C–V. As seen in Fig. 4, the C–V technique confirmed that this sample was p-type (positive slope under reverse bias), with calculated carrier concentration of $\sim 10^{14}$ cm^{-3}.
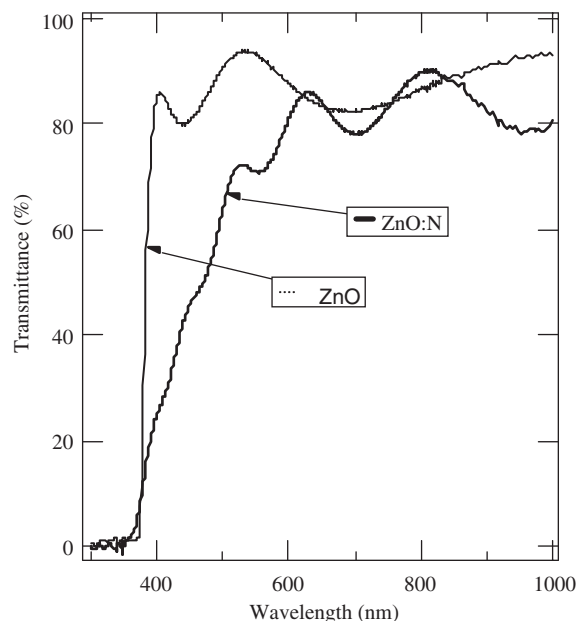
The p-type behavior was achieved only with the growth temperatures of about 400–450 °C. The best electronic properties achieved in this temperature range were on the sapphire substrate with carrier concentration of 8.36×10^{17} cm^{-3}, Hall mobility of 4.55 cm^2/V s, and resistance of 1.64 Ω cm. At growth temperatures lower than 400 °C, the film deposition rate was low and the film was n-type. When deposition temperatures were increased to 500 °C, the film reverted to n-type. We will discuss the temperature dependence of conducting type in the later sections.

3.2. Impurity and defect complexes analysis

In this work, we focus on the effects of hydrogen and carbon impurities. Hydrogen is an impurity that can be present in ZnO made by many fabrication techniques [3,9,23–25]. An isolated interstitial H is predicted to be exclusively donor in ZnO, i.e., it always exists in the form of an H$^+$ and bonds with the host O atom [26]. Carbon impurities are of special concern with MOCVD-grown films because of the metal-organic precursors that are used. Previous work has demonstrated that this growth technique results in bulk carbon concentrations much higher than other growth techniques such as reactive sputtering [12]. In n-type ZnO, the carbon could substitute on the O site and be an acceptor. A recent study indicated that carbon could exist as a donor in ZnO in several forms [27]. For example, in semi-insulating or p-type ZnO, carbon can form diatomic species with oxygen or nitrogen and share an oxygen site.

The hydrogen and carbon impurity levels in the ZnO films were studied by SIMS depth-profiling. The measure-

Table 1
Electrical properties of ZnO films deposited on glass substrate at deposition temperature of 400 °C

Doping condition	Sample ID	CC (cm^{-3})	μ (cm^2/V s)	ρ (Ω cm)	Conductivity type
Undoped	L3353.2	-8.42×10^{18}	3.2	0.235	n
	L4084.1	-8.38×10^{16}	6.3	11.8	n
N-doped	L3357.2	2.90×10^{14}	579	37.2	p
	L4098.2[a]	8.36×10^{17}	4.55	1.64	p

(For Hall measurement, the error bars are very small for carrier concentrations higher than 10^{15} cm^{-3} and mobilities greater than 1 cm^2/V s. In this table, the sample L3367.2 has a large error bar. Carrier concentration data was measured in the region between 2.9×10^{14} and 4.8×10^{14} cm^{-3}.
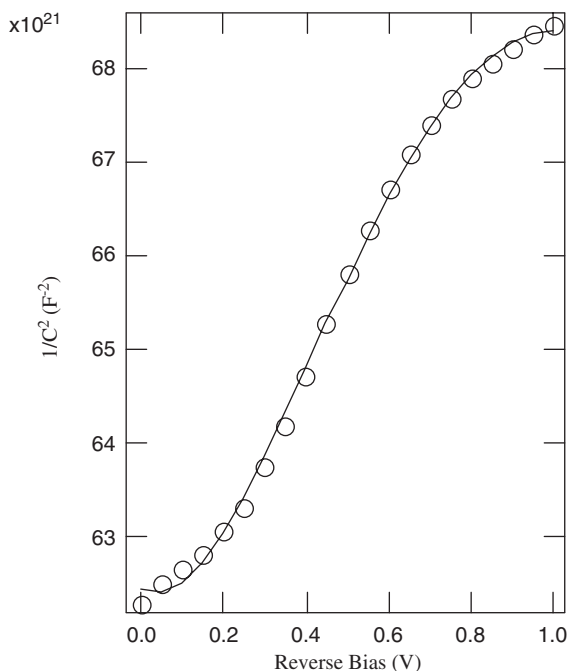
[a] Sapphire substrate.

Fig. 4. Measured C–V characteristics of $1/C^2$ vs. reverse-bias voltage on nitrogen-doped ZnO film. The film is 1.8 μm thick and deposited on a glass substrate.
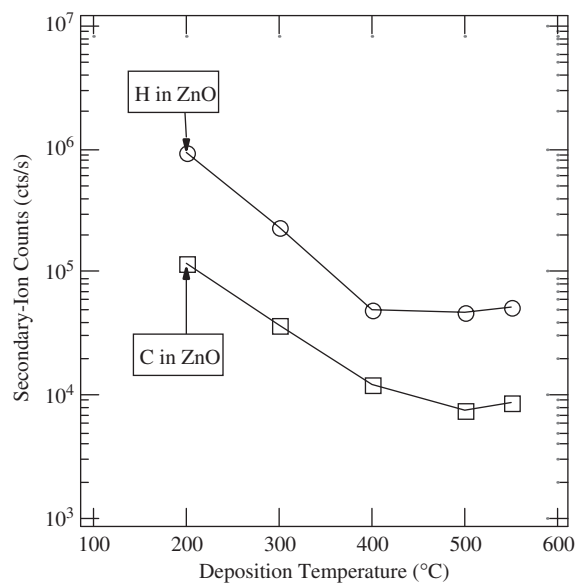

Fig. 5. A SIMS analysis of hydrogen and carbon concentration on the MOCVD-fabricated ZnO samples. The ZnO films were deposited at 400 °C with DEZ and O$_2$ flow rate of 1 and 100 sccm, respectively.

ment on an undoped ZnO film fabricated with MOCVD was used as a benchmark. The hydrogen and carbon concentration as a function of growth temperature for undoped ZnO film is shown in Fig. 5. The hydrogen and carbon concentrations are high at low deposition temperature. As the deposition temperature increased, both hydrogen and carbon concentrations decreased and likely stabilized around 400 °C. The similar dependence of carbon and hydrogen concentrations on deposition temperature indicates that carbon and hydrogen possibly exist together as defect complexes.

For nitrogen-doped ZnO films, the dependencies of the hydrogen and carbon concentration on the growth temperature are different from the case of unintentionally doped ZnO films. Fig. 6 shows that, in the ZnO:N samples, the hydrogen and carbon concentrations did not monotonically decrease as deposition temperature increased. The samples grown at 400 °C had the lowest hydrogen and carbon concentrations. As the deposition temperature
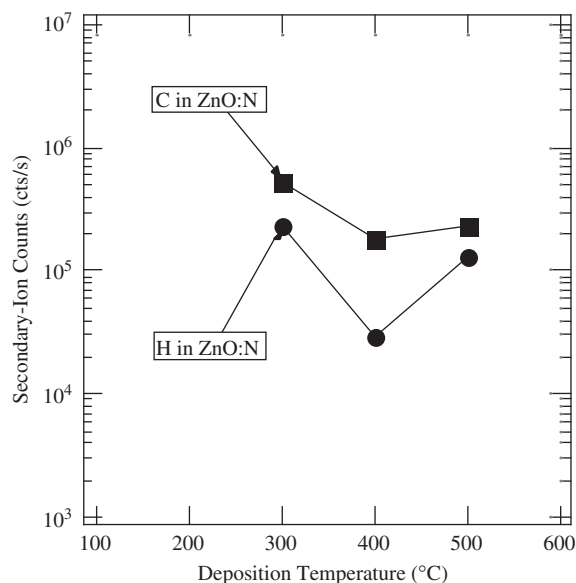

Fig. 6. A SIMS analysis of hydrogen, carbon, and nitrogen concentration on MOCVD-fabricated ZnO:N samples. The ZnO:N films were deposited at 400 °C with DEZ and NO gas flow rate of 1 and 36 sccm, respectively.

increased to above 400 °C, hydrogen and carbon concentrations both increased again. If we compare the hydrogen and carbon concentrations between the nitrogen-doped and undoped samples, we find that the hydrogen concentrations are about the same level. However, the carbon concentrations in nitrogen-doped samples are about ten times higher than those in the undoped samples. A possible explanation for the increased carbon impurities in the ZnO:N samples will be provided later in this paper. In any case, it is clear that under current film growth conditions, when NO gas used as an oxidizer instead of O_2 gas, the carbon concentrations in the ZnO film increase.

The FTIR results strongly support the hypothesis that at least some of the carbon and hydrogen co-exist as defect complexes in the undoped ZnO. Fig. 7 shows the FTIR absorbance spectra in the 2750–3050 cm^{-1} region. Two absorbance spectra were taken from the undoped and nitrogen-doped ZnO samples that were both deposited at 400 °C. On the undoped ZnO film (dotted line), we observed a series of sharp absorption peaks in the range consistent with CH stretch-mode frequencies. These specific peaks correlate well with the observed frequencies of the CH_x ($x = 1$, 2, and 3) stretch modes [25,28]. Combined this with our impurity analyses results, we believe that in our MOCVD-fabricated ZnO films, a large fraction of carbon is present in the form of CH_x defect complexes. These complexes most likely come from metal-organic precursors.
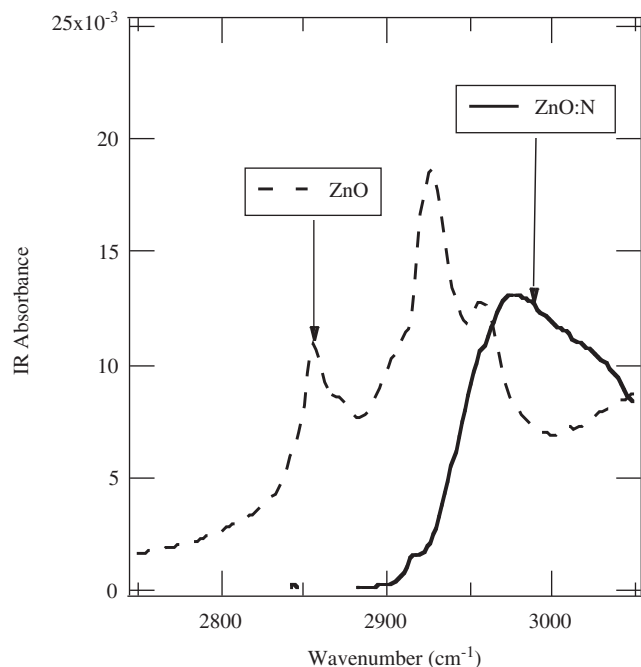
FTIR absorbance spectra of the ZnO:N sample further indicated that the NO gas affects the formation of the CH_x complexes in the ZnO film. Although SIMS data show the increase in carbon concentration for the ZnO:N sample, Fig. 7 shows that with nitrogen doping (solid line), the sharp IR absorbance peaks associated with the CH_x complex are largely decreased. The new broad peak emerges [19] around 3020 cm^{-1} (assigned as N_O–H peak [29]). This observation indicates that the use of NO gas as a precursor reduces the absorption of CH_x radicals on the surface of the substrate and/or that the existence of nitrogen in the ZnO film strongly attracts the impurity H and promotes the break-up of CH_x defect complexes. The other possibility is that with nitrogen doping, a reaction between nitrogen and carbon occurs, which we discuss next.

There is some correlation between carbon and nitrogen in the nitrogen-doped ZnO film. SIMS results indicated that the carbon concentrations in the ZnO:N films are generally higher than those in undoped ZnO films. Fig. 8 shows that for the nitrogen-doped ZnO films, very strong IR absorption peaks exist in the range of frequencies consistent with NC, NN, and CO modes [19]. Based on first-principles calculations, the formation energies of the NC and NN complexes are much lower than for CO [27]. Therefore, the peaks around the wave number of 1840 cm^{-1} are quite possible due to the NC and NN complexes. Our previous work suggests that the NC

Fig. 7. FTIR absorbance spectra, showing the 2750–3050 cm^{-1} region, were taken from undoped (dotted line) and nitrogen-doped (solid line) ZnO films. Both ZnO samples were deposited at 400 °C. The absorption peaks, which correlate well with the frequencies of the CH_x ($x = 1$, 2, and 3) stretch modes [25,28], are clearly shown on the undoped ZnO film, but not on the nitrogen-doped film.
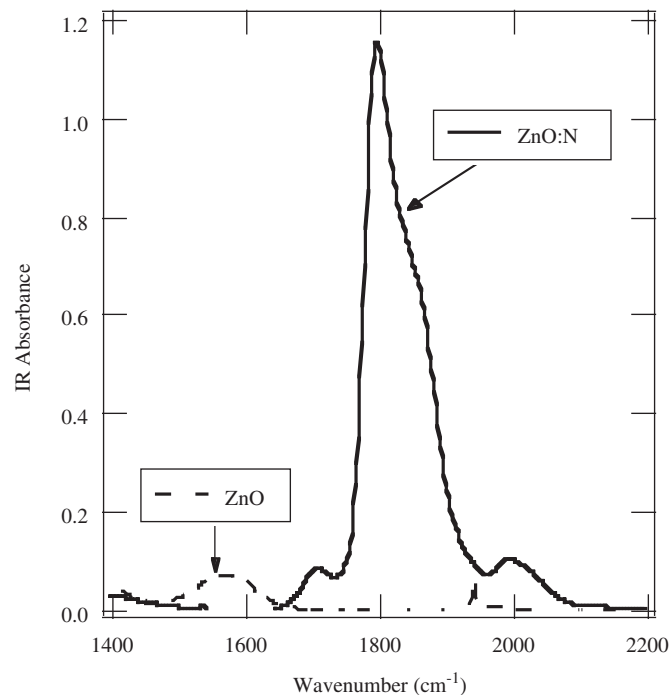

Fig. 8. FTIR absorbance spectra, showing the 1400–2200 cm^{-1} region, were taken from the same samples as Fig. 7. Compared with the undoped (dotted line) ZnO film, the nitrogen-doped (solid line) ZnO film has very strong absorption peaks in the frequency region possibly due to NC, NN, and CO stretch modes.

complex is far more likely in the MOCVD-formed ZnO:N film, compared with the NN defect complex [12]. Therefore, in the ZnO:N film fabricated with the DEZ and NO gas, the majority of the IR absorption peaks around the wave number of 1840 cm^{-1} may be due to the NC complex.

In order to produce high quality p-type ZnO:N, carbon contamination must be reduced. However, identifying and reducing the carbon incorporation pathways for MOCVD grown ZnO:N is quite difficult. The decomposition kinetics of DEZ under vacuum or inert atmospheres are understood fairly well [30,31], but the presence of O_2 or NO in the growth chamber will significantly effect the decomposition chemistry. Ethyl (C_2H_5) radicals and ethylene (C_2H_4) are expected to be highly reactive with O, N, and NO, leading to many pathways for carbon incorporation [32–36]. These reaction products may then incorporate in the film as the CH_x and NC species evident in Figs. 6–8. The high reactivity of ethyl and ethylene with N may also account for the differences in carbon incorporation between the doped and undoped films. Further work on the kinetics of ZnO:N growth and carbon incorporation is ongoing.

3.3. The possible compensation/passivation effects by hydrogen and carbon

Hydrogen passivation appears to be a very important issue for p-type ZnO doping. Isolated interstitial hydrogen was predicted to be an exclusive donor (H^+) in ZnO [37]. The interstitial H_2 molecule was predicted to be unstable in ZnO, except in an extreme n-type (Fermi level (E_F) is very close to the conduction-band minimum). The calculated formation energy (per H atom) of the H_2 molecule in ZnO is shown in Fig. 9, in comparison with the formation energy of an isolated H^+ and N_O–H complex in ZnO. Under a Zn-rich conditions, the formation energy of the H_2 molecule in ZnO has a higher formation energy than isolated H^+ and N_O–H complexes in almost the entire range of the Fermi energy.

The H_2^* complexes, which have been predicted to be stable in GaP:N and metastable in GaN, have high formation energy in ZnO and are thus unlikely to exist [38]. That H_2^* complexes are predicted to be unstable in ZnO is mainly because H^- is not stable in ZnO [39]. A H_2^* complex can be viewed as a complex between H^+ (bonded with O) and H^- (bonded with Zn).

For nitrogen-doped ZnO, one of the hydrogen passivation effects has been discussed in detail in a previous paper [29]. We also investigated the possibility of forming the N_O–H_2 complex. In Fig. 9, the calculated formation energy of the N_O–H_2^* complex in ZnO is shown (solid line) in comparison with the sum of the formation energy of an isolated H^+ and N_O–H complex (dotted line) in ZnO. Because the N_O–H complex has a neutral charge state, there is no Coulomb driving force for the complex to bind with another H^+ to form a N_O–H_2^* complex. Indeed, it is more difficult to form a N_O–H_2^* complex than an isolated H_2^* (which is also not stable) in ZnO. Therefore, the main
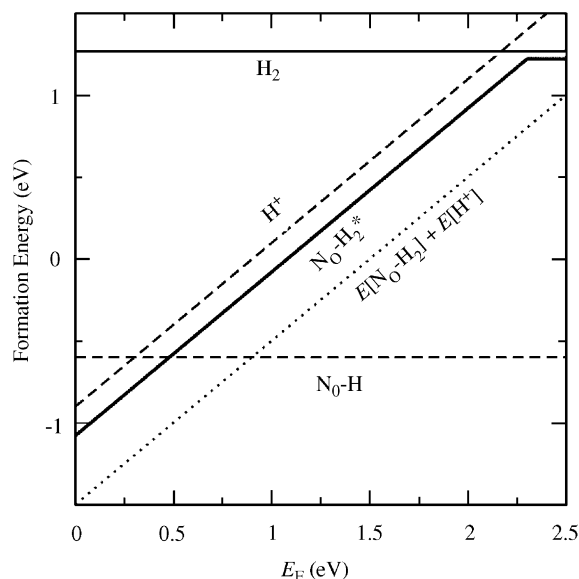

Fig. 9. The formation of the N_O–H_2^* complex. Dashed lines represent the formation energies of N_O–H complex and an isolated H^+ defect. The solid lines represent the formation energy of the N_O–H_2^* complex. The dotted lines show the sum of the formation energies of the N_O–H complex and an isolated H^+ defect. The N_O–H_2^* complex has a total formation energy higher than the sum of individual defects, which means the complex is unstable. The Zn-rich condition, N_2 phase precipitation limits (for N chemical potential), and H_2 phase precipitation limits (for H chemical potential) were used in the calculations. The formation energy of the H_2 molecule in ZnO is also shown. The E_F is relative to the valence-band maximum.

effect of hydrogen impurities in nitrogen-doped ZnO should be to form N_O–H neutral complexes, and thus to passivate the N_O acceptors.

From the above discussion, we can see that for an undoped ZnO, carbon impurities most likely exist as CH_x defect complexes. In the case of nitrogen doping, there are fewer CH_x complexes and other forms of carbon impurities such as the NC complexes are present. Based on first-principles calculations, we investigated several carbon-related defects in ZnO. Interstitial carbon (C_i) was found to be a donor, whereas substitution carbon (C_O) is a neutral or deep acceptor. Both C_i and C_O have high formation energies; therefore, they should not exist in high concentration. The N_O and C_i strongly bound to form a (NC)$_O$ complex. The strong binding energy suggests that under equilibrium Zn-rich conditions, (NC)$_O$ defect complexes are likely to form. Among carbon-related defects, the (NC)$_O$ complex has a lower formation energy than C_i and C_O. The predictions well support the experimental observation that the carbon solubility increases in the nitrogen-doped samples in comparison to the undoped samples.

First-principles calculations predict that at almost any Fermi level (except very near the conduction-band minimum), the (NC)$_O$ is a donor, stable in the 1^+ charge state, and has a vibrational frequency of 1995 cm^{-1} [27]. Therefore, the increased carbon concentration in the ZnO:N films will compensate the N_O doping effect.

4. Summary

We have discussed hydrogen and carbon impurities and their potential compensation/passivation effects in MOCVD-fabricated and nitric oxide-doped ZnO:N films. Compositional, optical, electronic, and element chemical states characterization were performed comparatively on both undoped and nitrogen-doped samples.

By MOCVD growth using NO doping, we can achieve very high nitrogen-doping concentration in ZnO films. However, hydrogen and carbon are unintentionally doped into our MOCVD-fabricated ZnO:N films. The carbon concentrations increase greatly in nitrogen-doped samples, suggesting that the unintentionally doped carbon impurities prefer to form defect complexes with nitrogen. Because of the strong bonding between hydrogen and carbon with nitrogen, the $(N_O–H)^0$ and $(NC)_O^{1+}$ defect complexes have quite low formation energies and could exist in large concentrations. Our result illustrates that with MOCVD growth of N-doped ZnO, strict control of carbon and hydrogen concentrations may be required to achieve high carrier concentrations in p-type ZnO:N films.

Acknowledgments

References

[1] C.R. Goria, N.W. Emanetoglu, S. Liang, W.E. Mayo, Y. Lu, M. Wraback, H. Shen, J. Appl. Phys. 85 (1999) 2595.
[2] J. Hu, R.G. Gordon, Solar Cells 30 (1991) 437.
[3] K. Minegishi, Y. Koiwai, Y. Kikuchi, K. Yano, M. Kasuga, A. Shimizu, Jpn J. Appl. Phys. 36 (1997) L1453.
[4] M. Joseph, H. Tabata, T. Kawai, Jpn J. Appl. Phys. 38 (1999) L1205.
[5] Y.R. Ryu, S. Zhu, D.C. Look, J.M. Wrobel, H.M. Jeong, H.W. White, J. Crystal Growth 216 (2000) 330.
[6] X. Li, Y. Yan, T.A. Gessert, C. Dehart, C.L. Perkins, D. Young, T.J. Coutts, Electrochem. Solid State 6 (2003) C56.
[7] X.-L. Guo, H. Tabata, T. Kawai, J. Crystal Growth 223 (2001) 135.
[8] T. Aoki, Y. Shimizu, A. Miyake, A. Nakamura, Y. Nakanishi, Y. Hatanaka, Phys. Stat. Sol. B 229 (2002) 911.
[9] A.B.M.A. Ashrafi, I. Suemune, H. Kumano, S. Tanaka, Jpn J. Appl. Phys. 41 (2002) L1281.
[10] J.F. Rommeluere, L. Svob, F. Jomard, J. Mimila-Arroyo, A. Lusson, V. Sallet, Y. Marfaing, Appl. Phys. Lett. 83 (2003) 287.
[11] T.M. Barnes, K. Olson, C.A. Wolden, Appl. Phys. Lett. 86 (2005) 112112.
[12] C.L. Perkins, S.-H. Lee, X. Li, S.E. Asher, T.J. Coutts, J. Appl. Phys. 97 (2005) 034907.
[13] K.-K. Kim, H.-S. Kim, D.-K. Hwang, J.-H. Lim, S.-J. Park, Appl. Phys. Lett. 83 (2003) 63.
[14] G.D. Yuan, Z.Z. Ye, L.P. Zhu, Q. Qian, B.H. Zhao, R.X. Fan, C.L. Perkins, S.B. Zhang, Appl. Phys. Lett. 86 (2005) 202106.
[15] K. Nakahara, H. Takasu, P. Fon, A. Yamada, K. Iwata, K. Matsubara, R. Hunger, S. Niki, J. Crystal Growth 237-239 (2002) 503.
[16] J.M. Bian, X.M. Li, X.D. Gao, W.D. Yu, L.D. Chen, Appl. Phys. Lett. 84 (2004) 541.
[17] A. Tsukazaki, A. Ohtomo, T. Onuma, M. Ohtani, T. Makino, M. Sumiya, K. Ohtani, S.F. Chichibu, S. Fuke, Y. Segawa, H. Ohno, H. Koinuma, M. Kawasaki, Nat. Mater. 4 (2005) 42.
[18] B.S. Li, Y.C. Liu, Z.Z. Zhi, D.Z. Shen, Y.M. Lu, J.Y. Zhang, X.W. Fan, R.X. Mu, D.O. Henderson, J. Mater. Res. 18 (2003) 8.
[19] B.M. Keyes, L.M. Gedvilas, X. Li, T.J. Coutts, J. Crystal Growth (2005) (in press)
[20] S.B. Zhang, J.E. Northrup, Phys. Rev. Lett. 67 (1991) 2339.
[21] S. Limpijumnong, S.B. Zhang, S.-H. Wei, C.H. Park, Phys. Rev. Lett. 92 (2004) 155504.
[22] S.-H. Wei, S.B. Zhang, Phys. Rev. B 66 (2002) 155211.
[23] X. Li, Y. Yan, T.A. Gessert, C.L. Perkins, D. Young, C. Dehart, T.J. Coutts, J. Vac. Sci. Technol. A 21 (2003) 1342.
[24] E. Kaminska, A. Piotrowska, J. Kossut, R. Butkute, W. Dobrowolski, R. Łukasiewicz, A. Barcz, R. Jakieła, E. Dynowska, E. Przezdziecka, M. Aleszkiewicz, P. Wojnar, E. Kowalczyk, Phys. Stat. Sol. C 2 (2005) 1119.
[25] N.H. Nickel, K. Fleischer, Phys. Rev. Lett. 90 (2003) 197402.
[26] C.G. Van de Walle, Phys. Rev. Lett. 85 (2000) 1012.
[27] S. Limpijumnong, X. Li, S.B. Zhang, S.-H. Wei, Appl. Phys. Lett. 86 (2005) 211910.
[28] G.-C. Yi, B.W. Wessels, Appl. Phys. Letts. 70 (1997) 357.
[29] X. Li, B.M. Keyes, S.E. Asher, S.B. Zhang, S.-H. Wei, T.J. Coutts, S. Limpijumnong, C.G. Van de Walle, Appl. Phys. Lett. 86 (2005) 122107.
[30] J. Ye, S. Gu, S. Zhu, S. Liu, W. Liu, X. Zhou, L. Hu, R. Zhang, Y. Shi, Y. Zheng, J. Crystal Growth 274 (2005) 489.
[31] H. Dumont, A. Marbeuf, J.-E. Bouree, O. Gorochov, J. Mater. Chem. 3 (10) (1993) 1075.
[32] W. Tsang, R.F. Hampson, J. Phys. Chem. Ref. Data 15 (3) (1986) 1087.
[33] D.L. Baulch, C.J. Cobos, R.A. Cox, P. Frank, G. Hayman, T. Just, J.A. Kerr, T. Murrels, M.J. Pilling, J. Troe, R.W. Walker, J. Warnatz, J. Phys. Chem. Ref. Data 23 (1994) 847.
[34] G. Parakevopoulos, C.A. Winkler, J. Phys. Chem. 71 (1967) 947.
[35] L.J. Stief, F.L. Nesbitt, W.A. Payne, S.C. Kuo, W. Tao, R.B. Klemm, J. Chem. Phys. 102 (1995) 5309.
[36] G. Pratt, I. Veltman, J. Chem. Soc. Faraday Trans. 72 (1976) 2477.
[37] C.G. Van de Walle, Phys. Stat. Sol. B 229 (2002) 221.
[38] A. Janotti, S.B. Zhang, S.-H. Wei, Phys. Rev. Lett. 88 (2002) 125506.
[39] S. Limpijumnong, J.E. Northrup, C.G. Van de Walle, Phys. Rev. B 68 (2003) 075206.